AN EXPERIMENTAL FACILITY FOR THE STUDY OF UNSTEADY FLOW IN TURBOPUMPS

by

Nicolas R. Goulet

Ingénieur des Arts et Manufactures,
Ecole Centrale de Paris, 1988

SUBMITTED TO THE DEPARTMENT OF AERONAUTICS AND ASTRONAUTICS
IN PARTIAL FULLFILMENT OF THE REQUIREMENTS FOR
THE DEGREE OF

MASTER OF SCIENCE IN
AERONAUTICS AND ASTRONAUTICS

at the

MASSACHUSETTS INSTITUTE OF TECHNOLOGY
May 1989

Signature of Author_____
Department of Aeronautics and Astronautics
May 1989

Certified by_____
Dr. Belgacem Jery
Assistant Professor of Aeronautics and Astronautics
Thesis supervisor

Approved by_____
Professor Harold Y. Wachman
Chairman, Department Graduate Committee

AN EXPERIMENTAL FACILITY FOR THE STUDY OF
UNSTEADY FLOW IN TURBOPUMPS

by

Nicolas R. Goulet

Submitted to the Department of Aeronautics and Astronautics in May 1989,
in partial fulfillment of the requirements for the degree of
Master of Science in Aeronautics and Astronautics

ABSTRACT

The conception, design and preliminary modelling of an experimental facility aimed at the study of unsteady flow in centrifugal pumping systems have been conducted. The design is driven by the need to determine the fluid dynamic phenomena governing the performance and stability of low specific speed pumps when operated well below their design flow conditions.
The underlying principle is to provide a variable response system for the test pump to interact with. The dynamic behavior of the pump itself can then be studied in a controlled environment.
A closed, water recirculating, loop featuring a large, fully transparent, pump and a set of compliant plenums has been chosen as a test bed. Provisions are made for carrying out extensive, steady and time resolved, internal flow measurements. The techniques involved include pressure mapping with rotating instrumentation as well as qualitative and quantitative flow visualization.

In addition to a linear stability calculation used to determine the dimensions of the loop as well as the small perturbation behavior (frequency and damping) and the detailed engineering of the system components, an analytical effort has been initiated.

A time resolved, lumped parameter, model is developed to predict the unsteady non-linear behavior of the pumping system. In particular, results similar to those previously established for surge in open loop compression systems are derived and discussed.
An analysis of the local flow characteristics within the volute passage is used as a basis for a simple model to determine off-design operating conditions in centrifugal pumps. The results show how the mismatching of the volute and impeller performances affects the shape of the characteristic. This model is also used to assess the effect of shroud leakage flows on the performance and a simple correlation between the overall flow and the shroud leakage flows is established. The validity of this method is evaluated, based on comparison with existing data.

Thesis supervisor: Dr. Belgacem Jery.
Title: Assistant Professor of Aeronautics and Astronautics.

Acknowledgements

It is late now, and soon I will trudge over to the department headquarters in what will be the culmination of almost two years of . . . work? When I look back, It is obvious to me that I didn't do it alone. To all those who have helped me, even if you are not aware of it (if you are reading this, chances are you are!), thank you. Now, it is the tradition that I name here those that have left the strongest impression on me, but if you do not figure in the list below, don't despair, very few people will probably ever read this.

Special thanks to:

My advisor, Dr. Belgacem Jery, for his guidance throughout this research and for putting up with my frenzy to graduate. Also to Professor Greitzer for his valuable discussions and appropriate criticisms.

Tom Tyler, Paul Westhoff and Paul Hermann from Sundstrand Corporation for their support.

Holly, Diana, Karen and Nancy for their help with the details.

Viktor, Jim, and Roy for their help around the lab.

My office mates Reza, Yi-Lung, and Charlie for proving to me that you are never alone when you are a graduate student.

Jeff, whom I wish a good continuation and the best of luck with his new family.

Dr. Tan, for showing me that buying the New York Times in the morning is not a futile effort and Professor Epstein for making me *believe* that VersaCAD is in fact a useful tool to work with.

Viktor for his unbeatable comments on the general surroundings, watches, cars and many others.

Jimmy, Vincent, Philippe and Veronique for all the fun and the good times. For the sailing, the soaring, the parties, the rows....for being my friends.

All my other friends, here and in Europe, who contributed in their own way to this work.

I must mention here my parents and Lucinda, who have always backed me with love and affection, even from thousands of miles away.

Finally a little note to Catherine, for the inspiration.

Financial support was provided by the National Science Foundation and Sundstrand Corporation during the course of this work, and it is gratefully acknowledged.

'Things should be made as simple as possible,
but not simpler'

Albert Einstein

Table of contents

List of figures

Nomenclature

$A_{i_{ref}}$: --- Reference area of the duct section i (m^2).

$A_i(x)$: --- Area at coordinate x (m^2).

a_i: --- Nondimensional area.

$$= \frac{A_i}{\pi D_2 b_2}$$

B: --- B parameter.

$$= \frac{U}{2.\omega_{osc} L}$$

b_2: --- Discharge width of the impeller (m).

b_1: --- Shroud-casing clearance at the impeller discharge (m).

b_s: --- Shroud labyrinth seal clearance (m).

C: --- Volute tangential velocity (m/s).

C_{m1}: --- Impeller inlet meridional velocity (m/s).

C_{m2}: --- Impeller discharge meridional velocity (m/s).

C_{lm}: --- Meridional leakage velocity (m/s).

C_p: --- Diffuser pressure recovery coefficient.

C_s: --- Labyrinth seal average axial velocity (m/s).

C_{u2}: --- Impeller discharge tangential velocity (m/s).

D_1: --- Inlet diameter of the impeller (m).

D_2: --- Discharge diameter of the impeller (m).

D_s: --- Labyrinth seal diameter (m).

D_h: --- Hydraulic diameter (m).

D_t: --- Section diameter of the inner tube (m).

f: --- Similarity factor (reduction factor).

$$= \frac{N_o}{N}\left(\frac{H}{H_o}\right)^{1/2}$$

--- Critical shaft frequency (Hz).

F: --- Total thrust load (N).

F_b: --- Back shroud thrust (N).

F_f: --- Front shroud thrust (N).

g: --- Acceleration of gravity (m/s^2).

H: --- Total head (m or ft).

h: --- Volute height (m).

K_i: --- Dynamic head loss coefficient.

K_{m1}: --- Entrance velocity constant.

K_{m2}: --- Capacity constant.

K_u: --- Speed constant.

k: --- Dynamic head loss coefficient.

L_i: --- Length of duct (m).

L_p: --- Blade passage 'length' (m).

$\dot{m}$: --- Mass flow (kg/s).

n: --- Number of discrete elements used to discretize the volute.

N: --- Rotational speed (rpm).

N_s: --- Specific speed.

$$= \frac{\Omega \sqrt{Q}}{\sqrt[4]{gH^3}}$$

N_{ss}: --- Suction specific speed.

N_t: --- Number of tubes in each tank.

P_i: --- Pressure in the plenum i (Pa).

--- Inlet static pressure (Pa).

$P(r)$: --- Impeller static pressure (radial distribution) (Pa).

$P_b(r)$: --- Back shroud static pressure (radial distribution) (Pa).

$P_f(r)$: --- Front shroud static pressure (radial distribution) (Pa).

P_v: --- Fluid vapor pressure (Pa).

ΔP_s: --- Impeller static pressure rise (Pa).

ΔP_t: --- Pressure drop through the throttle (Pa).

ΔP_p: --- Pressure rise through the pump (Pa).

R_e: --- Reynolds number.

$$= \frac{U_{tip} D_2}{\nu}$$

R_i: --- Inlet radius (m).

--- Inner radius of tank (m).

R_o: --- Discharge radius (m).

--- Outer radius of tank (m).

R_s: --- Shaft radius (m).

R_t: --- Inner tube median radius (m).

Q: --- Volumetric flow rate (m^3/s or gpm).

t: --- Time (s).

U: --- Impeller tip speed (m/s).

V_i: --- Volume of air contained in plenum i (m^3).

--- Velocity of the fluid in the duct i (m/s).

w: --- Linear weight of the shaft (kg/m).

Z: --- Number of blades.

β: --- Relative blade discharge or incidence angle.

ρ: --- Density (kg/m^3).

γ: --- Specific heat ratio.

--- Absolute discharge angle.

ξ: --- Instability parameter.

$$= B^2 \cdot \left(\frac{\partial \Psi_{pump}}{\partial \Phi} \right) \cdot \left(\frac{\partial \Psi_{throttle}}{\partial \Phi} \right)$$

--- Loss factor.

λ: --- Friction loss factor.

--- Eigen value.

ζ: --- Length ratio.

χ_i: --- Non-dimensional area.

--- Area ratio.

σ: --- Cavitation number.

$$= \frac{P_i - P_v}{\frac{1}{2} \rho U_{tip}^2}$$

--- Slip factor.

μ: --- Dynamic viscosity (SI).

ν: --- Kinematic viscosity (SI).

η: --- Efficiency.

ω: --- Angular velocity (rad/s).

ω_{red}: --- Reduced frequency of the oscillations.

$$= \frac{\omega_{oscillations}}{\omega_{shaft}}$$

ω_{osc}: --- Angular velocity of the oscillations (rad/s).

ω_{shaft}:--- Angular velocity of the shaft (rad/s).

Sometimes noted: Ω.

Φ_{uns}: --- Instability inception flow coefficient.

Φ: --- Flow coefficient.

$$= \frac{\dot{m}}{\rho \pi D_2 b_2 U}$$

φ: --- Volute local flow coefficient.

Ψ: --- Head coefficient.

$$= \frac{\Delta P}{\frac{1}{2} \rho U^2}$$

Operators:

$\partial( )/\partial t$: Partial derivative.

$d( )/dt$: Total or substantial derivative.

$\delta( )$: Perturbation quantity.

$\Delta( )$: Differential quantity.

$\widetilde{( )}$: Non-dimensional quantity.

$\overline{( )}$: Steady state quantity.

$\Re( )$: Real part.

$\Im( )$: Imaginary part.

CHAPTER I

Introduction

I.1 Background

The recent trend in fuel injection and hydraulic systems, whether for new generation gas turbine engines or advanced space propulsion systems, is toward higher pressure ratios and relatively lower flow rates. This range of operation is optimally obtained with low specific speed centrifugal pumps whose small geometry and high rotational speed make them convenient for use in the demanding environment of aerospace applications.

However, some of the operating regimes associated with these applications, such as those corresponding to the landing approach or coasting phase of a fighter jet flight, require flows below 2% of nominal design conditions. Traditionally, such flow rates were achieved through a bypass; but, given the high power density of these small pumps (typical impeller diameters are about 3 cm), fluid overheat can become unacceptable for bypass operation. For this and other reasons (weight reduction, space limitations...etc) direct throttling is sometimes necessary over the entire range of operation.

There is, however, a major problem associated with this requirement, namely the possibility of unstable oscillations when the pump operates in the positively sloped portion of its characteristic. This occurs at flows well below Best Efficiency Point (BEP), in an area where other centrifugal compression systems are known to exhibit surge. Unfortunately, almost all the present knowledge on surge instability is based on gas compression systems. One of the most important factors for these systems was shown to be the coupling between the actual pumping element and the rest of the system. Many analyses have been developed

(e.g. [1], [2], [5]) and they all pinpoint the B parameter, which characterizes the ratio of pressure forces to inertial forces in the system, as the fundamental non-dimensional parameter associated with this coupling. It is still unclear however, whether the instability inception and growth mechanisms are the same, in the case of a gas [2], as in the case of the relatively incompressible fluid addressed in this study.

The work described in this thesis originated in the need to develop low specific speed pumps capable of sustained stable operation at the very low flow regimes described above. The objective is to go beyond the immediate need to alleviate the severe oscillations encountered during initial development tests, and to try and establish a more fundamental understanding of the instability mechanism(s) in this family of pumping systems.

The scope of this thesis is therefore the conception, design, and preliminary modelling of an experimental facility which will serve as a testbench for the investigation of turbopump instability and of unsteady flow within centrifugal pump components. First, the various possibilities available will be examined to justify the choice of a closed loop configuration. The lumped parameter analysis developed in [1] will be extended to more complex systems and serve as an analytical basis for the dimensioning of the loop. It will also provide a means for comparing the phenomenon observed with classic surge in gas compression systems.

The mechanical design will then be reviewed, and a model proposed to predict the time resolved and the steady state behavior of the test facility. This model will complement the lumped parameter analysis described earlier and help drawing possible parallels between the instability of concern here and surge.

Finally, a simple model shall be developed to show how some of the local flow properties can contribute to the overall performance of the pumping

element. This model will be refined after the results of the experiments planned for the next phase of the investigation are known and analyzed.

I.2 Statement of problem

Test measurements conducted as part of an industrial effort to develop a family of low specific speed centrifugal pumps revealed severe pressure oscillations. The situation is one in which the configuration of the system is imposed by the customer resulting in limited flexibility during the design phase of the pump. The design requirements call for these centrifugal pumps to (i) match this particular system configuration and (ii) operate stably over a specific flow range (i.e. down to 2% flow by direct throttling, no bypass allowed). The limited data collected during development tests typically show these oscillations to start at flows below 40% of Best Efficiency Point (BEP), with their amplitudes reaching up to 50% of design pressure rise (cf figure 1.1). The frequencies remain generally around 5% of shaft rotational frequency (which is higher than that of surge but lower than that of rotating stall in gas compression systems).

The pumping system used in the foregoing development tests is completely passive, in the sense that the pump is the only component capable of a net energy input to the flow. It can therefore be inferred that the oscillations are sustained by the pump. The mechanism of this input might or might not be similar to the one described in [1] and summarized on figure 1.3, but, in any case, externally triggered instabilities (structural interactions for example) or externally forced vibration modes will not be addressed.

As stated above, the instabilities occur at flows well below BEP, and there is a serious lack of adequate tools needed to understand this flow regime. One has to contend with the inherently viscous and three dimensional nature of the flow. Near shutoff, throughflow velocities are small and viscous shear is strong. Velocity triangles are distorted and there exists a severe mismatch between the various components (inducer, impeller, diffuser and volute). Moreover angles of

attack increase, airfoil wakes become thicker and separation and stall become predominant.

Conceptually, one can view the impeller as a mechanical device that accelerates the flow which is then diffused to recover pressure or potential energy. However the real picture is much more involved as many secondary problems arise:

- The centrifugal acceleration can lead to overspeeding and eventually cavitation due to the lowering of the pressure in the tip regions of the blades.
- Pressure recovery through diffusion implies the existence of an unfavorable pressure gradient that can induce boundary layer transition and separation. The increase in cross-section also amplifies existing perturbations such as wakes from the impeller blades or the diffuser vanes (when these exist).
- The circumferential non uniformity of the volute can also create potential disturbances in the area of the tongue, as was pointed out in [2]. These in turn will travel downstream and upstream and will be amplified if the pressure gradient is unfavorable.
- The trailing vortex core from the impeller can produce important local depressions in the fluid. When associated with cavitation these can be a major source of complications in the flow field.

Clearly, based on the current status of knowledge of these complex flow regimes, a purely analytical approach to the problem is unlikely to yield any significant near term results. On the other hand, further experimental evidence could be very beneficial in singling out the phenomena controlling the instabilities. This fact represents the philosophy underlying the design of the facility. It will have a strong impact on the design because it drives the major objectives of this project. These will now be reviewed and a research approach shall be defined to try and satisfy them.

I.3 Objectives and research approach

It has been established in the literature that, when operated as part of an otherwise passive system, pumps can sustain dynamic instability along that part of their characteristic which is positively sloped. This can happen due to either a static instability criterion or a dynamic instability criterion (figures 1.2, 1.3 and [1], [2] and [5]). Analysis of the data provided in [3] and [6] confirmed this fact in the case of interest. It was concluded (on this basis) that any comprehensive investigation of the observed instabilities will have to deal, at some stage, with the issue of determining what factors control the slope of a centrifugal pump characteristic when it is operating well below design flow conditions.

This matter is compounded by various other issues that must also be considered. They include the necessity to determine the mechanisms of inception and evolution of the instabilities and the need to establish guidelines on the role of each individual component in the overall performance of the pump. The effect of geometric modifications will also be explored.

The overall objective is therefore to obtain a good physical understanding of the phenomena and then establish proven design guidelines which would allow stable operation of centrifugal pumps at low flow. In other words the goal is to gain insight into the fluid mechanics rather than propose a series of parametric, machine specific, 'fixes'.

In view of the difficulty to develop adequate analytical tools, it was decided that the most useful avenue to do this was an experiment in which the actual hardware may be scaled up while preserving all the relevant non-dimensional flow parameters. Relatively simple (but conclusive) internal flow measurements can be carried out and used to narrow down the number of potential candidates on which further detailed measurements and refined theoretical models will concentrate.

A two-phased approach was thus adopted. The first phase concentrates on the design and testing of a rig which will be used to determine the scope of further detailed experiments and facilitate analytical modelling. Necessary insight into the problem will thus be obtained. The second phase can then concentrate on those experiments and expand the existing knowledge on internal flow phenomena in centrifugal pumps.

Realization of the objectives described above hinges upon the ability in the first stage to reproduce the unstable operation of the pump in a controlled laboratory environment using scaled up hardware. This thesis will seek an approach based on this imperative and will justify the choices of such an approach.

The design calculations (cf. Chapter II) show that it is possible to reproduce system instabilities with scaled up hardware. However, various issues must be settled beforehand:

- What type of rig is more suitable (open loop vs closed loop) ?
- What kind of scaling should be adopted for the pump ?
- How should the rest of the system be modelled ?
- What choice of working fluid is suitable (water vs air vs Jet fuel)?
- What should determine the design of the test section ?

The question concerning the type of rig is a relatively easy one to settle. Given a rough estimate of the scaling ratio of the pump (about 20, cf. III.1.1), a performance evaluation (nominal flow should be around 0.05 m^3/s) shows that the volumes of fluid considered are impractical in any other context than that of a recirculating system. A closed loop approach is therefore imperative. Moreover, it has certain advantages with respect to techniques such as seeding, corrosion prevention, etc..., which are more easily controllable in a closed environment.

The scaling of the actual device is an issue of pure geometric similarity and is a well accepted practice. Flow coefficients, head coefficients and specific speed are preserved. The details of the scaling procedure appear in Chapter III.

As far as modelling the system is concerned, only one approach seems realistic: To try and create a system that is easily controllable and that is capable of exhibiting the same response as in development tests where the instabilities were first observed. This implies that the frequencies observed are the system frequencies (analogous to the Helmoltz frequency described in [1]) and that the B parameter [1] can be simulated. It is also important to duplicate the onset of instability on the characteristic so as to ensure the damping factors are identical to the original ones. This actually corresponds to creating a 'black box' with a determinable and controllable response. Mechanical [1] and electrical [2] analogies can be used to create a series of inertances and compliances (for example with a combination of air bags and ducts). The detail of this method is developed in Chapter II together with the determination of the optimal parameter combination for such a system.

For the working fluid, water is the natural choice: compressibility is thus avoided, two phase flow and suction specific speed can be simulated, flow visualization is convenient. Its density and viscosity allow a realistic range of Reynolds numbers. For regimes where the Reynolds matching might be considered inadequate, additives such as glycerine can extend the range. Finally, water is the easiest and least expensive fluid to work with experimentally.

The test section is one of the most important components of the rig. Its design must be guided by the scope of experiments to be conducted. The two-phased approach adopted earlier is reflected in the organization of the actual experiments. These are:

- First phase:

Validation of the rig and determination of areas of interest in which more detailed experimental and theoretical investigation will be conducted. The types of data that correspond to this approach are:

(i) overall rig performance data, including flow and head coefficient ranges, cavitation performance, and system stability maps; the variables are pump speed, inlet pressure, throttle setting, and air content with some emphasis on the low flow areas of the characteristic.

(ii) ensemble-averaged velocity profiles, including the inlet, the impeller, the volute, and the pipe diffuser. These will be obtained through LDV (laser doppler velocimetry). Provision for this must be made during the mechanical design of the test section.

(iii) unsteady and time averaged static pressure, concentrated mostly at the impeller discharge, the volute tongue, and the diffuser; the frequencies and phases of unsteady signals are essential in pinpointing the nature and source of any mechanism that may contribute significantly to the overall behavior of the pumping element (impeller rotating stall, impeller-volute or impeller-diffuser interaction).

(iv) simple photographic flow visualization experiments using tufts and die injection techniques.

• Second phase:

The full scope of these second stage measurements cannot be finalized until the results of the first stage are known and analyzed. Suffice it to say at this point that more concentrated measurements should be performed, including phase locked and time resolved pressure and velocity maps of the local flow features of interest, such as inlet distortions, impeller and diffuser stall, impeller volute

interactions, etc... The techniques used will include, in addition to those described for stage one:

(i) rotating, static pressure probes.

(ii) qualitative and quantitative flow visualizations possibly using a metal vapor laser in conjunction with a high speed video camera and image processor.

The questions to be answered should deal with the relation between the mechanisms of unsteady operation and the pump's internal geometry. They should also assess the impact of detailed flow characteristics on the overall performance.

The mechanical design of the test section will have to take into account the implementation of the instrumentation described above. As will be shown in Chapter III, these considerations have a strong impact on the design. The final configuration of the rig is a direct consequence of such considerations and this thesis will try and follow the logic that has driven its design.

In the second Chapter a linear analysis will be developed to determine the range of variables and the dimensioning of the loop components. This study will also yield an estimate of the expected response of the system to small perturbations (in terms of frequency and response).

The third Chapter deals with the engineering of the rig. The scaling procedure is detailed and all the mechanical design solutions will be justified. Also, the operating restrictions, such as critical speeds and thrust loading, are determined to ensure proper operating limits.

The fourth Chapter describes the simulation and modelling developed to predict the operation of this facility. A time resolved overall dynamic simulation will be used to predict the operating characteristics of the system in surge and determine its transient response. The other model will use a simple, one

dimensional analysis of the flow in the volute to evaluate the impact on the performance of the mismatch between various components at off-design conditions.

CHAPTER II

Theoretical basis for facility design (linear perturbation model)

II.1 Theoretical basis

The object of this chapter is to explore the scope of pratical realizations once a closed loop rig configuration has been selected. The dominant factors in the dynamic response of the system shall be determined, together with the variable ranges necessary to complete the scaling correctly. To do this, it is convenient to consider a 'generalized' loop with an arbitrary number of elements divided into four categories:

- Inertial elements in which the fluid is incompressible. These are mainly the piping sections.
- Compliant elements in which energy can be accumulated through the isentropic compression of a given gas (in this case simply air). These are considered distributed discretely along the system in the form of plenums containing calibrated air bags (so no gas fraction is considered in the fluid).
- Purely resistive elements that exhibit a quasi parabolic behavior as far as their characteristic is concerned. The throttle is one of these.
- Active components that have the possibility to input energy into the system if the phase of the oscillatory phenomena is correct, as is shown in [1]. These include the pump itself but also systems such as a siren valve that might be used to force the system oscillations instead of relying on the natural frequencies of the loop.

For each of the above elements, all the steady state parameters are assumed known (volume, pressure, steady state characteristic and of course the operating

point). The fluid is taken to be incompressible with a density ρ and the air in the compliance bags has a specific heat ratio γ.

For each piping section, viscosity effects (skin friction) and singular pressure drops will be lumped into a single quadratic loss coefficient that describes the parabolic behavior of these phenomena.

The analysis shall be based upon the following elementary flow equations:

- Momentum for each piping section.
- Mass conservation for each plenum.
- Isentropic compression in each air bag.

From these one can derive a first order differential system which in turn can be linearized around the steady state operating point. The complex eigen values of this system will describe the global behavior of the loop under a given small perturbation.

The first step is therefore to setup the system in a form that is convenient for a numerical treatment. A computational code will then yield the real and imaginary parts of the eigen values associated with the system. The 'B' and instability parameters (defined in section II.2) can then be obtained for a series of operating points along the pump characteristic. The combination of the dominant eigen value's real and imaginary parts ($\Re(\lambda)$ & $\Im(\lambda)$) determine the stability of the system:

$$\left.\begin{matrix}\Im(\lambda)=0\\ \Re(\lambda)<0\end{matrix}\right\} \Rightarrow \text{Static stability}$$

$$\left.\begin{matrix}\Im(\lambda)\neq 0\\ \Re(\lambda)<0\end{matrix}\right\} \Rightarrow \text{Dynamic stability}$$

$$\left.\begin{matrix}\Im(\lambda)=0\\ \Re(\lambda)>0\end{matrix}\right\} \Rightarrow \text{Static instability}$$

$$\left.\begin{matrix}\Im(\lambda)\neq 0\\ \Re(\lambda)>0\end{matrix}\right\} \Rightarrow \text{Dynamic instability}$$

II.1.1 System definition and equations

One of the most attractive aspects of a closed loop rig is also one of its drawbacks. Any perturbations in the flow will be recirculated together with the working fluid. For this reason it was decided to arbitrarily make one of the plenums large enough to uncouple, as much as possible, the upstream section from the downstream section (relative to the pump). This plenum will also serve as a reference in the labelling of the plenums and the piping sections.

Figure 2.1 represents a schematic view of the system as defined. The following notations have been adopted:

- The plenums are numerically indexed as their downstream piping section and contain a volume of air V_i at the pressure P_i. The only exceptions are the one upstream from the pump which has the attributes V_p and P_p and the one upstream of the throttle which has the attributes V_t and P_t. The mass flow through the pump is $\dot{m}_p$ and the one through the throttle $\dot{m}_t$, and so forth...
- The main plenum bears the index n and is upstream from piping section number one: We are considering n inertial elements and n+1 compliances in the loop.
- If other resistive elements are to be introduced in one of the piping sections they will have to be incorporated in the corresponding pipe loss coefficient. This does not restrict the scope of the calculation, it only requires a little preliminary calculation to obtain the desired form (for example if one wanted to introduce a cyclic resistance such as a siren valve).

• It is assumed that, due to an adequate design, the compliant volume in each plenum will effectively be that of the air bag it contains. This implies that the design of the air bags gives them a behavior close to that of a equal amount of air in solution and that the air bag/fluid interaction is efficient in terms of pressure loss.

• The following conventions will also be used:

l_i : length of each duct.

$A_{i_{ref}}$: reference area of each duct, defined by:

$$A_{i_{ref}} = \frac{l_i}{\int_0^{l_i} \frac{dx}{A_i(x)}}$$

ΔP_i : represents the loss in the piping due to friction, bends and any other singularities. It also accounts for eventual external damping such as a pump, a throttle or any other discrete resistance.

The following equations can then be derived:

Volume conservation for the plenums:

$$1 \le i \le n \qquad \rho \frac{dV_i}{dt} = \dot{m}_{i+1} - \dot{m}_i \tag{2.1}$$

Isentropic transformation of the air contained in the air bags:

$$1 \le i \le n \qquad dV_i = -\frac{V_i}{\gamma P_i} dP_i \tag{2.2}$$

Momentum for the fluid contained in each piping section:

$$2 \le i \le n-1 \qquad \frac{l_i}{A_{i_{ref}}} \frac{d\dot{m}_i}{dt} = P_{i-1} - P_i - \Delta P_i$$

$$\frac{l_1}{A_{1_{ref}}}\frac{d\dot{m}_1}{dt}=P_n - P_1 -\Delta P_1$$

$$\frac{l_n}{A_{n_{ref}}}\frac{d\dot{m}_n}{dt}=P_{n-1} - P_n -\Delta P_n \qquad (2.3)$$

Substituting equations (2.2) in (2.1) yields a first order differential system of 2n equations:

$$1 \le i \le n-1 \qquad -\frac{\rho V_i}{\gamma P_i}\frac{dP_i}{dt}=\dot{m}_{i+1} - \dot{m}_i$$

$$-\frac{\rho V_n}{\gamma P_n}\frac{dP_n}{dt}=\dot{m}_1 - \dot{m}_n$$

$$2 \le i \le n-1 \qquad \frac{l_i}{A_{i_{ref}}}\frac{d\dot{m}_i}{dt}=P_{i-1} - P_i - \Delta P_i$$

$$\frac{l_1}{A_{1_{ref}}}\frac{d\dot{m}_1}{dt}=P_n - P_1 -\Delta P_1$$

$$\frac{l_n}{A_{n_{ref}}}\frac{d\dot{m}_n}{dt}=P_{n-1} - P_n -\Delta P_n \qquad (2.4)$$

Now, ΔP_i has two components, one due to the quadratic losses (friction and singularities) in the piping and another due to external damping sources (induced by foreign elements in the flow: pumps , throttles, screens etc..):

$$\Delta P_i = K_i \tfrac{1}{2} \rho V_i^2 + \Delta P'_i$$

Which can also be written:

$$\Delta P_i = \frac{K_i}{2}\frac{\dot{m}_i^2}{\rho A_i^2} + \Delta P'_i \qquad (2.5)$$

$\Delta P'_i$ is the pressure drop due any discrete element that might be included. Obviously, this notation is convenient for any elements not having a parabolic characteristic, but we shall also use it to describe the throttle response (which is nevertheless parabolic) since we shall use it to determine the operating point (see II.1.2).

The 2n equations go from 1 to n for the 'mass' equations and from n to 2n for the 'pressure' equations. The system matrix has a diagonal composed of two n^{th}. order matrices and is zero elsewhere. The upper right matrix corresponds to the mass flow terms and the lower left matrix corresponds to the pressure terms. It can be written:

$$
\left|
\begin{array}{ll}
 & \dfrac{d\dot{m}_1}{dt} = \dfrac{A_{1_{ref}}}{l_1}\left(P_n - P_1 - \Delta P_1\right) \\
2 \le i \le n-1 & \dfrac{d\dot{m}_i}{dt} = \dfrac{A_{i_{ref}}}{l_i}\left(P_{i-1} - P_i - \Delta P_i\right) \\
 & \dfrac{d\dot{m}_n}{dt} = \dfrac{A_{n_{ref}}}{l_n}\left(P_{n-1} - P_n - \Delta P_n\right) \\
1 \le i \le n-1 & \dfrac{dP_i}{dt} = \dfrac{\gamma P_i}{\rho V_i}\left(\dot{m}_i - \dot{m}_{i+1}\right) \\
 & \dfrac{dP_n}{dt} = \dfrac{\gamma P_n}{\rho V_n}\left(\dot{m}_n - \dot{m}_1\right)
\end{array}
\right. \qquad (2.6)
$$

Now, a perturbation method can be applied to this system. Each variable X is replaced by the sum of its steady state value $\bar{X}$ and its perturbation component δX (i.e. X becomes $\bar{X}+\delta X$) so that the averaged terms are simplified (they satisfy the steady state equations) and we are only left with the first order terms (of an equivalent Taylor expansion). The dynamic response of the passive and active

elements is now measured by the slope of their characteristic as in [1]. The final result is a first order linear differential system.

$$
\left|
\begin{array}{l}
\dfrac{d\delta\dot{m}_1}{dt} = \dfrac{A_1}{l_1}\left(\delta P_n - \delta P_1 - \left(\dfrac{K_1 \dot{m}_1}{\rho A_1^2}\right)\delta\dot{m}_1 \right) \\
\quad \vdots \\
\dfrac{d\delta\dot{m}_p}{dt} = \dfrac{A_p}{l_p}\left(\delta P_{p-1} - \delta P_p - \left(\dfrac{K_p \dot{m}_p}{\rho A_p^2}\right)\delta\dot{m}_p + \left(\dfrac{d\Delta P_{pump}}{d\dot{m}}\right)\delta\dot{m}_p \right) \\
\quad \vdots \\
\dfrac{d\delta\dot{m}_t}{dt} = \dfrac{A_t}{l_t}\left(\delta P_{t-1} - \delta P_t - \left(\dfrac{K_t \dot{m}_t}{\rho A_t^2}\right)\delta\dot{m}_t + \left(\dfrac{d\Delta P_{throttle}}{d\dot{m}}\right)\delta\dot{m}_t \right) \\
\quad \vdots \\
\dfrac{d\delta\dot{m}_n}{dt} = \dfrac{A_n}{l_n}\left(\delta P_{n-1} - \delta P_n - \left(\dfrac{K_n \dot{m}_n}{\rho A_n^2}\right)\delta\dot{m}_n \right) \\
\quad \vdots \\
\dfrac{d\delta P_1}{dt} = \dfrac{\gamma P_1}{\rho V_1}\left(\delta\dot{m}_1 - \delta\dot{m}_2\right) \\
\quad \vdots \\
\dfrac{d\delta P_n}{dt} = \dfrac{\gamma P_n}{\rho V_n}\left(\delta\dot{m}_n - \delta\dot{m}_1\right)
\end{array}
\right. \qquad (2.7)
$$

Since the expansion has been truncated at the first order, all the terms other than the perturbation terms are to be evaluated at the steady state operating point as defined on the characteristic. For the mass flow in particular, the flux is equated through all sections, as this is a condition for equilibrium:

$$\dot{m}_1 = \ldots = \dot{m}_i = \ldots = \dot{m}_n = \dot{m}_p$$

Note that the pressures P_i and the volumes V_i in the compliances do not correspond to the system at rest but to an operating equilibrium point.

II.1.2 Nondimensionalization

Before examining a concrete method of solving for this system, it is important to describe it with the parameters that are available. As written previously, it is dimensional, which means that the coupling of the loop itself and the pumping element(s) can be treated separately. The conventional non-dimensional parameters are relative to the pump's operational characteristics (speed, geometry, etc...) and are defined as follows:

- flow coefficient: $\Phi = \dfrac{\dot{m}}{\rho \pi D_2 b_2 U}$

- head coefficient: $\Psi = \dfrac{\Delta P}{\frac{1}{2} \rho U^2}$

Where: U is the impeller tip speed.
$\pi D_2 b_2$ is the impeller discharge area .

So:

$$\Delta P = \frac{1}{2} \Psi \rho U^2$$

$$\dot{m} = \rho \pi D_2 b_2 U \Phi$$

The pump slope will be:

$$\frac{d\Delta P}{d\dot{m}} = \frac{U}{2 \pi D_2 b_2} \cdot \left(\frac{d\psi}{d\phi} \right)_{pump} \qquad (2.8)$$

The value of $\left(\dfrac{d\psi}{d\phi} \right)_{pump}$ is known from the non-dimensional (Ψ, Φ) curve. This curve can be fitted with a variety of functions, the most popular being a third degree polynomial as it simulates the shape of the characteristic in both

forward and reverse flow. In the present study the data from [3] and [6] are used since they correspond to the development pump that will be scaled.

The throttle is modelled as a simple orifice (in the experiment a butterfly valve is used). Its characteristic can be considered parabolic:

$$\Delta P = K_t \, {}^1\!/_2 \, \rho V^2$$

$$\Delta P = K'_t \ . \text{ (dynamic head in the throttle duct)}$$

$$\Delta P = K'_t \frac{\dot{m}_2^{\,2}}{2 \rho A_t^2} \left(\Phi \frac{\dot{m}_2}{\dot{m}_1} \right)^2 \tag{2.9}$$

At the steady state operating point $\dot{m}_2 = \dot{m}_1$, and so the throttle slope as a function of the flow coefficient is:

$$\frac{d\Delta P_t}{d\dot{m}} = \frac{K'_t \dot{m}}{\rho A_t^2} = \frac{K_t \pi D_2 b_2 U}{A_t^2} \Phi \tag{2.10}$$

K_t is the unknown in this equation and, to calculate it, it is necessary to know the effective operating point of the system. This requires evaluating the shape of the global loop resistance curve (as seen by the pump). It will be parabolic because we are only considering losses that can be estimated linearly with respect to the dynamic head:

The losses in the piping amount to the sum of all the elementary losses experienced by each piping section:

$$\sum_{i=0}^{N} \Delta P_i = \sum_{i=0}^{N} \frac{K_i \rho \pi^2 D_2^2 b_2^2 U^2}{2 A_i^2} \Phi^2 \tag{2.11}$$

The expression is similar for the throttle:

$$\Delta P_t = \frac{K'_t \rho \pi^2 D_2^2 b_2^2 U^2}{2 A_t^2} \Phi^2 \qquad (2.12)$$

The losses are additive throughout the loop so the overall loop resistance curve can be expressed as follows:

$$\psi = \Phi^2 \left(\sum_i \frac{K_i \pi^2 D_2^2 b_2^2}{A_i^2} + K'_t \frac{\pi^2 D_2^2 b_2^2}{A_t^2} \right) \qquad (2.13)$$

The operating point corresponds to the intersection of the curve defined by equation (2.13) and the pump characteristic $\Psi_p(\Phi)$. If Φ_0 is the flow coefficient at this operating point, the equilibrium condition is:

$$\psi_p(\Phi_0) = \Phi_0^2 \left(\sum_i \frac{K_i \pi^2 D_2^2 b_2^2}{A_i^2} + K'_t \frac{\pi^2 D_2^2 b_2^2}{A_t^2} \right) \qquad (2.14)$$

And:

$$K'_t = A_t^2 \left(\frac{\psi_p(\Phi_0)}{(\Phi_0 \pi D_2 b_2)^2} - \sum_i \frac{K_i}{A_i^2} \right) \qquad (2.15)$$

Moreover, one can assume that most of the pressure drop takes place in the throttle itself (this hypothesis shall be validated further on), so:

$$\frac{K'_t}{A_t^2} \gg \sum_i \frac{K_i}{A_i^2} \qquad (2.16)$$

Applying this to (2.15):

$$K'_t = A_t^2 \left(\frac{\psi_p(\Phi_0)}{(\Phi_0 \pi D_2 b_2)^2} \right) \qquad (2.17)$$

By combining (2.7), (2.8), (2.10) and (2.17) the following formulation is derived:

$$-\frac{K_t \cdot \dot{m}_t}{\rho A_t^2} + \left(\frac{d(\Delta P_{throttle})}{d\dot{m}}\right) = -\frac{K_t}{A_t^2}(\pi D_2 b_2 U)\Phi_0 - \frac{2\psi_0}{\Phi_0}\frac{U}{2\pi D_2 b_2}$$

$$-\frac{K_p \cdot \dot{m}_p}{\rho A_p^2} + \left(\frac{d(\Delta P_{pump})}{d\dot{m}}\right) = -\frac{K_p}{A_p^2}(\pi D_2 b_2 U)\Phi_0 + \frac{U}{2\pi D_2 b_2}\left(\frac{d\psi}{d\Phi}\right)_{pump} \qquad (2.18)$$

These equations relate the terms in (2.5) which couple the loop with the active pumping element through the non-dimensional parameters that characterize it. The geometric data, the slope of the characteristic at the operating point and the operating point itself are all that is needed to determine the linearized response of the whole loop to a given combination of pumping elements. The relations would be the same if any more active elements were introduced, only one of them would be chosen as a reference (for the steady state mass flow), and the performance of the other elements would be related to it.

II.1.3 Validity of the hypotheses

In the dimensioning process, it was assumed that the pressure drop took place mainly in the throttle:

$$\frac{K'_t}{A_t^2} \gg \sum_i \frac{K_i}{A_i^2}$$

Typically, for the type of system considered, the total losses in the piping do not exceed four or five dynamic heads (the pipes are large and the flows medium: average velocities are on the order of 1 m/s). Moreover the reference areas are all of the same order and the denominators can be simplified. There is only K_t left to evaluate.

Realistic values for the operating point coordinates can be taken as:

$$\Phi_0 = 5\ 10^{-2}$$
$$\Psi_0 = 5.5\ 10^{-1}$$

The corresponding throttle curve will be:

$$\Psi = 220 \cdot \Phi^2$$

And the pressure drop across the throttle is:

$$\Delta P_t = \frac{\Psi_0}{\Phi_0^2} \frac{\dot{m}^2}{2 \rho \pi^2 D_2^2 b_2^2}$$

This can also be written:

$$\Delta P_t = \frac{\Psi_0}{\Phi_0^2} \frac{\left(\rho A_t^2 V\right)^2}{2 \rho \pi^2 D_2^2 b_2^2} = \frac{1}{2} K'_t \rho V^2$$

And finally:

$$K'_t = \frac{\Psi_0 A_t^2}{\Phi_0^2 \pi^2 D_2^2 b_2^2}$$

Numerically (for the derivation of the geometrical values D_2 & b_2 refer to chapter III):

$$A_t = 3.24\ 10^{-2}$$
$$D_2 = 0.609$$
$$b_2 = 1.27\ 10^{-2}$$

$$\boxed{K'_t = 4 \cdot 10^2}$$

K'_t is two orders of magnitude higher that K_i, so the approximation is quite valid. The major part of the pressure drop does take place in the throttle and for the *determination of the operating point* one can neglect the losses in the piping (even more so at low flows as velocities are reduced). However these losses have a damping effect on the perturbations that cannot be neglected. Indeed, the stability boundary is in a region where the pump slope is only very slightly positive (near the peak of the head curve) and even a small amount of damping can significantly alter the system behavior. So it is very important to properly estimate the pipe loss coefficients as these can alter the stability conditions for system 2.5.

II.2 Solution procedure and analysis

II.2.1 Numerical solution of the problem

The final objective is to extract the eigen values of the system (2.7). To do this a simple algorithm is developed in appendix D. All the parameters of the loop are specified by the user and the pump characteristic is input through a separate procedure that recreates the equations derived in (II.1.2). The calculation is conducted along the following steps:

-1- Choose an operating point on the curve for which the instability characteristics are to be determined (the whole curve is scanned over an operator defined interval, sequentially)

-2- Construct the differential system matrix using the dimensioning procedure described in section (II.1.2).

-3- Reduce it to an upper Hessenberg form.

-4- Extract the complex eigen values using a QR algorithm.

-5- Eliminate the physically unsatisfactory results.

-6- Calculate the reduced frequency, the B parameter and the instability parameter ξ for the various modes thus defined[1] .

-7- Reiterate on other flow coefficients to obtain the performance throughout the Ψ/Φ curve.

The output is arranged to give all the relevant information at each operating point along the characteristic: the natural frequency and damping in the dominant mode ($\Im(\lambda)$ and $\Re(\lambda)$), the B parameter and the instability parameter ξ. An example is given in appendix A and the point at which the system goes unstable (i.e. $\Re(\lambda)>0$ at Φ_{uns}) is highlighted. In this particular case instability inception takes place just below the peak of the characteristic. This confirms the information available from development tests (cf. figure 1.1). The slope of the

---

1 Note: For the definition of these parameters, refer to section II.2.2

characteristic only needs to be slightly positive to induce unstable operation of the system.

II.2.2 Analysis

The calculation described in the first part of this chapter enables one to establish the dynamic response of any given system. To determine a suitable configuration for the rig, one must first define the experimental goals in terms of the performance ranges resulting from the experimental variables to be controlled. A parametric study will then yield the behavior of the system relative to each individual variable.

II.2.2.1 Performance evaluation

In setting up the loop the main interest is to reproduce as exactly as possible both the *pump* and the *response of the system* on which the phenomena has been observed in a quantitative manner. This will be achieved by maximizing the number of non-dimensional parameters modelled and by inducing the instabilities at the same point on the characteristic.

The geometric scaling of the pump implies that the basic non-dimensional parameters are respected (cf. Chapter III) to ensure the similarity of the characteristic. The modelling of the system (exclusive of the pump) must rely on parameters that express the coupling between the system itself and the active element. The relevance of the B parameter has already been proven and investigated for surge in compressors where this coupling is dominant: [1], [2], [5] and [8]. The reduced frequency, on the other hand, is important to determine, if it exists, a relation between the instabilities and the geometry and performance of the impeller (i.e. rotating stall [8] and [27], wake effects [10], [11], [12] and [22], etc....).

These parameters, to be reproduced in the facility, are defined by[2]:

$$\omega_{red.} = \frac{\omega_{oscillations}}{\omega_{shaft}}$$

$$B = \frac{U}{2.\omega_{osc}L}$$

The performance envelope of the system must allow for substantial variations of these non-dimensional parameters. The design point of the system will reproduce the values of B and ω_{red} observed during development tests. The design should allow for the following intervals:

$$2\% < \omega_{red} < 20\%$$

$$0.05 < B < 0.5$$

Two other variables are significant in this problem. The unsteady flow coefficient Φ_{uns} (point at which the system becomes unstable on the characteristic) and the instability parameter ξ defined by:

$$\xi = B^2 . \left(\frac{\partial \Psi_{pump}}{\partial \Phi} \right) . \left(\frac{\partial \Psi_{throttle}}{\partial \Phi} \right)$$

The duplication of the flow coefficient at which instability inception takes place ensures the same damping is present in the experiment as in the original tests. For the open loops described in [1], [2] and [5], instability inception occurs

---

2 Note: Upon examination of the expressions below, it is obvious that at a given running speed the simultaneous knowledge of ω_{red} and B will automatically set the length L_p of the duct containing the pump. This is one of the constraints used in the definition of the system.

when $\xi = 1$. The behavior of ξ should therefore allow an assessment of the effect on the closed loop of the coupling between a finite main plenum with the rest of the system.

II.2.2.2 The system

The code developed is designed to support a system containing up to ten separate volumes of air. To limit unnecessary calculations, this study shall only comprise the case of two pressure volumes. As it turns out the simpler system satisfies the present modelling so from now on referrence will be made to the configuration described in figure 2.2.

The system adopted is analytically described by a first order linear differential system (i.e. equation 2.7) of four unknowns that is solved according to the first part of this chapter. A typical output from the numerical solver is shown at the end of appendix D. The whole characteristic is scanned, and for each value of Φ the corresponding complex eigen values are given (there are two modes as the system is of order 2)). The point at which the system becomes inherently unstable is pointed out and corresponds to a positive real part in the dominant eigenvalue. The second vibration mode is damped throughout the whole characteristic (it corresponds to the case in which the flows in the two ducts oscillate in opposite phase).

There are five experimental parameters that can vary independently: P_1, V_1, V_2, L_1 and L_2. The use of a standard 'baseline' is considered to simplify the study. It will be taken to be a configuration whose unsteady characteristics correspond to the original system (ω_{red}, B and instability inception). The marginal effect of each variable will be examined with respect to this baseline. The trends and range possibilities revealed in this way can then be exploited to calculate the performance envelope of the rig.

II.2.2.3 Parametric study

- Baseline

In the determination of the baseline various considerations must be taken into account:

- The main plenum volume should be as large as possible.
- The length of the pump leg is set .
- The length of the throttle leg is not relevant (as will be proved further along).
- The pressure in the main plenum cannot go below 0.4 Atm because of the hydrostatic head due to the physical location of the rig (for more details refer to section III.2).

The following configuration is adopted[3]:

Volume:	-main plenum: 750 liters.
	-small plenum: 300 liters.
Pressure:	-main plenum: 0.75 Atm.
	-small plenum: 1.65 Atm.
Length:	-Pump leg: 10.25 m.
	-Throttle leg: 3 m.
Pump:	-Rotor tip speed: 13.5 m/s.

- Effect of the main plenum volume (V_2)

The value of V_2 is varied from 200 to 1000 liters. The plots of reduced frequency, B parameter and Φ_{uns} are shown on figure 2.3.

---

3 Note: These values represent only one possibility that yields the desired non-dimensional parameters. A certain amount of subjectivity has been employed in it's determination and the constraint of physical location has influenced a few choices (i.e. the positioning of the two plenums on the same level).

The reduced frequency decays logarithmically when V_2 increases. This is due to the fact that once the main air volume becomes large with respect to the smaller one, it 'uncouples' the system and its marginal effect on the response decreases. This is a desirable feature as one would like to control the frequency with as few variables as possible. V_2 can be maintained constant at its original value without restricting the performance of the rig and simplicity is gained in the control of the response.

- Effect of the small plenum volume

In this case V_1 was scanned from 1000 liters to a very small value: 5 liters. This large range is justified by the fact that this is one of the driving variables for the system: The curves in figure 2.4 confirm this fact.

It appears clearly that the best range is from 0 to about 500 liters. By going to very small volumes one can reach the upper limits of the desired frequency range (the limit being no compliance between the pump and the throttle; which is equivalent to having a close coupled valve).

There is another effect that becomes apparent at very low volumes: The displacement of the instability onset. When the B parameter drops, the point at which the system goes unstable (i.e when the real part of the eigen value turns positive) appears at a lower flow coefficient. The system is stabilized. The same effect is described in [1], [2] and [5] and corresponds to having less compliance between the pump and the throttle. The limit represents a close coupled throttle configuration which, in the case of an incompressible fluid, will completely stabilize the system.

The instability parameter ξ does not predict the onset of unstable behavior in the same way as for an open loop (it is generally around 0.3 at instability onset and definitely below 1). One must assume that the effects due to the existence of

two separate modes modify the energy input to the oscillations (which is phase related) and advances the onset of instability. The system is not completely 'uncoupled' as far as the two plenums are concerned (the compliance of the main air bag is not really infinite) and the simple instability criterion used for first order systems is no longer valid.

- Effect of the overall pressure (defined through P_1)

The effect of varying the pressure of the two air bags is reflected in figure 2.5. These graphs show that the reduced frequency can be substantially lowered by decreasing the pressure in the air bags. Nevertheless, one must bear in mind that the system is limited by a minimum pressure which is simply the hydrostatic height of water (approximately 0.4 atm.) in the inlet section to the pump (cf. III.1.2.3).

- Effect of the pump duct length

The object here is to determine the optimal length of the ducting containing the test section. *A priori* it will be an operating constant but one can conceive of diverse systems to vary it in a discrete manner. As discussed before the baseline value is set, so this is simply a study of possibilities. The results are shown on figure 2.6.

It turns out that the effect is the same as by lowering the pressure, except that the B parameter varies with the same trend as the frequency. The amplitude of the variation is quite strong (50%), so, in conjunction with a decrease in pressure, this could be a way of broadening the range of the rig (notwithstanding the technical difficulties of implementing such a system)

- Effect of the throttle duct length

The plots are extremely simple (cf figure 2.7) and the effect of this variable is not discernable.

The explanation is straightforward and was used by Greitzer [1] to model open loop pumping systems. The pressure drop in the throttle is due essentially to the quasi-steady throttling characteristics of the device. The resistance is very large in comparison with the inertance terms and therefore the inertia of the fluid in the duct, which depends on the length of the duct, does not affect the behavior of the system.

II.2.2.3 Instability growth features

Another aspect of the problem is the variation of the instability parameters (frequency and damping) as the operating point moves along the characteristic. Their variation must be considered if one intends to use the dynamic characterization of the system to actively control the instabilities..

Figure 2.8 illustrates the variations of frequency and damping coefficients for the harmonic solution to system 2.7. The instability inception point is described when the damping coefficient becomes positive. This point also corresponds to the maximum of the frequency. Waves in the negatively sloped region of the characteristic are strongly damped and have a frequency below the Helmoltz frequency of the system (this will be confirmed in the first part of Chapter IV). At flow rates below Φ_{uns} the frequency also decays but, depending on the system B parameter, nonlinear effects become dominant and this analysis is no longer valid. One should note here that this decrease in frequency is not the same as the one associated with an increase in B (as described in IV.1). It occurs at fixed system parameters and reflects the trend towards static instability when $\omega \rightarrow 0$. Moreover, the condition for static instability cannot be reached simply because the dynamically unstable state will occur long before, as illustrated on the figure.

Another notable feature is the change in the slope of the damping when conditions change from static to dynamic, in other words when $Im(\lambda) \neq 0$. The dynamic characteristics of the system change as the divergence or the convergence become purely exponential instead of oscillatory. Finally, one can note the trend of the instability parameter ξ. It is actually very steep near Φ_{uns} so it is difficult to say how much different things are in this case from an open system where $\xi=1$ at Φ_{uns} ([1], [2] and [5]).

II.2.3 Conclusions and loop dimensioning

The parametric study has highlighted the dominant variables in the system and defined the ranges that should be encompassed by the design of the loop. However, it is important to realize that some of these characteristics have been set by practical considerations (cost, space, etc...). What is important is that the original goals have been satisfied. The following variables will be used to control the system:

-Small plenum volume.
-Air bag pressure.
-Pump duct length.

The proposed ranges are the following:

-Volume: from 5 to 500 liters.
-Pressure: from 0.4 to 1 Atm.
-Length of the pump duct: initially 10.25 m and eventually 20 m.

It should be noted that, in the case of the longer pump leg, the B parameter will not be scaled correctly. This will only be done if a very low reduced frequency is desired regardless of B.

The performance envelope of the rig can be summarized as follows:

- Maximum frequency/minimum B:
  - $-P_1$=0.75 atm.
  - $-V_1$=10 l
  - $-L_1$=10.25 m.

  $-\omega_{red}$ = 25%
  -B = 0.058

- Minimum frequency/maximum B (initial length):
  - $-P_1$=0.4 Atm.
  - $-V_1$=500 l.
  - $-L_1$=10.25 m.

  $-\omega_{red}$ = 3.5%
  -B = 0.40

- Minimum frequency/maximum B (extra length):
  - $-P_1$=0.4 Atm.
  - $-V_1$=500 l.
  - $-L_1$=20 m.

  $-\omega_{red}$ = 2.5%
  -B = 0.3

It turns out that the extra length is necessary to reach values of ω_{red} below 3%. The system must be forced into a very low frequency that requires large volumes, low pressures and large inertias (i.e. long lengths).

For the sake of simplicity the design will be conducted without the possibility of adding an extra length to the pump duct. The final decision concerning its implementation can be deferred for the moment, as the range obtained without it is still satisfactory.

In concluding this study it should be reemphasized that the major components of the loop have been satisfactorily dimensioned. Although many details will be defined with respect to other considerations, such as space and experimental procedure, the overall performance (in terms of unstable operation) will be guaranteed by the guidelines established. Moreover, the code makes it possible to predict the linear system behavior at any operating condition, if the experimental results prove that the type of instability encountered has been effectively modelled. Finally, it should be mentioned that the numerical code developed here could easily be modified to include other effects that might become apparent or desirable at a later stage in the experimentation (for example a more realistic model of the pump or active oscillators).

CHAPTER III

Description of facility design

III.1 Test section

One of the most important elements in the design of the whole rig is the test section, or model pump. This section provides a review of the main guidelines followed during this process. They are based on the following objectives:

- Modelling the original characteristics to ensure geometric similarity and equivalent performance.
- Maximizing the dimensions of the model to facilitate the integration of internal instrumentation.
- Maximizing the amount of transparent material to provide maximum optical access for measurements involving LDV and light sheet techniques.
- Ensuring that as many options as possible have been left open, including possibilities such as dynamic loads due to radial and axial offsets.
- Ensuring a modular build that will facilitate the modification of each component (impeller, volute, diffuser). This is necessary to study the impact of individual modifications on the performance.
- Respecting the usual budget and laboratory space limitations.

III.1.1 Scaling

The main scaling parameter for centrifugal pumps is the specific speed N_S, defined as:

$$N_s = \frac{\Omega \sqrt{Q}}{\sqrt[4]{gH^3}} = \frac{2\sqrt{\pi \frac{b_2}{D_2} \Phi}}{\sqrt[4]{\Psi^3}} \qquad (3.1)$$

A dimensional form is more commonly used, and is more directly related to the operating characteristics of the pump:

$$N_s = \frac{N.\sqrt{Q}}{\sqrt[4]{H^3}} \qquad \left(\frac{rpm.\sqrt{gpm}}{ft^{0.75}}\right) \tag{3.2}$$

It has long been established ([22], [23], [24], [30]) that the duplication of this parameter enables one to scale the dimensions and obtain the same non-dimensional characteristic (Ψ,Φ) curve, as long as geometric similarity is achieved. The specific speed as a type number is constant for all similar pumps and does not change with speed for the same pump. It is a criterion for similarity of centrifugal pumps in the same way that Reynolds number is a criterion for pipe flow (Figure 3.1 shows various impeller shapes and their corresponding specific speeds): This represents the basis for the scaling of all the 'hydraulic' dimensions in the model.

Now, the principle above dictates two relations involving four variables: the head H, the flow Q, the rotational speed N and the impeller diameter D_2 which serves as a geometrical reference for the model. Two of them must therefore be determined arbitrarily according to the priorities of the design. In this case the desire for internal instrumentation and extensive flow visualization (as well as the desire for a relatively low speed) suggest increasing D_2. A compromise between this objective and cost-practicality considerations results in D_2=61cm (2 ft). The head H can then selected to yield a reasonable volute backplate thickness. This is due to the fact that this plate must sustain the whole static pressure rise of the impeller and is therefore the limiting structure in the test pump. On the other hand, excessive thicknesses must be avoided in view of the Laser measurements which are sensitive to refraction and diffraction in the Plexiglass. After some iterations, H is set at 9.14m (30 ft) which corresponds to a thickness of 2.5 cm (1").

The similarity relations can be expressed as follows:

$$f = \frac{N_o}{N}\left(\frac{H}{H_o}\right)^{1/2} \tag{3.3}$$

$$f^3 = \frac{N_o}{N}\frac{Q}{Q_o} \tag{3.4}$$

$$f = \frac{D_{2_o}}{D_2} \tag{3.5}$$

Once the values of H and D_2 are known (H=30 ft and D_2=24"), 3.2, 3.3 and 3.4 determine N and Q. A summary of the pump performance thus derived is included in Figure 3.3.

Various other design constants are used in the calculation of the geometrical characteristics of the pump. The detail of their derivation can be found in [23]. Only a summary is included here:

- Speed constant:

$$K_u = \frac{U}{\sqrt{2gH}} \tag{3.6}$$

- Capacity constant:

$$K_{m2} = \frac{c_{m2}}{\sqrt{2gH}} \tag{3.7}$$

- Eye velocity constant:

$$K_{m1} = \frac{c_{m1}}{\sqrt{2gH}} \tag{3.8}$$

A plot of these constants as functions of the ratio of impeller eye diameter to impeller discharge diameter and specific speed is given in Figure 3.2. It is important to note that K_u also depends on the number of vanes and therefore on the blade loading, but this effect shall not be discussed here as an existing design is being scaled.

These constants can be related to the head and flow coefficients at BEP in the following manner:

$$\Psi = \frac{1}{2.K_u^2} \tag{3.9}$$

$$\Phi = \frac{c_{m2}}{U} = \frac{K_{m2}}{K_u} \tag{3.10}$$

The combination of expressions (3.1) through (3.8) enables one to derive all the important geometric and operating parameters relevant to the model (D_1, D_2, B_2, etc...). These are summarized in Figure 3.3.

The Reynolds number R_e and the cavitation number σ are also important non-dimensional numbers affecting the design. They control the ability of the rig to simulate transition and cavitation phenomena in the test pump. They are defined as follows:

$$R_e = \frac{U_{tip} D_2}{\nu} \tag{3.11}$$

$$\sigma = \frac{P_i - P_v}{\frac{1}{2} \rho U_{tip}^2} \tag{3.12}$$

Where:

- U_{tip}: Impeller tip speed.
- D: Impeller diameter.
- ν: Kinematic viscosity of the working fluid.
- P_i: Inlet static pressure.
- P_v: Fluid vapor pressure.

The performance summary in Figure 3.3 shows a comparison of the original values with those obtained in the case of this study. The R_e matching is satisfactory and the operating ranges in both the original pump and the model

are beyond the transition Reynolds number. For σ it is more difficult to obtain a good similitude. However, this is not a major problem as the inlet static pressure can be reduced, and the role of cavitation in the present study is only hypothetical. There is limited experimental evidence concerning its effect on the unsteady performance of the pump.

One can also determine the power and torque necessary to drive the model. The hydraulic power needed to raise the total head of the fluid by H is:

$$P = Q \rho g H \tag{3.13}$$

So, considering an overall efficiency η of about 60%, as was observed during development tests:

$$P = (Q \rho g H)/\eta \tag{3.14}$$

Numerically:

$$P = 6.7 \text{ kW (9 Hp).}$$

The shaft torque is defined by:

$$\Gamma = P/\omega_{shaft} \tag{3.15}$$

Numerically:

$$\Gamma = 125 \text{ N.m}$$

III.1.2 Mechanical design

Several considerations entered in the mechanical design of the test section components. Emphasis was put on satisfying the maximum number of constraints, but compromises were inevitable in some cases. This section presents a review of these considerations and compromises and a detailed description of the resulting design solutions.

III.1.2.1 Materials

One of the main constraints is, as pointed out before, the necessity for very good optical access to all the flow passages. Several transparent materials such as Plexiglass™, Lucite™ and Lexan™ have been considered. A comparison of their basic properties is shown in Figure 3.4. Plexiglass is the best choice because of its higher Young Modulus and flexural strength and because it has a smaller thermal expansion coefficient. Finally, its machining properties make it more attractive for components such as the impeller which require several delicate machining operations.

III.1.2.2 Stress evaluation

The major concern is for the dynamic load stresses on the rotating impeller. These are evaluated using methods developed in detail in references [4], [25] and [26] which shall not be repeated here. The results can be summarized as follows:

- Blade stresses:
  - Radial: $\sigma_t < 1.5\ 10^5$ Pa.
  - Tangential: $\sigma_t < 1\ 10^4$ Pa.
- Shroud stresses:

  $\sigma_{max} < 2\ 10^5$ Pa.
- Deflections:

  Based on the Young Modulus the maximum relative deflection encountered at nominal operating conditions is:

$$\varepsilon_{max} < 1.4\ 10^{-4}$$

Clearly stresses will not be a major problem for this rig. The only bearing they have had on the design is for the dimensioning of the backplate (cf. p: 49)

III.1.2.3 Component description and layout

The basic idea behind the configuration of the test section is a modular conception to facilitate geometrical modifications on individual components.

The impeller has and outer diameter of 61cm (2 ft) and an inlet diameter of 20 cm (8"). It consists of four full blades and four splitter blades with a backswept discharge. It is shrouded and the inlet tube serves as a wear ring for the sleeve seal (Figure 3.10). There is an inlet contraction with a half angle of 16º reproducing the geometry of the original HPU (High Pressure Unit).

There is no vaneless diffuser and the volute is of the rectangular type. Its circumferential profile is made up of four circular arcs and it is sandwiched between the back and front plates. The discharge area at the tongue is $5.8\ 10^{-3}\ m^2$ and the recirculating area is $1.68\ 10^{-3}\ m^2$.

The pipe diffuser is conical with a half angle of 4º. It has an area ratio of 25 and connects directly to the 8 inch (nominal diameter) pipe used to build the loop (cf. III.2). It is also constructed out of transparent material so that flow distortions could easlily be observed (cf. IV.2.3.3). It is connected to the volute by a seal-ring and a transition piece which ensure a smooth transition from the rectangular volute throat.

Figure 3.5 shows an overall view of the test section. The motor assembly is not on the drawing but is mounted vertically above the test section. It is connected to the shaft just above the slip-ring with a flexible drive coupling. A Lebow torquemeter is also included in this assembly. A 15 Hp, synchronous motor is used, in conjunction with a variable frequency controller. Care is taken to reduce mechanical vibrations by using elastomeric dampers under the stand and on the inlet and outlet pipes. A fairing is placed in the inlet pipe to eliminate perturbations arising form the geometry of the damper.

Figure 3.6 illustrates the details of the shaft and bearing arrangement. A double row Conrad bearing absorbs the radial loads and a matched pair of 15º. contact tandem bearings absorb the thrust loads (cf. Appendix A). The backplate seal is conceived to allow operation under eccentric conditions (cf. III.1.2.4). A system of three tie-rods (not shown in the figure) is used to stiffen the whole assembly and ensure concentricity of the impeller and the casing to within 15 μm when operated under worst case dynamic loads. These supports are anchored on the main supporting frame.

Figure 3.7 shows the detail of the seal behind the volute. The seal itself is a preloaded lip seal and the back shroud leakage flow can be controlled by three outlets in the seal housing. Any fluid escaping past the seal will be evacuated before it reaches the bearings. The reader can refer to Figure 3.8 to see the arrangement for the transition from volute to diffuser as well as the horizontal configuration and modularity of the components. This Figure also enables one to appreciate the extent of optical access that has been achieved. The hatched circle in the center represents the inaccessible area taken up by the transmission.

Finally Figure 3.9 gives an isometric view of the whole assembly. Details of the flow path and the sleeve seal are also shown in the isometric views on Figure 3.10.

III.1.2.4 Eccentric and offset operation

The decision to provide for small axial and radial offsets of the impeller position within the volute adds some complexity to the design of the rotor assembly, in particular to the hydrodynamic load estimations needed for rotor critical speed calculations. However, this feature will be very helpful in assessing the potential role of volute-impeller interaction forces. Indeed, these have been shown to have a destabilizing effect in some cases ([31], [32]). The axial offsets are implemented with variable thickness shims. The radial offsets on the other hand require that the bearing housing be contained in a triple eccentric sleeve

arrangement (Figure 3.10). Rotation of the inner sleeve (containing the housing) with reference to the outer one provides a means of continuously varying the amount of offset. The direction of offset can then be varied by rotating the outer sleeve within the main support sleeve. The stiffening rods mentioned above must be adjusted accordingly to maintain the verticality of the shaft assembly.

III.1.3 Operational analysis

The object of this section is to examine two of the most important operational parameters in the rig: the shaft critical speeds and the thrust loading.

III.1.3.1 Shaft critical

The simplest possible model in this case is that of an overhung impeller. It is as follows:

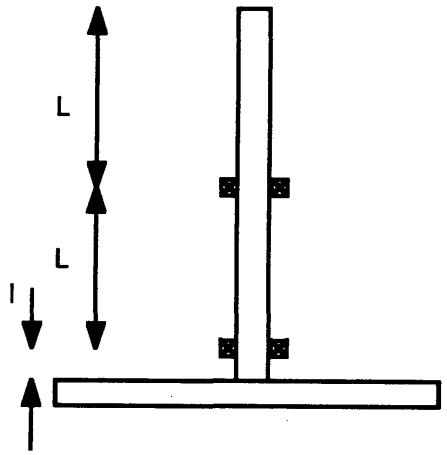

The corresponding data are:

- $g = 9.81\ m/s^2$.
- $\rho = 8\ 10^3\ Kg/m^3$.
- $R_2 = 0.0254$ m. • $R_1 = 0.0127$ m.
- $w = g\ \rho\ \pi\ (R_2^2 - R_1^2) = 120$ N/m.

- L =0.250 m. - l = 0.1 m.
- $E = 29.10^6$ lb/in^2 = 200 GPa = 2.10^{11} N/m^2.
- $I_s = \int_s r^2 ds = 2\pi \int_s r^3 d\theta\, dr = \frac{\pi}{2}\left(R_2^4 - R_1^4\right) = 6.129\,10^{-7}\ m^4$.

Dunkerley's formula is used to calculate the first critical:

$$\frac{1}{f_c^2} = \frac{1}{f_0^2} + \frac{1}{f_1^2} \tag{3.16}$$

Where:

f_c: Overall critical.

f_0: Shaft only critical.

f_1: Impeller only critical.

The shaft only critical is given by:

$$f_0 = c\sqrt{\frac{g\,EI}{w\,(2L)^4}} \tag{3.17}$$

The second mode of vibration for a hinged free configuration is used to model this situation(no bearing stiffness). Reference [26] gives the value for c:

$$\text{Hinged-free} \quad \Rightarrow c = 7.92$$

So

$$f_0 = 3.1 \text{ kHz.}$$

The impeller only critical is given by:

$$f_1 = \frac{1}{2\pi}\sqrt{\frac{3(L+l)\,g\,EI}{M\,L^2\,l^2}} \tag{3.18}$$

$$M = 100 \text{ N}$$

$$f_1 = 1.4 \text{ kHz.}$$

Finally:

$$\boxed{f_c = 1.27 \text{ kHz}}$$

This preliminary analysis does not consider the bearing stiffness (the hinged free assumption was made). A more complete calculation can be done using existing computational codes to calculate both the critical modes and their shapes. The results of this analysis are displayed on Figure 3.12 (critical frequencies) and on Figure 3.13 (mode shapes). It is clear from these that the operating range is well below any dangerous levels and that the preliminary estimation is in fact quite good (in the case of low bearing stiffness).

III.1.3.2 Thrust and radial loading

The details of the derivation are given in Appendix A. It should simply be mentioned here that the load directed in the downward direction was estimated to be under 6 KN (one thousand pounds). Radial loads are evaluated on the basis of a worst case approximation, i.e. when the rotor is running with an eccentricity of 1 cm. Given the characteristics of the bearings this implies a bearing life of:

- one million hours for the lower thrust bearings.
- half a million hours for the upper radial load bearings.

For all practical purposes the bearing life can be considered infinite and should not be a matter of concern in this rig.

III.2 Other loop components

The general loop construction is conducted with simple PVC (Polyvinyl Chloride) piping. It was chosen for ease of construction, availability and cost. Its compliance under the nominal operating conditions is minimal and Appendix B gives an estimation of the importance of this compliance relative to the plenum air bags.

The loop is configured over two floors as shown in Figure 3.14. The inlet pipe to the test section is 30 cm (12") in diameter and comes vertically up from the main plenum. The discharge pipe and the connection between the two plenums is 20 cm (8") in diameter and consists of a long straight portion after the diffuser and then a deaeration stack connected to a vacuum pump (cf. III.2.2). The throttling devices are located on the lower floor with the tanks and the transfer system.

III.2.1 Plenums

Chapter II detailed the analysis that led to the dimensioning of the gas volumes to be included in each one of the plenums. The object here is to achieve a simple yet efficient design of these tanks along the following guidelines:

- Best possible interaction between the air and the fluid to enhance the transfer of stored energy.
- The main plenum must have a large volume of fluid to uncouple the inlet from the discharge.
- The small plenum must contain as little fluid as possible in excess of the equivalent pipe volume to minimize momentum loss.
- Ease of modification and maintainability.

The idea behind the design is to use commercial automotive inner tubes as air bags. The main body of the fluid can then pass through the middle and the contact area is relatively high. Moreover these tubes are readily available at low

cost. A manifold and a regulator enable a precise control of the pressure inside these tubes. A pair of transducers serve as pickups for chamber pressure during operation.

In the small plenum these bags are centered around an eight inch inner diameter to ensure that there is a minimal loss of momentum relative to the inlet. The main plenum has a large 'dump' volume to dissipate the incoming perturbations and deliver a relatively smooth flow to the inlet pipe.

The configuration is described schematically in Figure 3.15. An exploded isometric view of this assembly presented in Figure 3.16 shows the positioning of the tubes inside the tank. A front flange is used to close off each tank and enhance access. The seal is achieved through a wide gasket that includes the bolt circle (40 durometer neoprene). Both tanks are rolled out of 5/8" thick 5083 Aluminum and corrosion is inhibited with Sodium Nitrite at a concentration of 1000-2000 ppm.

The final dimensions of the plenums are selected to fit given inner tube sizes while respecting the volumetric constraints dictated by the system performance requisites:

- Small plenum:
  - Max internal air volume: V_{air} = 500 liters.
  - Inner radius: R_i = 0.102 m.
  - Outer radius: R_o = 0.411 m.
  - Inlet: Ø 20 cm (8")
  - Outlet: Ø 20 cm (8")
  - Tube medium radius: R_t = 0.256 m.
  - Tube section diameter: D_t = 0.309 m.
  - Number of tubes: N_t = 3
  - Length: L = 1 m.
  - Approximate wall thickness: t = 4 mm.

- Main plenum:

Max internal air volume:	V_{air} = 1000 liters.
Inner radius:	R_i = 0.4 m.
Outer radius:	R_o = 0.644 m.
Inlet:	Ø 20 cm (8")
Outlet:	Ø 30 cm (12")
Tube medium radius:	R_t = 0.589 m.

Tube section diameter:	D_t = 0.244 m.
Number of tubes:	N_t = 5
Length:	L = 1.25 m.
Approximate wall thickness:	t = 4 mm.

- Maximum gauge pressures:
  - Burst: 2 Atm
  - Collapse: 0.4 Atm

III.2.3 Peripheral systems

III.2.3.1 Flow control devices

The main throttling system for the loop is composed of one 20cm (8") butterfly servovalve and one 2.5 cm (1") ball valve, also servo actuated, in a bypass configuration. They both have positioning systems that enable a prescribed voltage (2-5 Vdc for the large one and 1-6 Vdc for the small one) to be input with automatic position hunting that ensures a better repeatability.

III.2.3.2 Transfer & storage system

The transfer system is designed to contain the whole capacity of the loop so as to avoid losing all the deaerated, filtered (0.3 μm), and corrosion treated water each time the loop is opened.

For this a large polyethylene molded tank was installed with a two way pumping setup as described in Figure 3.17.

III.2.3.3 Deaeration system

The deaeration system adopted here was chosen for its simplicity and for its proven performance at the MIT Ocean Engineering Water Tunnel. It consists of a stack, located at the highest point of the loop, in which a partial vacuum can be pulled. The fluid is then circulated slowly allowing the air to rise up through the vertical section of 20 cm (8") piping and come out of solution at the interface. The stack can be totally closed off to avoid any accumulation of air that could act as a compliance. A sketch of the system is shown on Figure 3.18.

III.3 Instrumentation

The instrumentation reviewed here comprises only those instruments needed in the preliminary phase of the investigation . The objective in this phase is to obtain the steady and unsteady performance of the system and to determine whether the selected approach is suitable. For this reason, the main focus is on mass flow, pressure and total pressure measurements. Future instrumentation such as needed for LDV measurements and light sheet flow visualizations will not be addressed here. Simple flow visualization will provide qualitative understanding of the flowfield and will be part of this preliminary investigation. Also discussed later are the type and location of instruments needed for detailed pressure measurements to validate the results from the modelling presented in Chapter IV.

The following section describes the system instrumentation as illustrated on Figures 3.19. Figure 3.20 describes the location of the more detailed pressure instumentation necessary to the completion of the first phase measurements.

III.3.1 Flow and pressure instrumentation

For the initial investigation, only the variables relevant to a lumped parameter analysis of the system need to be considered :

• Mass flow: For measuring the flow rate, a hot film sensor is used because of its good response. Although very high unsteady frequencies are not expected, it is important to resolve the blade passing frequency (100 Hz) and some of its harmonics. The probe is a TSI model 1269W ruggedized side flow and it is located in the inlet pipe 90 cm below the impeller inlet to ensure a clean flow free of any swirl that could be induced by the impeller. The velocity profile in the duct will be assumed to be self-similar in unsteady operation (the time scale of the variations is quite large) and calibrations shall be conducted to verify this. The signal conditioning is provided by a TSI model 1050 Anemometer system.

• Pump pressure rise: Both the static and total pressure rise through the pump are measured at the inlet (before the contraction) and at the diffuser exit. The inlet static tap is located 30 cm below the impeller inlet and the exit static tap is located 15 cm downstream from the diffuser exit.

Static pressure: The probes used are Druck PDCR-820 silicon strain gauge bridge. The operating range is 0 to 50 psig with a full scale output of 100 mV at 10 Vdc excitation and they have a 0.1% repeatability. Signal conditioning and excitation voltage is provided by Division Instruments type 2310 Signal conditioner amplifiers.

Total pressure: The probes used are Kulite XTM-190 series miniature ruggedized pressure transducers with a piezoresistive strain gage bridge. The operating range is once again 0 to 50 psig with a full scale output of 75 mV at 10 Vdc excitation and the repeatability is 0.25% FSO (Full Scale Output). Signal conditioning and excitation voltage is provided by the same amplifiers as the static transducers. They are located at the same stations as the static taps.

• Plenum pressure: The pressure in each tank is measured with an Omega amplified voltage output, silicon diaphragm type transducer. They feature an operating range of 0 to 50 psig and a 1 to 6 Vdc output at 8 Vdc excitation. Repeatability is 0.25% FSO. Obviously these probes do not require any amplification and their output is fed directly into the A/D system. They are mounted on the air bag manifold on each plenum and also serve to calibrate the compliance in each plenum.

• Miscellaneous: Other static pressure measurements are taken on each plenum with analog indicators to ensure the tanks are within their correct operating limits. There is also an absolute pressure pickup in the deaeration stack to monitor the overall pressure level of the loop during the deaeration process

and during testing. Temperature is also measured in the plenums although fluid heating is not a major concern given the low power levels involved.

III.3.2 Data acquisition & processing

The data acquisition on this rig is controlled with a Macintosh II personal computer and Data Translation A/D card. A schematic of the whole setup is shown in Figure 3.21. The output from the two static, the two total and the hot film probes is fed, after signal conditioning, into a DT707 connection board and from there to the motherboard. The speed pickup on the shaft also goes directly into the system with a panel display in parallel.

The two throttles are controlled with the analog outputs in the board and can be operated from the panel with a potentiometer assembly.

The leakage flow through the back shroud is controlled with a small manual valve and has an analog pressure display.

The pressure in the air bags is controlled, as we said before, by a manifold and a regulator. The output from the two monitoring transducers is also input with the analog inputs to the A/D board.

The A/D board itself is a DT211-PGH Forerunner™ high level input range. It has 16 single ended (8 double ended) analog inputs, 16 digital I/O lines and 2 independent analog outputs (up to 5V). Maximum throughput is 20 kHz and acquisition time is 20 μs. There are four software programmable gains and onboard memory for up to 1024 data samples.

The acquisition software used is Labtech Notebook™ which offers wide real time data analysis possibilities, including Fourrier analysis and simultaneous display of data during sampling.

CHAPTER IV

Dynamic simulations and modelling

IV.1 Constant speed time resolved model

The calculations described in Chapter II essentially yield the linear performance of the system at a given operating point (in terms of frequency and damping factor). However, it is also important to compute the behavior of the system when the linear approximation is no longer valid. This is especially true when there is a need to evaluate transients (i.e. determine the final equilibrium state from given initial conditions) or deep surge phenomena for which non-linear effects are very strong and a good part of the characteristic is swept in a single oscillation.

Calculations such as this have already been completed for open loop compression systems (axial and centrifugal) [2] and [27], the most common method being a time stepped Euler or Runge-Kutta solver. In the present study a generic dynamic systems code is used to solve the non-dimensional equations.

IV.1.1 Assumptions and equations

The most consequential assumption made here is that of constant wheel speed. In [2], it is shown that for a compression system, where wheel inertia and compressibility effects are important, substantial variations in speed induced by changes in torque must be accounted for. In the present case case this is not necessary for the following reasons:

- Compressibility effects are negligible in the pump itself and will only appear if cavitation is present. This is confirmed by the fact that the

available experimental data shows no evidence of the 'barking' mode which characterizes surge dominated by wheel inertia effects ([2], [5]).

• The speed in the present rig is kept at constant values (constant speed drive). This is justified by the fact that, in aircraft fuel system applications, it is difficult to conceive of the whole high speed spool of a gas turbine following speed fluctuations induced by the pump. The power supplied to accessories is only a fraction of total 'spool' output.

Another important hypothesis is that throughout all operating regimes the pump itself (in the actuator disk approximation) stays on its steady state characteristic. This simplification has been extensively used before with good results.

Finally, all the assumptions made in the derivation of equations (2.4) are adopted here. For a detailed discussion of these and the resulting equations, refer to Chapter II.

The equations characterizing the system behavior are:

$$
\left|
\begin{aligned}
\frac{d\dot{m}_1}{dt} &= \frac{A_{1_{ref}}}{l_1}\left(P_2 - P_1 - \Delta P_1\right) \\
\frac{d\dot{m}_2}{dt} &= \frac{A_{2_{ref}}}{l_2}\left(P_1 - P_1 - \Delta P_2\right) \\
\frac{dP_1}{dt} &= \frac{\gamma P_1}{\rho V_1}\left(\dot{m}_1 - \dot{m}_2\right) \\
\frac{dP_2}{dt} &= \frac{\gamma P_2}{\rho V_2}\left(\dot{m}_2 - \dot{m}_1\right) \\
\frac{dV_1}{dt} &= \frac{V_1}{\gamma P_1}\frac{dP_1}{dt} \\
\frac{dV_2}{dt} &= \frac{V_2}{\gamma P_2}\frac{dP_2}{dt}
\end{aligned}
\right. \qquad (4.1)
$$

Substituting for results in the following dimensional system:

$$\left|\begin{array}{l} \dfrac{d\dot{m}_1}{dt} = \dfrac{A_1}{l_1}\left(P_2 - P_1 - \dfrac{K_1}{2}\dfrac{\dot{m}_1^2}{\rho A_1^2} + \Delta P'_{pump}\right) \\ \dfrac{d\dot{m}_2}{dt} = \dfrac{A_{2_{ref}}}{l_2}\left(P_1 - P_1 - \dfrac{(K_2+K_t)}{2}\dfrac{\dot{m}_2^2}{\rho A_2^2}\right) \\ \dfrac{dP_1}{dt} = \dfrac{\gamma P_1}{\rho V_1}\left(\dot{m}_1 - \dot{m}_2\right) \\ \dfrac{dP_2}{dt} = \dfrac{\gamma P_2}{\rho V_2}\left(\dot{m}_2 - \dot{m}_1\right) \\ \dfrac{dV_1}{dt} = \dfrac{V_1}{\gamma P_1}\dfrac{dP_1}{dt} \\ \dfrac{dV_2}{dt} = \dfrac{V_2}{\gamma P_2}\dfrac{dP_2}{dt} \end{array}\right. \qquad (4.2)$$

To rewrite this system in non-dimensional form, the following definitions shall be used:

Flow:

$$\Phi = \frac{\dot{m}_1}{\rho\,\pi\,D_2\,b_2\,U} \qquad \tilde{\dot{m}}_2 = \frac{\dot{m}_2}{\rho\,\pi\,D_2\,b_2\,U}$$

Pressure:

$$\tilde{P} = \frac{P}{\frac{1}{2}\rho U^2} \qquad \Psi = \frac{\Delta p_{pump}}{\frac{1}{2}\rho U^2}$$

Volume:

$$\tilde{V} = \frac{\omega V}{\pi D_2 b_2 U}$$

Area:

$$\chi_i = \frac{\pi D_2 b_2}{A_i}$$

Length:

$$\zeta = \frac{l_2}{l_1}$$

B parameter:

$$B = \frac{U}{2 \omega l_1}$$

Time:

$$\tilde{t} = \frac{\omega t}{2 \pi}$$

Substituting these expressions in (4.2) yields:

$$\left(\omega \rho D_2 b_2 U\right) \frac{d\Phi}{d\tilde{t}} = \rho U^2 \frac{A_1}{l_1}\left(\tilde{P}_1 - \tilde{P}_2 - \left(\frac{K_1}{A_1^2}\pi^2 D_2^2 b_2^2\right)\Phi^2 + \Psi\right)$$

$$\left(\omega \rho D_2 b_2 U\right) \frac{d\tilde{\dot{m}}_2}{d\tilde{t}} = \rho U^2 \frac{A_2}{l_2}\left(\tilde{P}_2 - \tilde{P}_1 - \left(\frac{(K_2+K_t)}{A_1^2}\pi^2 D_2^2 b_2^2\right)\tilde{\dot{m}}_2^2\right)$$

$$\frac{d\tilde{P}_1}{d\tilde{t}} = 2\pi\gamma \frac{\tilde{P}_1}{\tilde{V}_1}\left(\Phi - \tilde{\dot{m}}_2\right)$$

$$\frac{d\tilde{P}_2}{d\tilde{t}} = 2\pi\gamma \frac{\tilde{P}_2}{\tilde{V}_2}\left(\tilde{\dot{m}}_2 - \Phi\right)$$

$$\frac{d\tilde{V}_1}{d\tilde{t}} = \frac{\tilde{V}_1}{\gamma \tilde{P}_1}\frac{d\tilde{P}_1}{d\tilde{t}}$$

$$\frac{d\tilde{V}_2}{d\tilde{t}} = \frac{\tilde{V}_2}{\gamma \tilde{P}_2}\frac{d\tilde{P}_2}{d\tilde{t}} \qquad (4.3)$$

Which, after a little algebra, becomes:

$$
\left|
\begin{aligned}
\frac{d\Phi}{dt} &= \left(\frac{2B}{\chi_1}\right)\left(\tilde{P}_1 - \tilde{P}_2 - \left(K_1 \chi_1^2\right)\Phi^2 + \Psi(\Phi)\right) \\
\frac{d\dot{m}_2}{dt} &= \left(\frac{2B}{\chi_2 \zeta}\right)\left(\tilde{P}_2 - \tilde{P}_1 - \left((K_2+K_t)\chi_2^2\right)\dot{m}_2^{\,2}\right) \\
\frac{d\tilde{P}_1}{dt} &= 2\pi\gamma\frac{\tilde{P}_1}{\tilde{V}_1}\left(\Phi - \dot{m}_2\right) \\
\frac{d\tilde{P}_2}{dt} &= 2\pi\gamma\frac{\tilde{P}_2}{\tilde{V}_2}\left(\dot{m}_2 - \Phi\right) \\
\frac{d\tilde{V}_1}{dt} &= \frac{\tilde{V}_1}{\gamma\tilde{P}_1}\frac{d\tilde{P}_1}{dt} \\
\frac{d\tilde{V}_2}{dt} &= \frac{\tilde{V}_2}{\gamma\tilde{P}_2}\frac{d\tilde{P}_2}{dt}
\end{aligned}
\right. \qquad (4.4)
$$

IV.1.2 Transient response of the system

As stated earlier, one of the main objectives of this time-resolved simulation is to obtain the details of transients which can occur in the rig during startup and operation. These include phenomena such as pressure surges and water hammer that could be of a destructive nature). To do this one can specify variables such as U and K_t as functions of time (i.e. to simulate a ramp-up in pump speed) and observe the overall evolution of various parameters with time.

The tendency of the system to become unstable can also be examined, by waiting for initial startup transients to dissipate and then varying K_t, for example. This will simulate most of the real development tests during which the flow was decreased with the throttle. In all cases a (Ψ,Φ) curve similar in shape to

the original HPU characteristic is used. Operating and geometric parameters are taken from the scaled up model (U, D_2, B_2).

The first set of computations described above is illustrated in Figures 4.1 through 4.3. The instant startup corresponds to a case in which the speed and throttle are set to the selected point almost instantly. The pressure surges through the pump section, together with the mass flow, in the initial phase of the transient. The smooth procedure, which corresponds to a soft ramp, has much more desirable features, in terms of pressure and mass flow loads. It is interesting to note how the pressure rise through the pump is constantly increasing towards the final equilibrium which represents the stable operating point of the whole system.

The second analysis is based on the transient from a stable operating point on the characteristic to a lower flow coefficient. The final locations on the curve are noted A through D and are represented in Figure 4.4. Four different cases have been treated and only the flow coefficient Φ, the head coefficient Ψ and the overall non-dimensional pressure rise $\widetilde{P_1} - \widetilde{P_2}$, are examined. When the final operating point is on the negatively sloped side of the characteristic the system is heavily damped. There is no energy input to the perturbation and the oscillations decay exponentially (cf. Figure 4.5). When the final operating point is on the positively sloped portion, and not too far from the peak, the system is still damped. This happens at point B where the exponential decay is much weaker than at point C.

Interesting behavior is obtained when Φ is reduced below the critical flow coefficient for the given system (this 'minimal stable flow' can be calculated using the linear approach from Chapter II). The oscillations become unstable and diverge towards a limit cycle: surge. As is shown in IV.1.3, the character of this surge depends very strongly on the system characteristics and the two sets of data (Figures 4.7 & 4.8) show how the oscillations are similar (indeed the system is identical in both cases, only the operating point changes). The terms 'mild' and

'deep' surge are used here only to denote the existence or not of reverse flow throughout the cycle. By forcing the average operating point (or the point on the characteristic which would be the operating point if the system were stable) down to a lower flow coefficient the amplitude increases but not the overall character of the instability.

IV.1.3 B parameter dependence

From foregoing considerations, it appears that what determines the type of unstable behavior is not the operating point one tries to impose on the system but the overall system characteristics. It is therefore important to evaluate the influence of the B parameter and compare the results for this closed loop case with the open loop results in other compression systems [1], [2], [5], [27]. One can not only examine the time histories but also the phase plane portraits for the flow coefficient and the overall system pressure rise $(\tilde{P}_1 - \tilde{P}_2)$ which, when compared to the characteristic, provide a good indication of the system behavior.

The B parameter for each different case is evaluated with the algorithm described in Chapter II. The values of 0.1, 0.15, 0.27 and 0.7 are studied. Although B=0.7 is impossible to achieve with the present rig, it is given here as a reference for comparison with some results from [27]. Each run is initiated from the same stable operating point at equilibrium and the same perturbation step is applied (corresponding approximately to point C on Figure 4.4). Only for B=0.7, where the relaxation time for the system is very large, is the perturbation induced before reaching a stable operating point. This has no bearing on the results as the system goes directly into surge. The limit cycle is attained almost instantly, as described in [5].

B=0.1 corresponds to a stable case. There is not enough compliance in the system to promote unstable behavior. This confirms the trend illustrated by Figure 2.4 which shows the minimum stable flow coefficient decreasing with B. The plot of the characteristic shows $\tilde{P}_1 - \tilde{P}_2$ spiralling towards the equilibrium

point. However for B=0.15 the system is already in a surge configuration which could technically be called deep surge since the flow coefficient does become negative during the cycle. Note how two or three periods are necessary to reach the limit cycle and that the shape of $\widetilde{P_1} - \widetilde{P_2}$ is still not very far from that of a linear perturbation (quasi-circular).

For B=0.27 the perturbations are no longer linear. As the system compliance increases, so does its relaxation time. The period of the oscillations grows relative to the Helmoltz frequency. Non-linearity becomes more important and the limit cycle of $\widetilde{P_1} - \widetilde{P_2}$ tends to 'hug' the characteristic on its negatively sloped side and in the reverse flow region. Moreover, the limit cycle is attained in a short time compared to the period of the oscillations. Finally, for the extreme case, B=0.7, the response of the system is slow, with a period almost double that of the Helmoltz resonator. It is completely non-linear.

The phase plane portraits can now be examined. For clarity only those with a limit cycle have been represented in Figure 4.13. There is a definite transition from quasi-linear behavior (circular trace) to the interesting shape described in the case of B=0.7. In fact one recognizes the signature of a Van-der-Pol oscillator; which means that by forcing the flow in this configuration there is a possibility for inducing quasi-periodic behavior in the system. Furthermore, this shows an easy way of classifying surge cycles according to their type of behavior and to the extent of non-linearity present in them. Traditionally mild surge corresponds to small amplitude perturbations, which induce a quasi circular trace on the phase plane. Deep surge, on the other hand, is characterized by its high level of nonlinearity due to the massive blowdown of the pressure chambers (the plenums in the present case). This appears quite strikingly on the phase plane portrait and enables a direct recognition when amplitude considerations might might not be enough to characterize the type of surge. Finally the degree of instability of the system is illustrated by the number of cycles required for the limit cycle to be reached. As B increases the system goes into surge more and more quickly. For B=0.7 the system enters surge almost instantly.

IV.2 Volute/impeller interaction in the presence of shroud leakage flows.

One of the main problems in the design of centrifugal pumps is the prediction of their characteristic. This implies a good understanding of the flow properties not only at design point but also at off-design conditions. At design point the principle is simple: kinetic energy is input into the flow through the work of the centrifugal body forces in the impeller. The volute simply acts as a collector and the total pressure is then recovered in the diffuser (which can in fact be located before or after the volute). However, at off-design conditions there is a severe mismatch between the various components, velocity triangles are distorted and it becomes difficult if not unrealistic to try and determine any operating parameters without a detailed investigation of the flow.

The present approach is based upon the work of Lorett and Gopalakrishnan [13]. Assumptions will be made that enable one to determine impeller performance without going into the details of the flowfield. This implies that a proper design procedure has been conducted for the blading in order to provide a correct flow at design point(loading, velocity triangles, speed, etc...). The basis for the calculation is a 1-D discretization of the volute passage to which continuity and momentum are applied. The interaction of the volute with the impeller is evaluated in the form of a momentum equation for radial acceleration in the blade passage.

IV.2.1 Nomenclature and Assumptions

The following sketch illustrates the conventions that shall be used. A more detailed picture of the vector notations is on page 79:

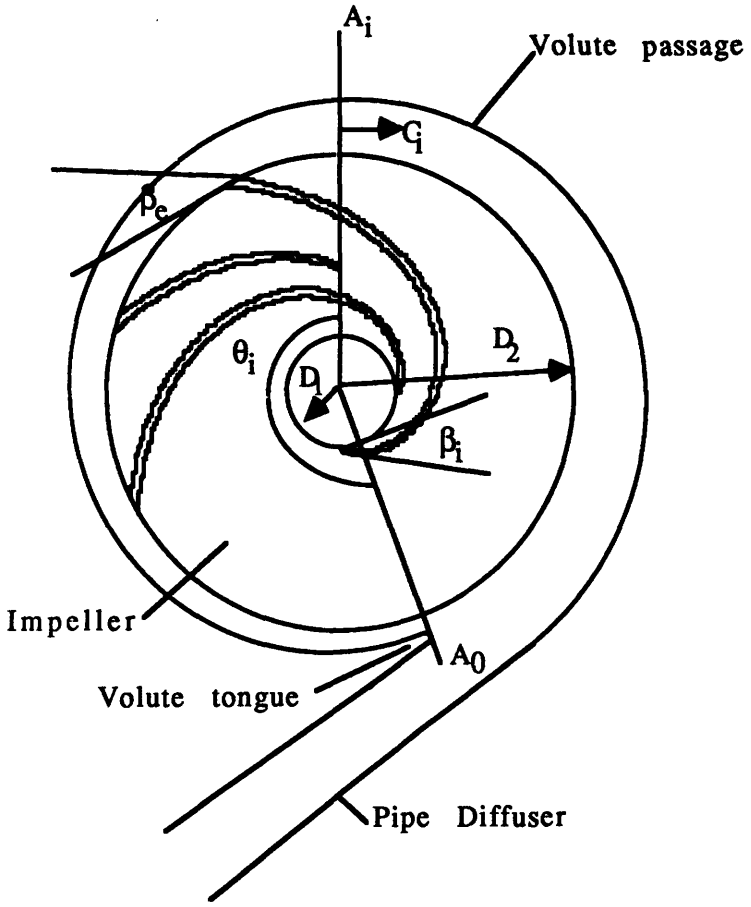

The main assumptions for this calculation are the following:

• There are no blade to blade variations of the impeller flow. It shall be treated as a two dimensional actuator disk (this is equivalent to an infinite solidity)

• The volute itself shall be considered thin. The radial variations in pressure and velocity are small. This is in contradiction with the conservation of angular momentum but the error thus committed is only of the order of 5% ($\Delta\Psi/\Psi \approx 5\%$).

• There is very good mixing in the volute. The momentum flux due to the incoming and departing flows is instantly transmitted to the main body of the

rotating fluid (a more detailed discussion of this argument shall be presented with the closure equations).

• The leakage flow rate is considered parabolic with respect to the volute static pressure (the leakage passages are treated as orifices). This implies that the meridional exit velocity of the fluid is:

$$C_{m1} = U\sqrt{\frac{\Psi}{k}}$$

An estimation of the loss coefficient k is given in Appendix C, together with some additional remarks concerning this simplification.

• The swirl at the beginning of the leakage path is the same as in the volute:

$$C_{u1} = C$$

• No inlet swirl is considered.

IV.2.2 Equations

The first step is to evaluate the impeller performance. The discharge velocity triangle is as follows:

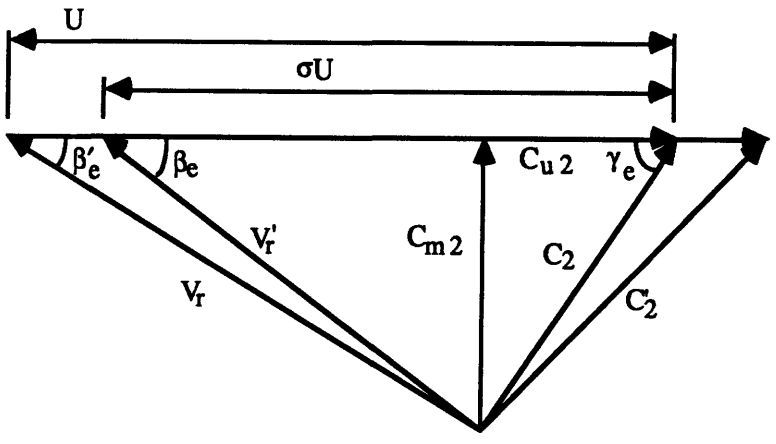

Where V'_r and C'_2 are the ideal (no slip) relative and absolute velocities and V_r and C_2 are the actual relative and absolute velocities. β_e is the blade discharge angle and β'_e is the flow discharge angle.

The following relations can be derived from this diagram:

$$C_2 = \sqrt{C_{m2}^2 + \left(\sigma U - \frac{C_{m2}}{\tan\beta_e}\right)^2} \tag{4.5}$$

$$C_{u2} = \sigma U - \frac{C_{m2}}{\tan\beta_e} \tag{4.6}$$

$$\beta'_e = \tan^{-1}\left(\frac{\sigma U - C_{u2}}{U - C_{u2}}\tan(\beta_e)\right) \qquad \gamma_e = \sin^{-1}\left(\frac{C_{m2}}{C_2}\right) \tag{4.7}$$

By definition:

$$C_{m2} = \Phi U$$

The slip factor σ is defined in this case as the ratio of the actual relative tangential discharge velocity to the ideal relative tangential discharge velocity.

The inlet velocity triangle is simpler, since no swirl is considered :

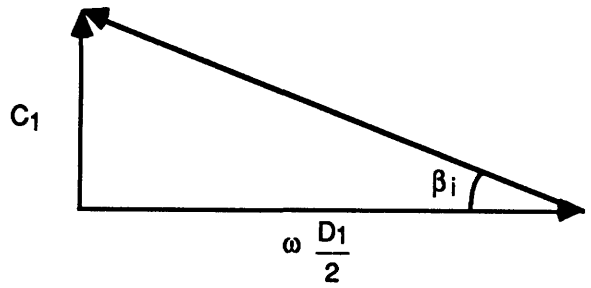

So:

$$C_1 = C_{m1} = \Phi.U.\chi_{im} \tag{4.8}$$

$$\chi_{im} = \frac{D_2 b_2}{D_1 b_1} \tag{4.9}$$

The absolute total pressure rise through the impeller can be written:

$$\Delta P_t = \Delta P_s + \frac{1}{2}\rho\left(C_2^2 - C_1^2\right) \tag{4.10}$$

Or:

$$\Delta P_t = \Delta P_s + \frac{1}{2}\rho\left(C_{m2}^2 + \left(\sigma U - \frac{C_{m2}}{\tan\beta_e}\right)^2 - C_1^2\right) \tag{4.11}$$

In terms of nondimensional coefficients:

$$\Psi_{tm} = \Psi_{sm} + \Phi^2\left(1 - \chi^2\right) + \left(\sigma - \frac{\Phi}{\tan\beta_e}\right)^2 \tag{4.12}$$

Thc Euler turbine equation can be expressed as follows:

$$C_{u2} = \sqrt{C_2^2 - C_{m2}^2} = \frac{\Psi_{tm} U}{2} \tag{4.13}$$

So combining (4.12) and (4.13):

$$\Psi_{sm} = \frac{2\sqrt{C_2^2 - C_{m2}^2}}{U} - \Phi^2\left(1 - \chi^2\right) - \left(\sigma - \frac{\Phi}{\tan\beta_e}\right)^2 \tag{4.14}$$

Or, considering (4.5):

$$\Psi_{sm} = \sigma^2 - \Phi^2\left(1 - \chi^2\right) - \frac{\Phi^2}{\tan^2\beta_e} \tag{4.15}$$

With, of course:

$$\Phi = \frac{C_{m2}}{U}$$

If one considers viscous losses in the impeller channel this expression becomes:

$$\Psi_{sm} = \sigma^2 - \Phi^2\left(1 - \chi^2\right) - \frac{\Phi^2}{\tan^2\beta_e} - \xi\left(\frac{C_{m2}}{\sin\beta_e}\right)^2 \tag{4.16}$$

The loss factor ξ depends on the geometry of the blade passage, the operating conditions and the working fluid. In this case, and for the sake of simplicity, it is taken to be constant over the whole range of Φ.

The second step is to consider the volute performance. To avoid confusion the flow coefficients in the volute will be lower case (φ) and the subscript i denotes the discrete element index.

The discretization applied to the volute consists of n equally spaced elements individually arranged as follows:

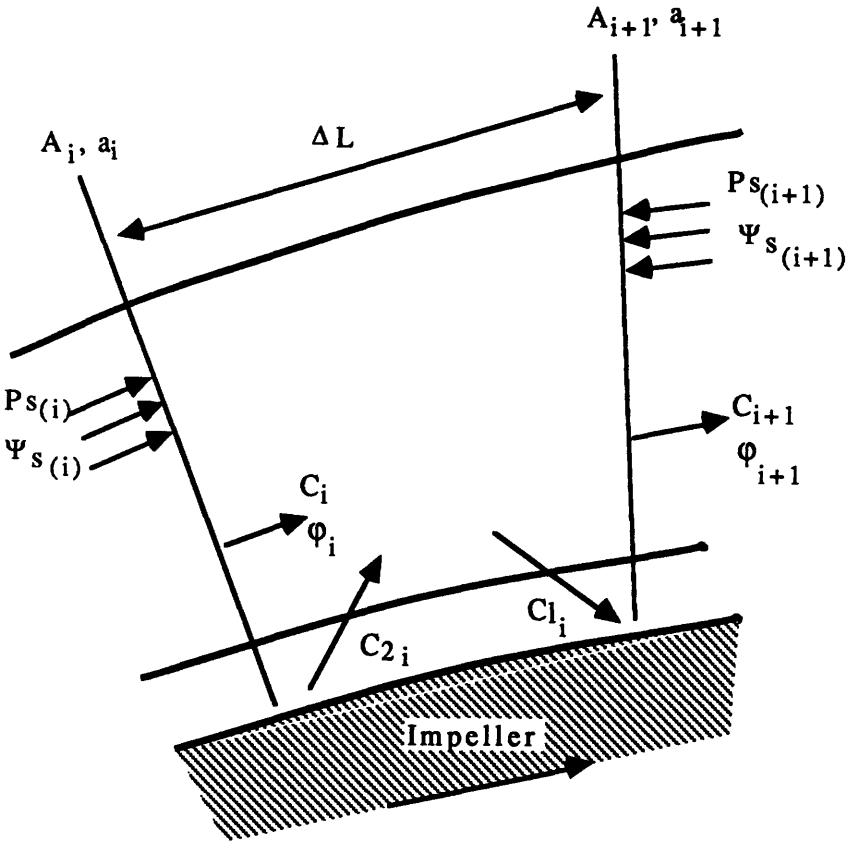

Continuity imposes that:

$$\varphi_{i+1} = \varphi_i + \frac{C_{m2i}}{n\,U} - \frac{C_{lmi}}{n\,U}\chi_1 \qquad (4.17)$$

As we assumed uniform conditions in a radial cross-section throughout the volute:

$$C_{i+1} = \frac{U.\varphi_{i+1}}{a_{i+1}} \tag{4.18}$$

Each element of the volute can be considered as a linear diffuser, and the elementary control volume is then modelled as follows:

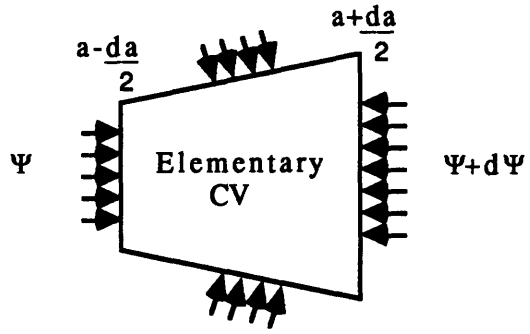

In nondimensional terms, the pressure forces on this element are:

$$\Sigma f = \Psi.(a-\frac{da}{2}) + \Psi.da - (\Psi+d\Psi).(a+\frac{da}{2}) = -a.d\Psi + o(d\Psi) \tag{4.19}$$

Given the discretization considered, this expression, combined with the momentum equation, becomes:

$$\frac{a_i + a_{i+1}}{2}\left(\Psi_{s(i+1)} - \Psi_{s(i)} + \Delta\Psi_{sf}\right) = -\frac{\text{Momentum flux in CV}}{\frac{1}{2}\rho\pi D_2 b_2 U^2} \tag{4.20}$$

where $\Delta\Psi_{sf}$ is the wall friction loss in the element:

$$\Delta\Psi_{sf} = \lambda\frac{\Delta L}{D_h}\left(\frac{C_i}{U}\right)^2 \tag{4.21}$$

λ is the friction coefficient and is dependent on the local Reynolds number and surface roughness. It is derived from the Moody diagram for pipe losses and in this case we shall approximate $\lambda(C_i)$ linearly. Initially, when we consider σ=1 in an ideal case, λ can be slightly overestimated to compensate for the momentum normally lost through σ.

Finally, the momentum equation for this element of volute can be written:

$$\Psi_{s(i+1)} = \Psi_{s(i)} - \Delta Y_{sf} + \frac{4}{a_i + a_{i+1}} \left(\varphi_i \frac{C_i}{U} - \varphi_{i+1} \frac{C_{i+1}}{U} + \frac{C_{mi} C_{u2i}}{n U^2} - \frac{C_{lmi} C_i}{n U^2} \right) \tag{4.22}$$

The most important effect of the interaction between the volute and the impeller is the acceleration or deceleration of the fluid in the blade passage. This depends on wether the volute static pressure is higher or lower that the static head of the impeller for the local discharge conditions. At this point it is important to assume that one can indeed consider a 'local' performance of the impeller (2-D actuator disk). The velocity in the passage has a magnitude:

$$V r_i = \frac{C_{m2i}}{\sin\beta_e} \tag{4.23}$$

Radial momentum in the blade passage is expressed by:

$$\frac{dVr_i}{dt} = \frac{U^2}{2.L_p} \left(\Psi_{sm(i)} - \Psi_{s(i)} \right) \tag{4.24}$$

The discretization of (4.24) yields the variation of meridional discharge velocity across the volute element.

$$\Delta C_{m2i} = \frac{\Delta t . \sin\beta_e . U^2}{2.L_p} \left(\Psi_{sm(i)} - \Psi_{s(i)} \right) \tag{4.25}$$

The final result is a system of equations that enables one to explicitly march through the volute and calculate the local operating conditions from an initial guess on C, C_{m2} and Ψ_s. It is now necessary to establish two closure equations that must be satisfied for those initial guesses to be considered valid. The first is trivial: the impeller meridional velocity must be continuous along the discharge and therefore:

$$C_{m2(n)} = C_{m2(0)} \tag{4.26}$$

The second is more involved and requires a some justification. The idea is to link C_n and C_0. But, due to the presence of the volute tongue and the variation of area from A_n to A_0, we must admit that there may be a numerical discontinuity in pressure and velocity. A momentum equation on a control volume including the tongue is not satisfactory: the assumption of radial uniformity in the passage breaks down because of the separation between the discharge and the recirculatory flows. Physically, there are potential effects of the tongue that will be felt several elements upstream and downstream and we can argue that, depending on the shape of the stagnation streamline, the flow pattern will act either as a diffuser or a contraction (cf. Figure 4.14). It therefore seems logical to use a formulation of total pressure conservation with a loss factor (which may in fact be variable with the flow regimes) that reflects the behavior of the flow that gets recirculated into the volute. In [31] a condition of total head conservation (without loss) was used with success. Losses will be considered here but their effect on the overall behavior shall be assessed (cf. IV.2.3.3). The condition is:

$$C_0 = U\sqrt{\frac{C_n^2}{U^2} + \left(\Psi_{sm(i)} - \Psi_{s(i)}\right).(1-\xi')} \qquad (4.27)$$

These two closure equations represent a convergence condition. Once we have calculated all the operating conditions we must verify the matching at the tongue and then reiterate until satisfactory convergence is achieved. The algorithm used is an underrelaxed steepest descent that evaluates the error over two successive iterations to ensure uniform convergence. The code is detailed in Appendix E, together with some convergence history diagrams.

Once this calculation is completed, a number of global operating parameters relative to the pump can be derived:

- Overall flow coefficient:

$$\Phi = \varphi_n - \varphi_0 \qquad (4.28)$$

- Leakage flow coefficient:

$$\Phi_l = \frac{\chi_1}{n} \sum_{i=1}^{n} \frac{C_{ml(i)}}{U} \tag{4.29}$$

- Volute exit total pressure coefficient:

$$\Psi_t = \Psi_{s(n)} + \frac{C_n^2}{U^2} \tag{4.30}$$

- Diffuser exit static pressure coefficient (overall pump head coefficient):

$$\Psi_t = \Psi_{sn} + C_p \frac{C_n^2}{U^2} \tag{4.31}$$

C_p is the pipe diffuser static pressure recovery factor at the given operating conditions. It is estimated based on the data in [25] and is initially assumed constant. The possibilities of its dependence on the flow regime shall be reviewed, together with an evaluation of the impact of such variations on the results.

- Overall hydraulic efficiency:

It can be written as the ratio of the total power input to the fluid by the pump to the power input to the fluid by the impeller. The overall power input to the fluid by the pump is:

$$P_o = \tfrac{1}{2} \pi D_2 b_2 \rho^2 U^3 g \, \Phi \Psi_{to} \tag{4.32}$$

The power input to the fluid by the impeller is:

$$P_i = \tfrac{1}{2} \pi D_2 b_2 \rho^2 U^3 g \sum_{j=1}^{n} \frac{C_{m2(j)}}{n\,U} \Psi_{t(j)} \tag{4.33}$$

Equation (4.13) gives:

$$\Psi_{t(j)} = 2 \frac{C_{u(j)}}{U} \tag{4.34}$$

So η can be written:

$$\eta = \eta_{imp} \frac{\sum_{j=1}^{n} \frac{C_{m2}}{nU} \frac{2\,C_{u(j)}}{U}}{\Phi\,\Psi_{to}} \tag{4.35}$$

In other words:

$$\eta = \eta_{imp} \frac{2}{n\,U^2\,\Phi\,\Psi_{to}} \cdot \sum_{j=1}^{n} C_{m2}\,C_{u(j)} \tag{4.36}$$

The prediction of η_{imp} requires a more detailed analysis of the flowfield inside the impeller. It must take into account the blade loading, secondary flow eddies, stall and separation, etc... In this case, it is simply approximated by a constant (η_{imp} =0.9) from [29].

Finally, it is important to note that the only input necessary for this model is the tongue static pressure coefficient $\Psi_{s(0)}$ and an initial guess on $C_{m2}(0)$ and C(0). Then, given geometry and impeller operating characteristics, one can derive the operating parameters of the pump. The determination of valid values for this tongue pressure coefficient is achieved by trial and error and, as it turns out, one value can yield more than one operating point. This requires fine tuning of the computational code to ensure convergence toward the solution nearest to the initial guess of boundary conditions $C_{m2}(0)$ and C(0) (and to avoid undamped oscillations between two equilibrium points of the numerical system).

IV.2.3 Results and discussion

It is obvious that there is a great deal of information that can be extracted from the method described above. Indeed, the main interest is not only focused on the prediction of the operating characteristics but also on the details of the flow

within the different components. The impact of the leakage flows on the performance must be determined and the distortion endured by the various elements at off-design conditions evaluated. To do this it is first necessary to examine the initial guesses or 'boundary conditions' that converge to a given operating point. All data will be referenced to the corresponding flow coefficient to facilitate interpretation.

IV.2.3.1 Boundary conditions

As stated above, it is $\Psi_s(0)$ that determines the overall operating point. Figure 4.15 describes $\Psi_s(0)$ as a function of the flow rate. One can observe that for $0.815 < \Psi_s(0) < 1$ there are two distinct possible flow coefficient that yield a solution to the equations. This does not mean the system is unstable because the overall flow rate is determined by the external throttling device. It is interesting to note that this induces a depressed region at low flow, just as is pointed out in [2]. The effect of leakage is minimal at very low flow rates as is illustrated in this Figure. However, there is a definite loss in pressure rise associated with this leakage at design conditions.

Figure 4.15 also includes the boundary conditions that satisfy the closure equations (4.26) and (4.27). The leakage flow has a noticeable effect on the impeller discharge velocity (at the tongue). This velocity is increased almost uniformly throughout the whole range of flows. The impeller must deliver more flow than necessary because of the loss through the shroud passages. It turns out the overall leakage flow (Φ_l) varies little with Φ (cf. IV.2.3.4).

IV.2.3.2 Circumferential profiles

Another interesting aspect of the problem is the circumferential distribution of the various parameters along the volute, especially at off-design conditions. Figures 4.16 through 4.19 illustrate these profiles and Figures 4.20 and 4.21 are three dimensional surface renderings of these quantities versus location

and flow rate. They are intended to give qualitative views only and will not be referenced directly. Moreover they do not give any information relative to the case with leakage flows.

The impeller discharge profiles show a very distinct effect of the leakage flows. The impeller delivers more flow in the presence of leakage and this extra flow is more or less uniformly distributed around the discharge. It is interesting to note, however, how the profiles become distorted at off-design conditions. At very low flows reverse flow can appear in the blade passage near the tongue region. This model does not take into account secondary flow patterns within the impeller channels which are due to blade-to-blade variations in pressure. At high flows the discharge velocity increases, creating a potential for high angles of attack on the tongue and therefore separated flow at the inlet to the pipe diffuser (cf. Figure 4.14).

The static pressure profiles present a more complex picture. At low flows there appears a depressed region near the tongue, but then everything tends to become uniform again near shutoff. This can be explained by the fact that, at very low flows, the volute appears as very large (i.e. infinitely large) collector with uniform pressure. At higher flows a negative gradient appears and the pressure decreases along the circumference. There is more flow than allowed by the cross-sectional area increase and the fluid is accelerated.

The volute tangential velocity profiles also show how the volute diffuses the flow below design point. One feature subject to discussion is the overall decrease in velocity as flow decreases. Indeed, one may argue that near shutoff the flow must be circulating at wheel speed in a solid body rotation and this would be true if the volute were symmetric and there was no skin friction. The fact is that, because at low flow C_{m2} is small, there is little tangential momentum injected into the volute. The losses due to friction and to the flow pattern in the tongue region (cf Figure 4.14) are enough to overcome this input and maintain a small

velocity. Moreover an increase in the slip factor σ probably contributes to this effect (less momentum is added to the volute flow).

IV.2.3.3 Overall performance

Another interesting aspect of this method is the prediction of the global performance of the pump. As stated earlier, the performance of the pipe diffuser was derived from [28] using the geometrical and operating characteristics (R_e, AR, Length, etc...). The pumping characteristics of the volute at various locations were derived from the data. These are summarized in Figure 4.22 and it is clear that the tongue is the area most affected by off-design distortions. Figure 4.23 illustrates the diffuser operating characteristics: inlet total and static pressure and discharge static pressure. It appears that this model indeed accounts for the loss of performance at lower flows and the negative slope in the characteristic. The impeller discharge absolute total pressure, whose profiles are represented on Figure 4.19 show a potential for much greater performance if the volute could be matched over a broader range of flows.

To evaluate the validity of this approach, a comparison to existing experimental data is presented in Figure 4.23. The qualitative agreement is good and the shape of the pressure rise curve is correctly predicted. There is, however, a discrepancy in the higher flow ranges. At low flow there is a high level of error on the experimental data because the development test system encountered unstable operation in that portion of the characteristic (this error is quantified on Figure 4.32). It is therefore prudent to review some of the assumptions made, and try to refine them.

In the initial approach the performance of the pipe diffuser has been assumed invariant. In reality, it clearly depends on the level of inlet distortion and therefore on the angle with which the flow impinges on the volute tongue (as in Figure 4.14). This angle of attack increases quite strongly with the overall flow rate and, to model the resulting decrease in diffuser performance, we can

simply assume a linear decay of C_p when the angle of attack increases beyond a given value (taken to be 4º for flat plate stall). These two trends are illustrated on Figure 4.24. The slope of the linear decay is chosen to best fit the experimental data. Therefore, this has but little value from the point of view of prediction until some more data are generated on this type of diffuser inlet distortion. Nevertheless the very good experimental fit obtained in this way (cf. Figure 4.23) seems to augur a simple verification of this feature. All the calculations described from now on will be conducted with this distribution of $C_p(\Phi)$.

Throughout the previous computations, the loss factor ξ' was taken to be a constant (ξ'=0.5) and this is not compatible with the physical interpretation given earlier. Indeed it depends on the shape of the stagnation streamline which in turn strongly depends on the flow regime (as illustrated in Figure 4.14) and on the angle of attack (illustrated in Figure 4.24). To determine the sensitivity of the model to this parameter ξ', the calculations are repeated for ξ'=0, 0.25, 0.75, 1 (including the variations of $C_p(\Phi)$ described earlier). The resulting characteristics are plotted in Figure 4.25 and it is obvious that the effect of ξ' is negligible. Only for ξ'=0 there is a noticeable deviation from the average when the flow coefficient increases beyond 0.07. A more detailed examination proves that the experimental fit is better for lower ξ' at low flows and higher ξ' at high flows. This confirms the qualitative explanation given in Figure 4.14.

The sensitivity to ξ' of the velocity and pressure profiles is illustrated in Figures 4.26, 4.27 and 4.28. The relative variations are small, confirming the non critical nature of the assumptions made to derive equation (4.27).

Finally, the effect of the slip factor σ can be assessed. Figure 4.30 illustrates the sensitivity of the calculation to variations of σ in the range of 0.75 to 1. In [2], σ was shown to exhibit a sharp decrease near shutoff for radial discharge compressors. In the present study, however, the picture is somewhat different as the geometry is backswept, so it is difficult to draw conclusive evidence as to what

the real behavior of σ is. Here again experimental evidence should clear the picture.

IV.2.3.4 Leakage flows and efficiency

In the previous section, it was shown that the effect of the leakage flows on the pressure rise of the pump is not very important. For the efficiency, however, this is not true. The power absorbed by the fluid recirculated through the labyrinth seal is considerable and therefore large variations in η are to be expected. However, this model does not take into account the losses due to secondary flow generated by blade-to-blade variations in pressure within the passages. Neither does it account for the losses induced at the impeller discharge by an eventual decrease in the slip factor σ (the loading increases if σ decreases and stall or separation may occur). This model will therefore not predict η correctly in areas where these phenomena are dominant.

Figure 4.30 illustrates the evaluation of η for $\xi'=0.5$ and $\sigma=1$. At low flows the losses due to the leakage are very important. If no leakage is assumed the limit of η as $\Phi \rightarrow 0$ is near 50% as opposed to 0% in the case of imperfect shroud sealing. At zero flow, power is still needed to drive the fluid through the seal. However, even in the case of no leakage, power is needed to drive the impeller at zero flow. This is due to recirculatory secondary flow patterns within the blade passages and other phenomena not modelled here.

Another effect of the leakage flows is the increase in Φ_{BEP} (Best Efficiency Point). This means that the pump will be run at lower design pressure rise than for an ideal case. When correlated to experimental data, the calculation including leakage yields a very good fit for the BEP.

To conclude this section we can examine the leakage flow rate as a function of overall flow rate. Figure 4.25 presents the plots Φ_l/Φ as a function of Φ/Φ_{des}

and a logarithmic scale showing that a simple correlation between leakage flows and overall flows can be written:

$$\frac{\Phi_l}{\Phi} = \alpha \cdot \left(\frac{\Phi}{\Phi_{des}}\right)^{-1} \tag{4.32}$$

Also, one last calculation is run considering all the parameters at values taken from literature or design data. It will provide an idea of the real value of this model to predict performance in a case where only the design operating conditions and the geometry are known. The results are plotted in Figure 4.32. Clearly, there is good agreement with the experimental data. The values of the various parameters are chosen as follows:

- $k = 1.5\ 10^4$ (from the derivation in Appendix C).
- $\sigma = 0.9$ (from Wiesner correlation)
- $\lambda = 0.02 - 0.005(Ln_{10}(R_e)-5)$ (linearization of the Moody diagram for pipe flow in the range of interest)
- $\xi = 0.5$ (Not a critical parameter (cf. Figure 4.25))

As proved by the results, this method yields some good performance predictions. With a simple inspection of the detailed flow, it enables one to show that the mechanism for inverting the slope of the characteristic at low flows is directly connected to the matching of the volute. Also the performance of the pipe diffuser appears to be quite important as it must endure some severe inlet distortions even when operating at design conditions. Finally the efficiency loss due to the leakage flows emphasizes the importance of the shroud seals. The validity of the method may be questioned very near shutoff, where certain assumptions probably break down, particularly so those concerning the operation of the impeller.

IV.2.3.5 Possible extensions of the model

One of the empirical assumptions in the model concerns the behavior of the pipe diffuser under various flow conditions. A more detailed modelling, based on flow visualization and measurements, would enable a more direct prediction of overall performance.

The one dimensional approach to the volute can be extended to two or even three dimensions. A more precise modelling of the mixing out of the impeller discharge momentum and of the flow pattern in the tongue region should then be possible. Also this method will eliminate the necessity for a numerical discontinuity at the tongue. A refined mesh will give enough insight into the flow geometry to fully determine the radial distribution of the parameters at the tongue location. This will enable one to determine the effect of geometrical modifications on the flow and understand the way they affect the performance.

Another important point is that this method only treats the case of a volute configuration. It can be extended to the case of a vaned or vaneless diffuser by applying conservation laws to each passage. Some modelling of the free vortex flow in the case of a vaneless diffuser and of the flow in the passage for a vaned diffuser will be necessary. One can also envision the necessity for wake modelling in the case of a vaned diffuser. Wake transport will then have to be taken into account.

CHAPTER V

Conclusions and recommendations

I.1 Conclusions

The design of an experimental facility for the investigation of unsteady flow in centrifugal turbopumps has been completed. All the design choices and performance requisites have been justified. Maximum flexibility from the experimental point of view has been kept in mind throughout the process.

The dimensioning of the loop is based on a linear calculation of the system behavior. This linear analysis also provides an estimation of the stability envelope and of the small perturbation growth parameters (frequency and damping).

The conception and design of the test section has been reviewed and the need for extensive internal flow measurements as well as qualitative and quantitative flow visualization has been stressed. The associated instrumentation has had a very strong bearing on most of the design choices (notably the fully transparent configuration and size adopted).

A time -resolved calculation of the system behavior has been conducted to determine a basis for comparisons with the experimental results. It shows that, with the selected geometry and system characteristics, all types of surge can be reproduced within the facility's performance envelope. The dependence of the phase plane portraits on the B parameter has also been evaluated.

Finally, a simple investigation of the volute flow in the presence of leakage flow has been initiated. It predicts the distribution of impeller discharge velocity,

volute tangential velocity, and volute pressure coefficients along the circumference of the volute. It also gives an estimation of the overall pump pressure rise. The efficiency of the pump is derived from this calculation and the results show that the shroud leakage flows are responsible for an important drop in efficiency throughout the flow range, more particularly at low flow rates.

The validity of this model is supported by good agreement with available experimental data. Observed discrepancies have been explained and various possibilities for extension and enhancement have been suggested.

I.2 Recommendations for future work

The work presented in this thesis is obviously only the first step in an extensive experimental and analytical investigation. At the time of this writing, rig construction has almost been completed and preliminary testing has begun. The initial results are encouraging and, although their extent is not large enough to draw any conclusions, they indicate that the design of the external rig is successful.

The experimental data that will be initially collected should be used to firmly validate the design procedure of the loop. Then, more detailed measurements should be aimed at validating the two simple models proposed here. Care should be taken with the volute model due to the fact that it assumes a discontinuity at the tongue that will not exist in reality.

The most interesting part of the experimentation will no doubt be the possibility to proceed, later on in the project, with a complete three-dimensional mapping of the flowfield inside the pump. This can be achieved using either the existing LDV system or a more sophisticated sheet laser to obtain photographic evidence of the flow phenomena. Whatever the outcome, this facility should provide some extremely valuable visual evidence on what has been until now a rather mysterious side of turbomachinery research.

References & Bibliography

[1] Greitzer E.M., "The stability of pumping systems. The 1980 Freeman Scholar Lecture". ASME Journal of Fluids Engineering, Vol. 103, June 1980.

[2] Fink D., "Surge dynamics and unsteady flow phenomena in centrifugal turbochargers". PhD Thesis, Department of Aeronautics and Astronautics, MIT, May 1988.

[3] Chheda N. R., "High speed centrifugal pump (27 GPM) performance and stability evaluation tests". Engineering Report #2217, Sundstrand Corporation, August 1983.

[4] Glessner J. W., "A method for analyzing the stresses in centrifugal impellers". ASME paper #54-A-167.

[5] Pinsley J.E., "Active control of centrifugal compressor surge". Master"s Thesis, Department of Aeronautics and Astronautics, MIT, October 1988.

[6] Tyler T., Westhoff P., Hermann P., Sundstrand corporation, Personal communications.

[7] Furst R. B., Burgess R. M., Gulbrandsen N. C., "Small Centrifugal Pumps for Low-Thrust Rockets". Journal of Propulsion, Vol. 3, No. 3, May-June 1987.

[8] Greitzer E. M., "Surge and Rotating Stall in Axial Flow Compressors". Engineering for Power, Vol. 98, No. 2, April 1976.

[9] Flueckiger G., Melling A., "Flow instability at the inlet of a centrifugal compressor". Journal of Engineering for Power, April 1981, Vol. 103.

[10] Krain H., "A study on centrifugal impeller and diffuser flow". ASME paper #81-GT-9.

[11] Yuasa T., Hinata T., "Fluctuating flow behind the impeller of centrifugal pump". Bulletin of the JSME, Vol. 22, N0. 174, December 1979.

[12] Mizuki S., Ariga I., Watanabe I., "A study of the flow mechanism within centrifugal impeller channels". ASME paper #75-GT-14.

[13] Lorett J. A., Gopalakrishnan S., "Interaction between impeller and volute of pumps at off design conditions". Transactions of the ASME, Vol. 108, March 1986.

[14] McNulty P. J., Pearsall I. S., "Cavitation Inception in Pumps". Journal of fluids engineering, March 1982, Vol. 104.

[15] Howard J. H. G., Mukker O. S., Naeem T., "Laser Doppler Measurements in a Radial Pump Impeller", ME Department, University of Waterloo, Ontario, Canada.

[16] Kannemans H., "Radial Pump Impeller Measurements Using a Laser Doppler Velocimeter". ASME paper #80-GT-94.

[17] Kannemans H., "Principles Of LDV measurements in Fully Transparent Pump". Paper #5.4, Fluid Mechanics Silver Jubilee Conference, November 1979.

[18] Howard J. H. G., Kittmer C. W., "Measured Passage Velocities in a Radial Impeller with Shrouded and Unshrouded Configurations". ASME paper #74-GT-66.

[19] Yadav R., Yahya S. M., "Flow Visualization Studies and the Effect of Tongue Area on the Performance of Volute Casings of Centrifugal Machines". Int. J. Mech. Sci. Vol. 22, pp. 651-660.

[20] Braisted D. M., "Cavitation induced Instabilities Associated with Turbomachines". Report #E184.2, California Institute of Technology, September 1979.

[21] Wislicenus G. F., "Preliminary Design of Turbopumps and Related Turbomachinery". NASA Reference publication #1170, October 1886.

[22] Eckardt D., "Detailed flow investigations within a high-speed centrifugal compressor impeller". ASME paper #76-FE-13.

[23] Stepanoff A. J., "Centrifugal and axial flow pumps". 2nd Edition. John Wiley & sons.

[24] Lobanoff V. S., Ross R. R., "Centrifugal pumps, Design and Applications". Gulf publishing co.

[25] Mattingley J. D, "Aircraft Engine Design". AIAA Education Series.

[26] Roark R. J., "Formulas for stress and strain".

[27] Greitzer E. M., "Surge and rotating stall in axial flow compressors. Part I and II". Engineering for power, Vol. 98, No. 2, April 1976.

[28] Runstadler P. W. Jr., Dolan F. X., Dean R. C. Jr., "Diffuser data book". Creare publication TN-186, May 1975.

[29] Japiske D., "Centrifugal compressor design and performance". Course held at Norwich, Vermont, October 1986.

[30] Sabersky R. H., Acosta A. J., Hauptmann E. G., "Fluid flow, A first course in fluid mechanics". 2nd Edition. Macmillan. pp. 391-470.

[31] Adkins D., "Analyses of hydrodynamic forces on centrifugal pump impellers". PhD Thesis, California institute of Technology, 1986.

[32] Jery B., "Experimental study of unsteady hydrodynamic forces on whirling centrifugal pump impellers". PhD Thesis, California institute of Technology, 1987.

FIGURES

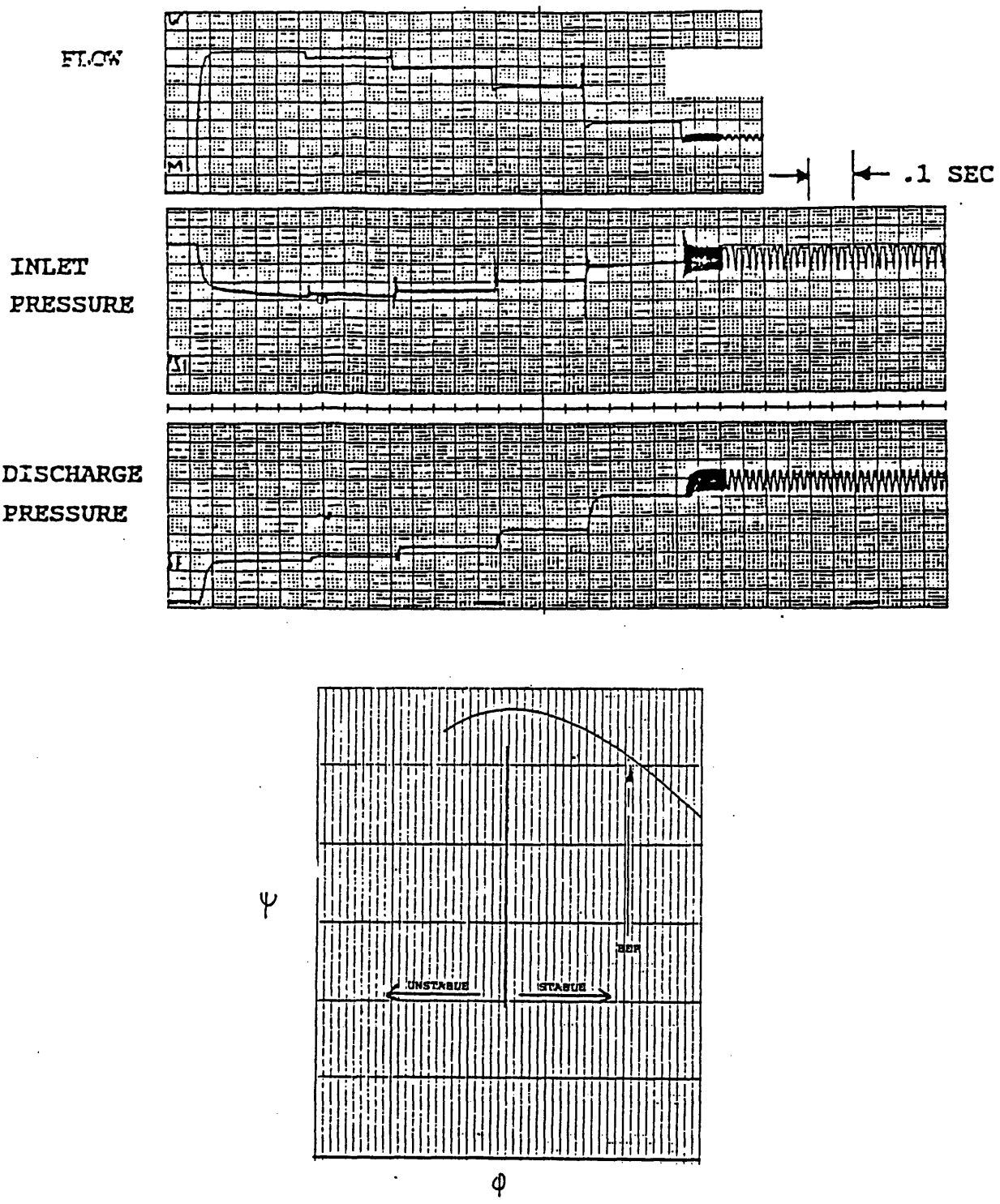

Figure 1.1: Typical unstable operation of low N_s pumps: Time traces and instability inception on the characteristic

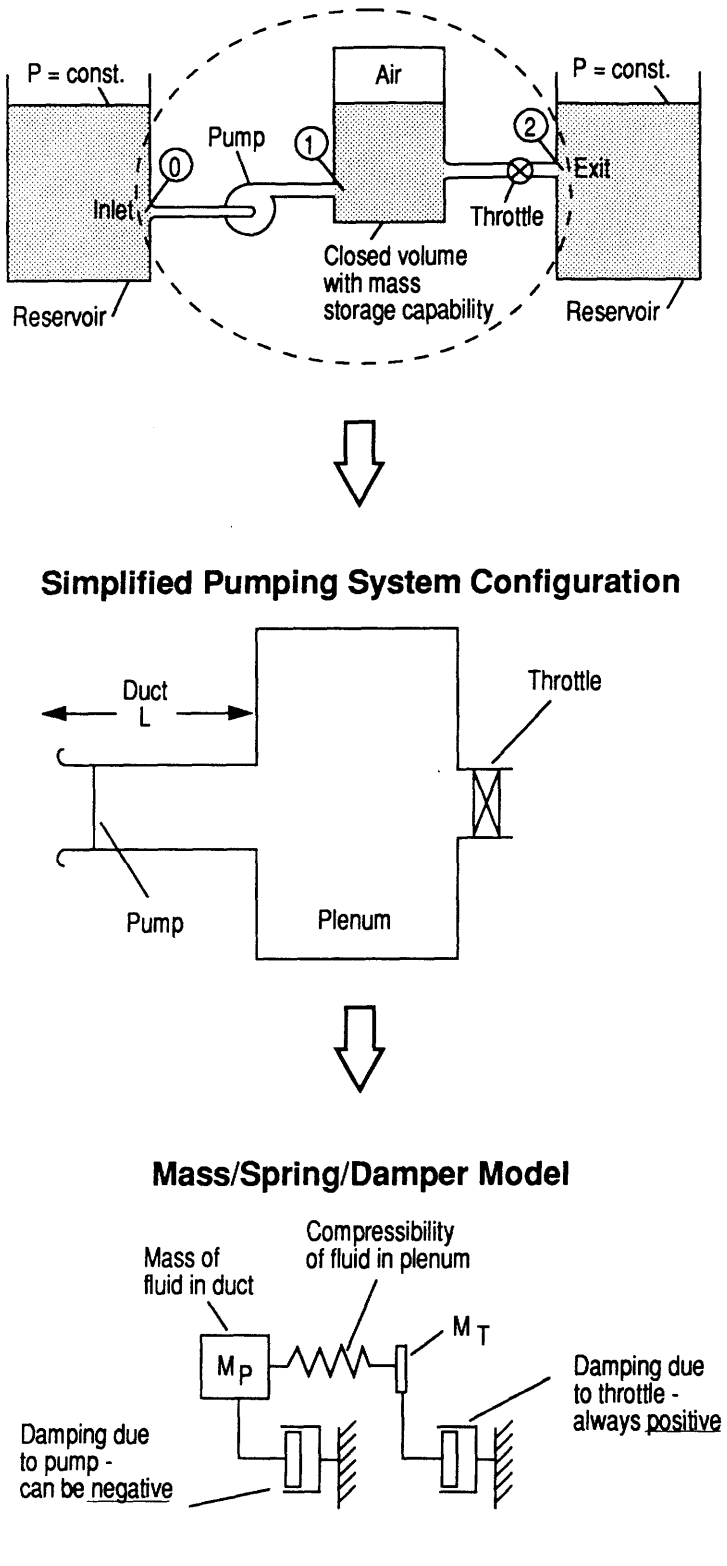

Figure 1.2: Basic pumping system and analogies (from [1]).

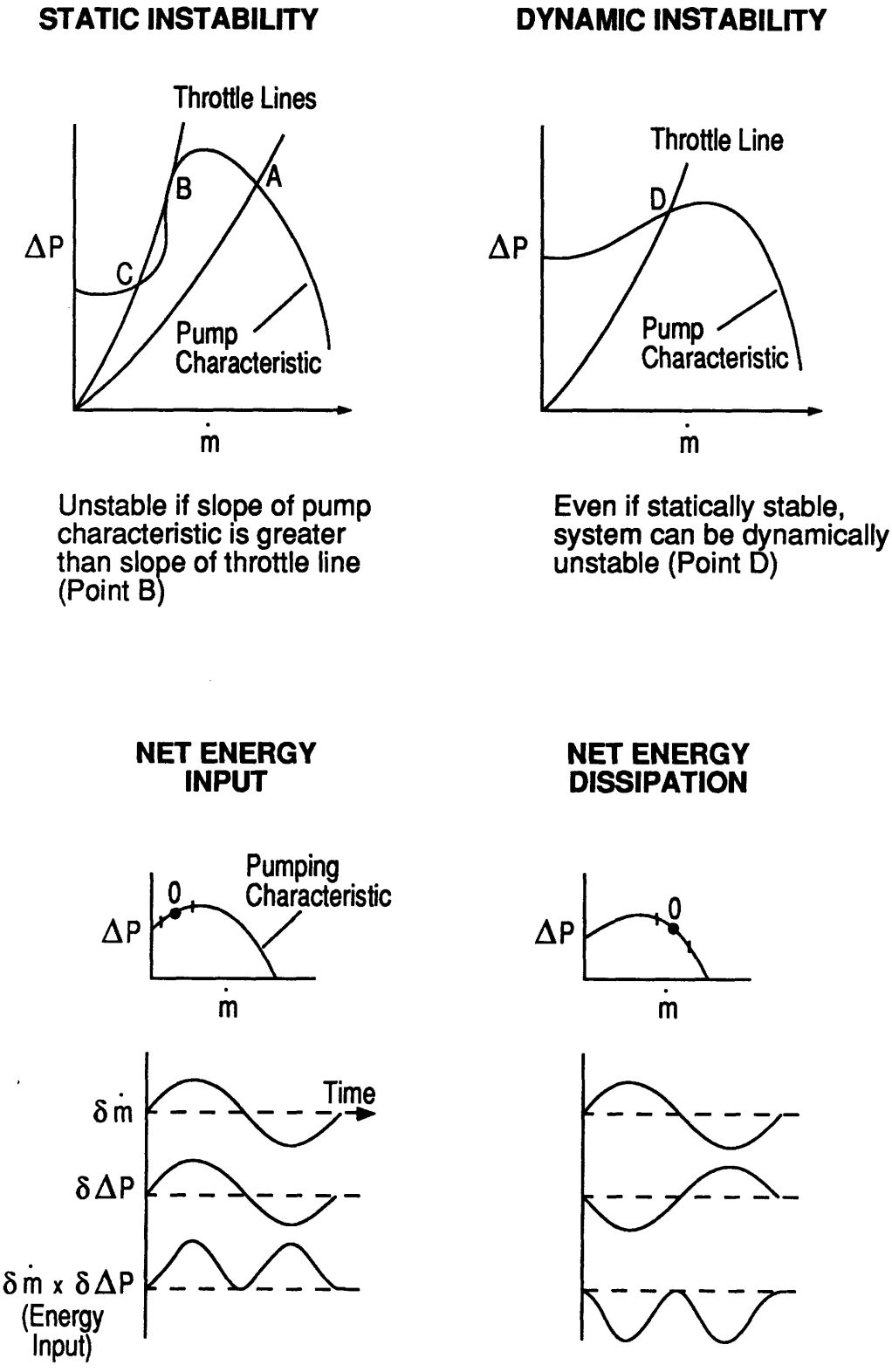

Figure 1.3: Instability modes and criterion (from [1]).

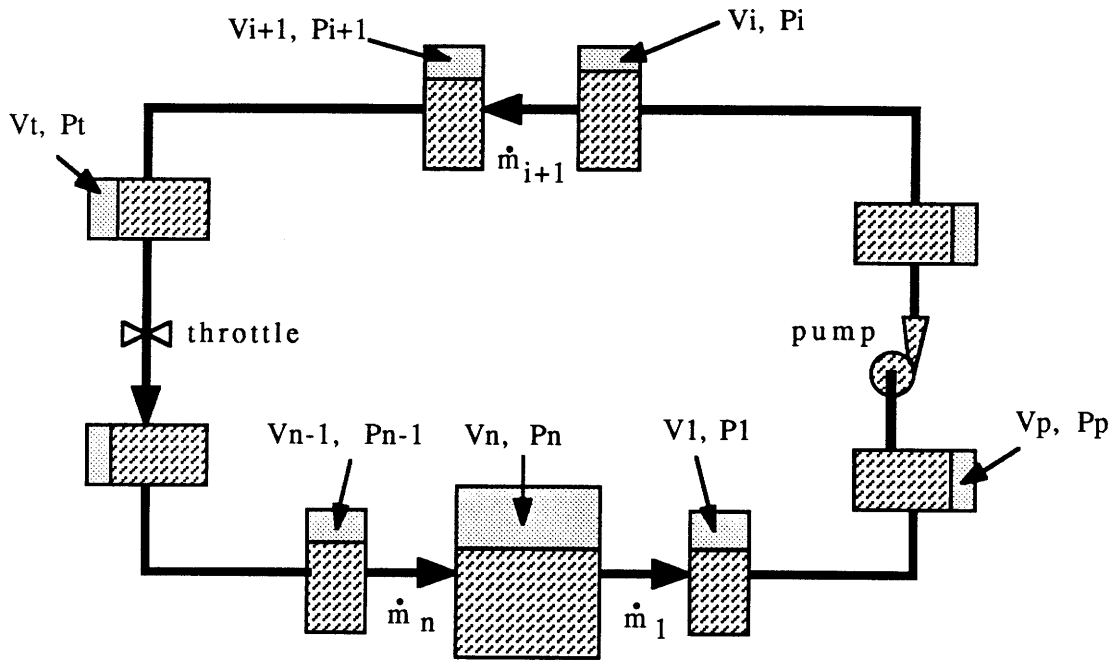

Figure 2.1: Schematic of the closed loop (general case): Definition of element notations and layout.

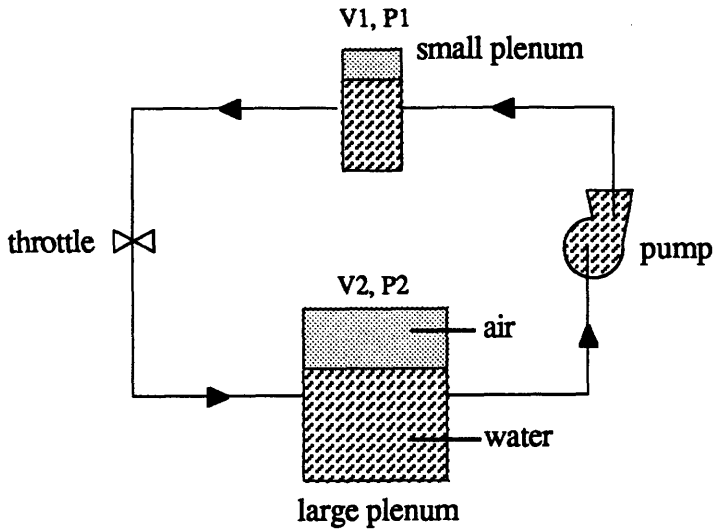

$$
\begin{cases}
\dfrac{d\delta\dot{m}_1}{dt} = \dfrac{A_1}{l_1}\left(\delta P_2 - \delta P_1 - \left(\dfrac{K_1 \dot{m}_1}{\rho A_1^2}\right)\delta\dot{m}_1 + \left(\dfrac{d\Delta P_{pump}}{d\dot{m}}\right)\delta\dot{m}_1\right) \\
\dfrac{d\delta\dot{m}_2}{dt} = \dfrac{A_2}{l_2}\left(\delta P_1 - \delta P_2 - \left(\dfrac{K_2 \dot{m}_2}{\rho A_2^2}\right)\delta\dot{m}_2 + \left(\dfrac{d\Delta P_{throttle}}{d\dot{m}}\right)\delta\dot{m}_2\right) \\
\dfrac{d\delta P_1}{dt} = \dfrac{\gamma P_1}{\rho V_1}\left(\delta\dot{m}_1 - \delta\dot{m}_2\right) \\
\dfrac{d\delta P_2}{dt} = \dfrac{\gamma P_2}{\rho V_2}\left(\delta\dot{m}_2 - \delta\dot{m}_1\right)
\end{cases}
$$

Figure 2.2: Schematic of the closed loop with equations (case of study): Simplifications for the case of study.

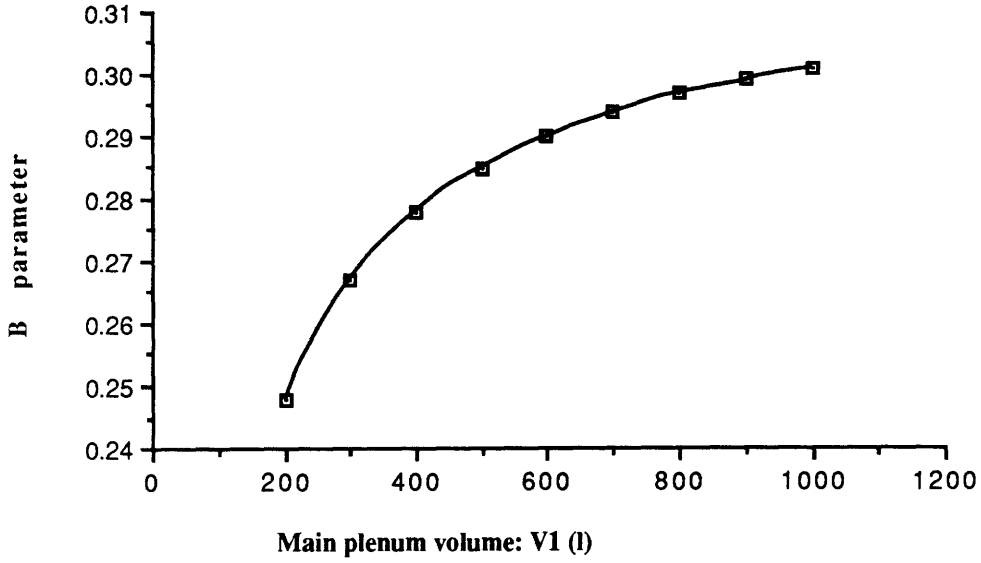

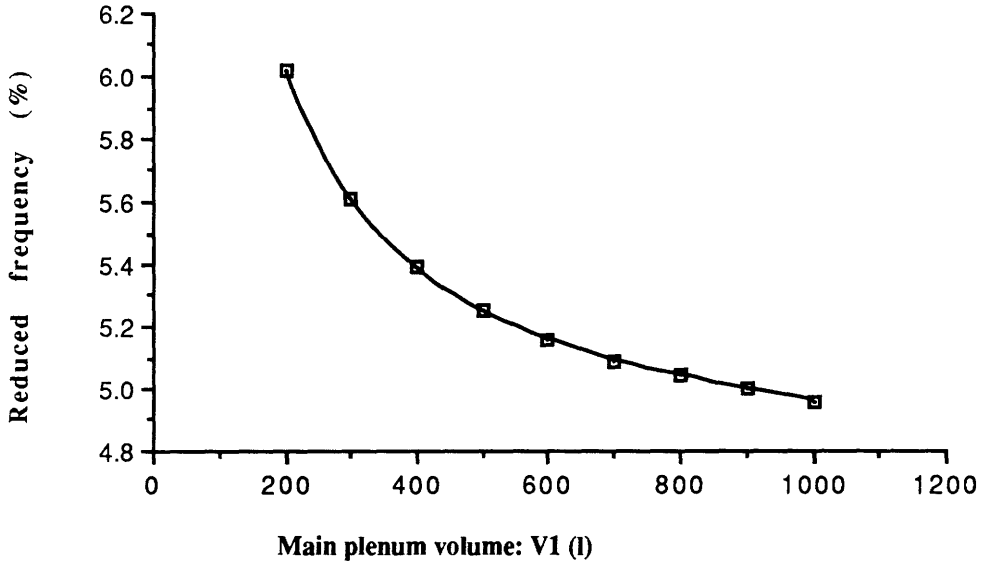

Figure 2.3: Effect of the main air volume on the system performance: Trends of B and ω_{red} vs V_1.

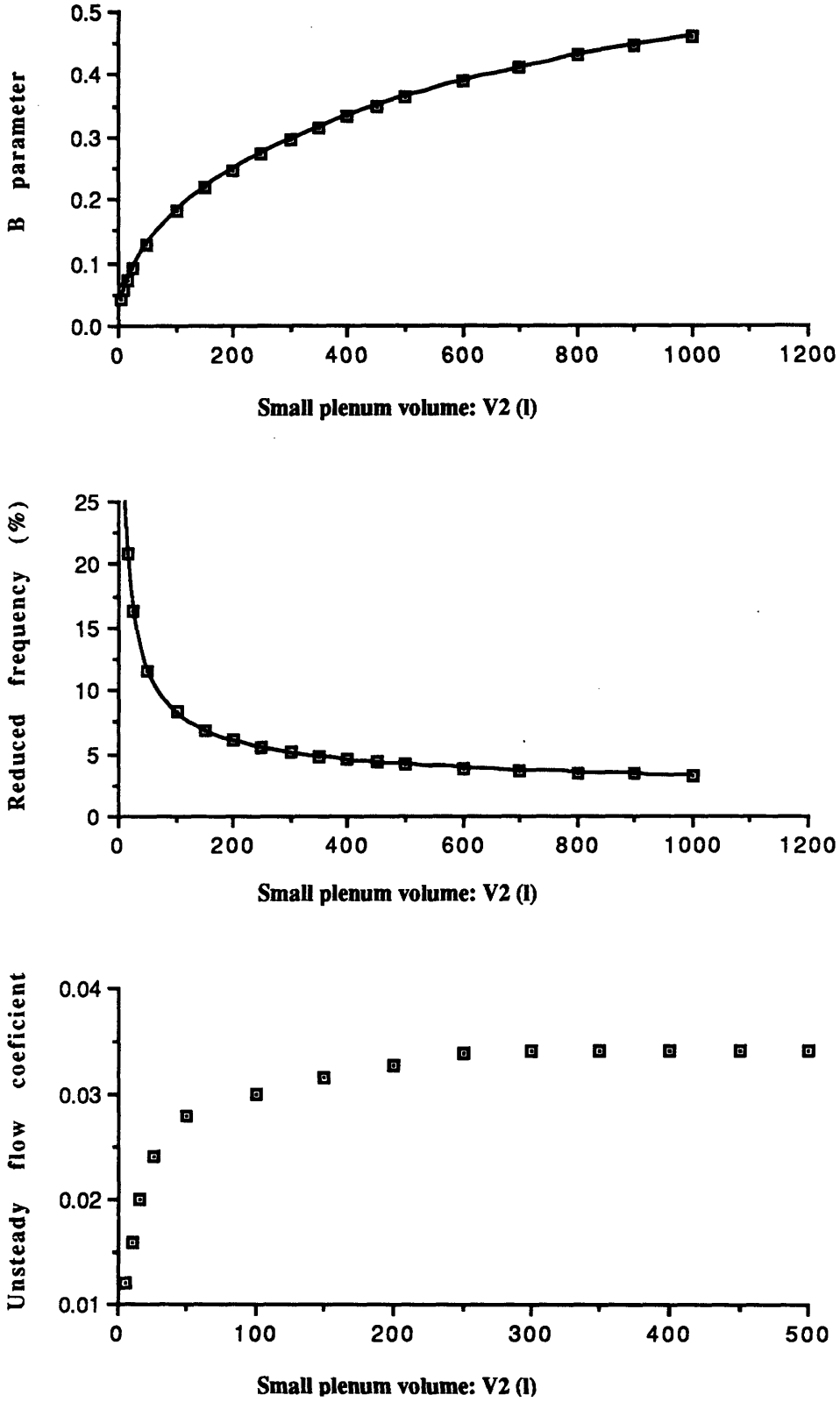

Figure 2.4: Effect of the small air volume on the system performance: Trends of B, ω_{red} and Φ_{osc} vs V_2.

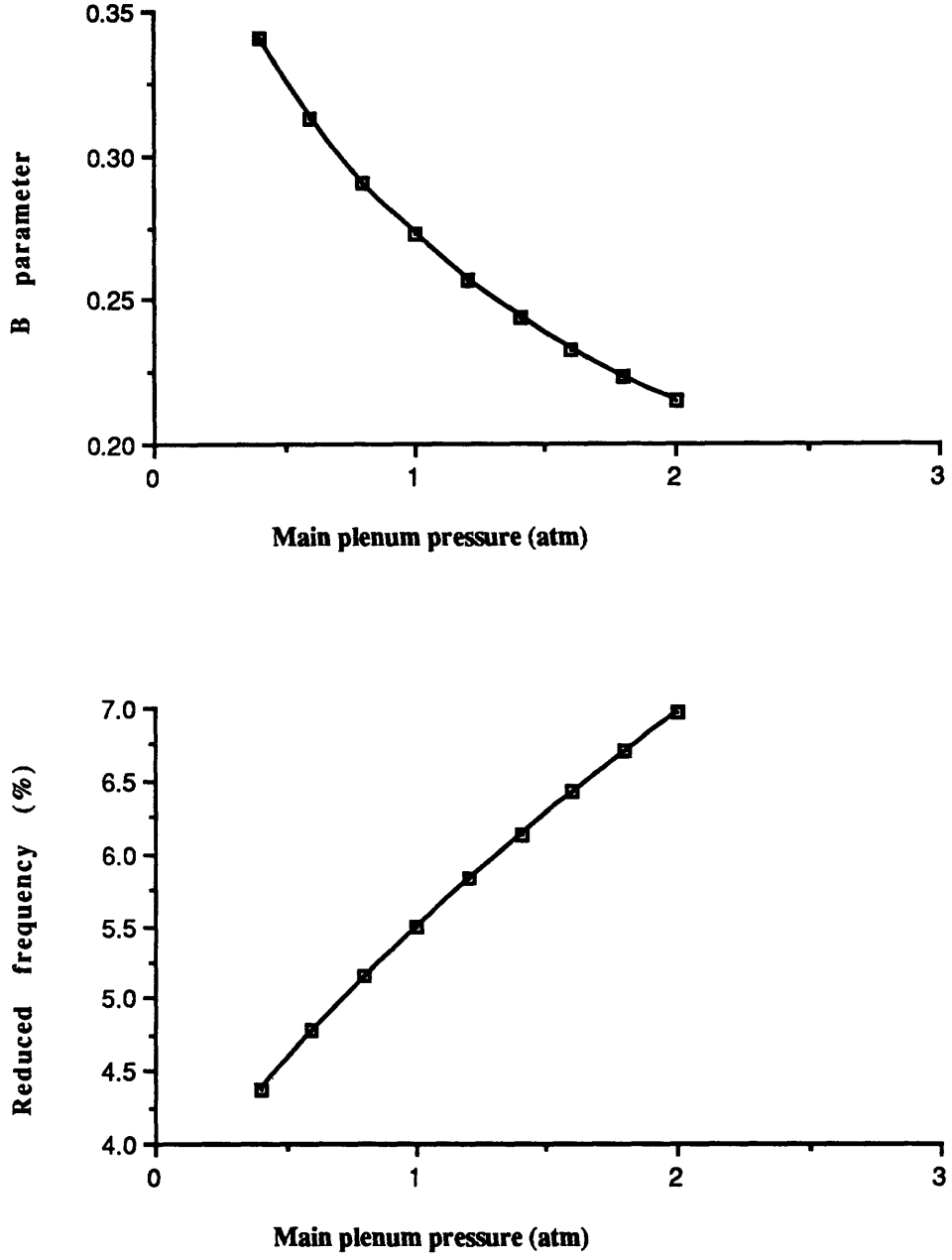

Figure 2.5: Effect of the overall pressure on the system performance: Trends of B and ω_{red} vs P_1.

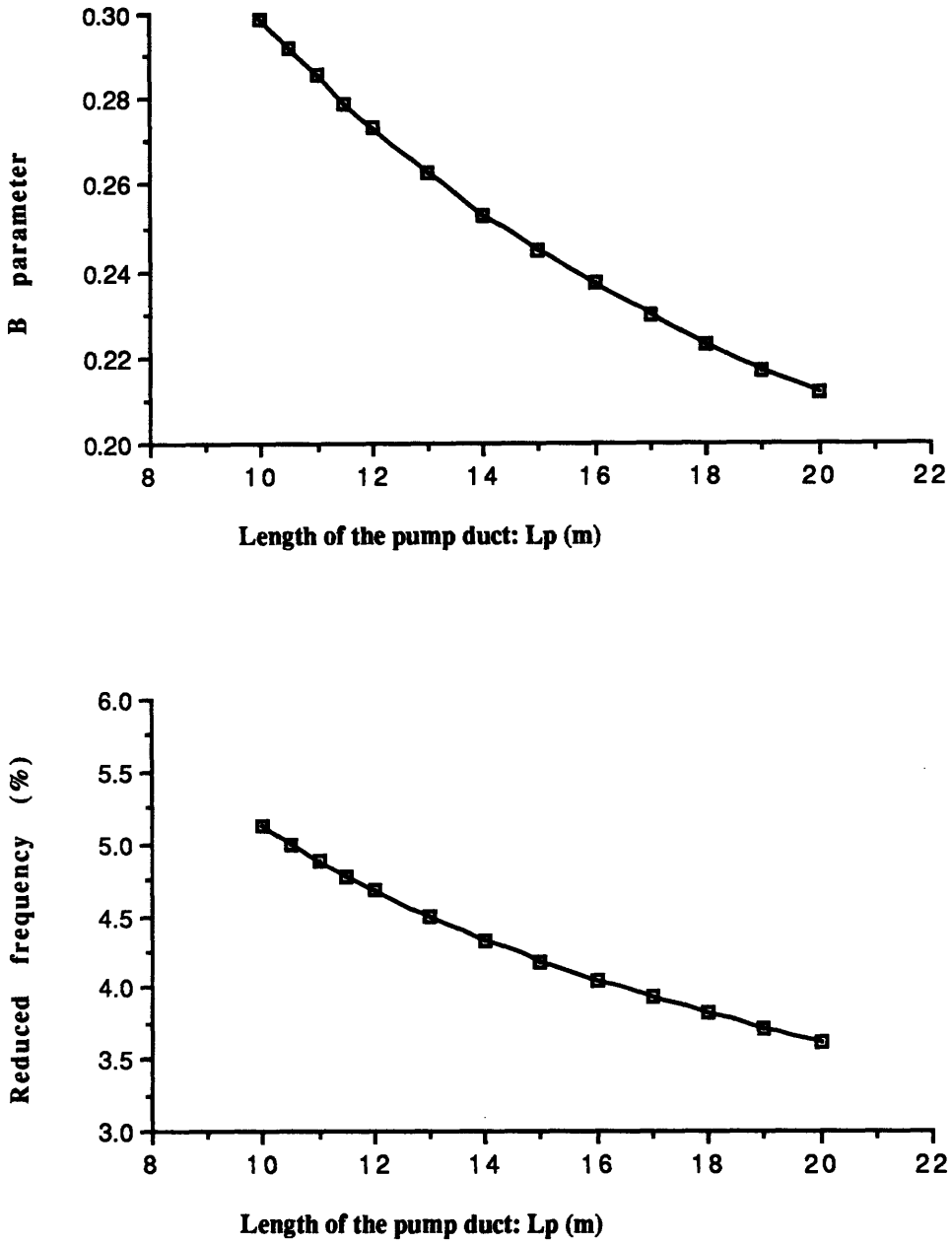

Figure 2.6: Effect of the test section duct on the system performance: Trends of B and ω_{red} vs L_p.

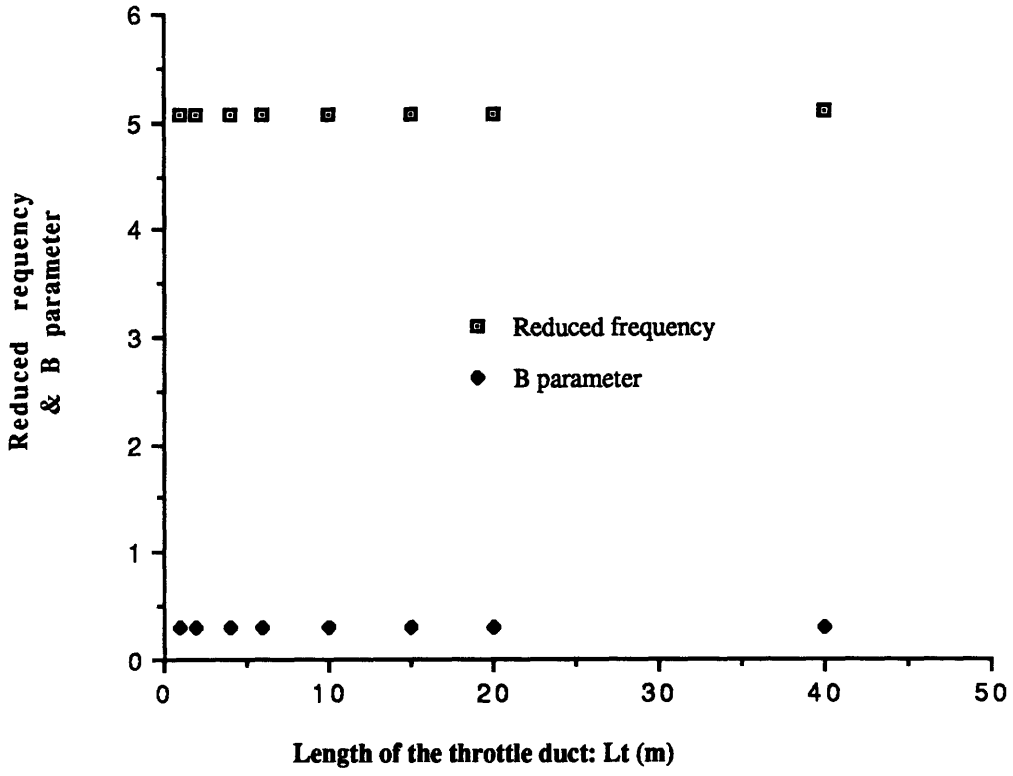

Figure 2.7: Effect of the throttle duct on the system performance: Trends of B and ω_{red} vs L_t.

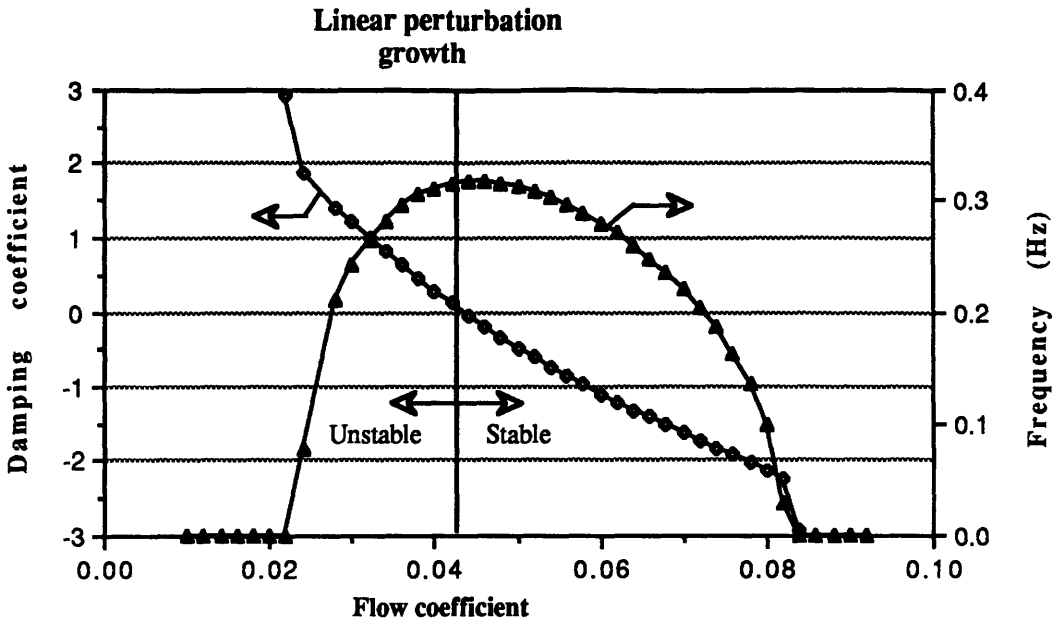

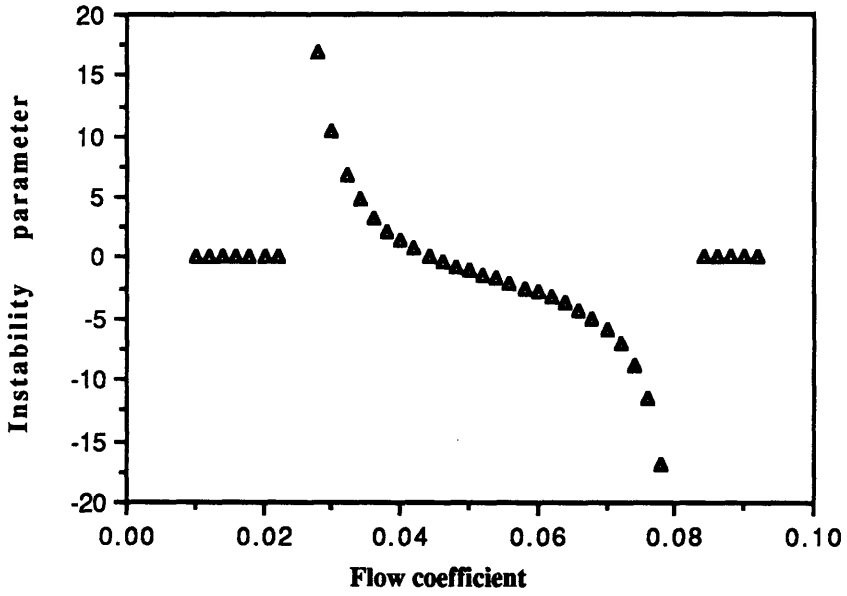

Figure 2.8: Instability growth features: Frequency, damping and ξ vs Φ.

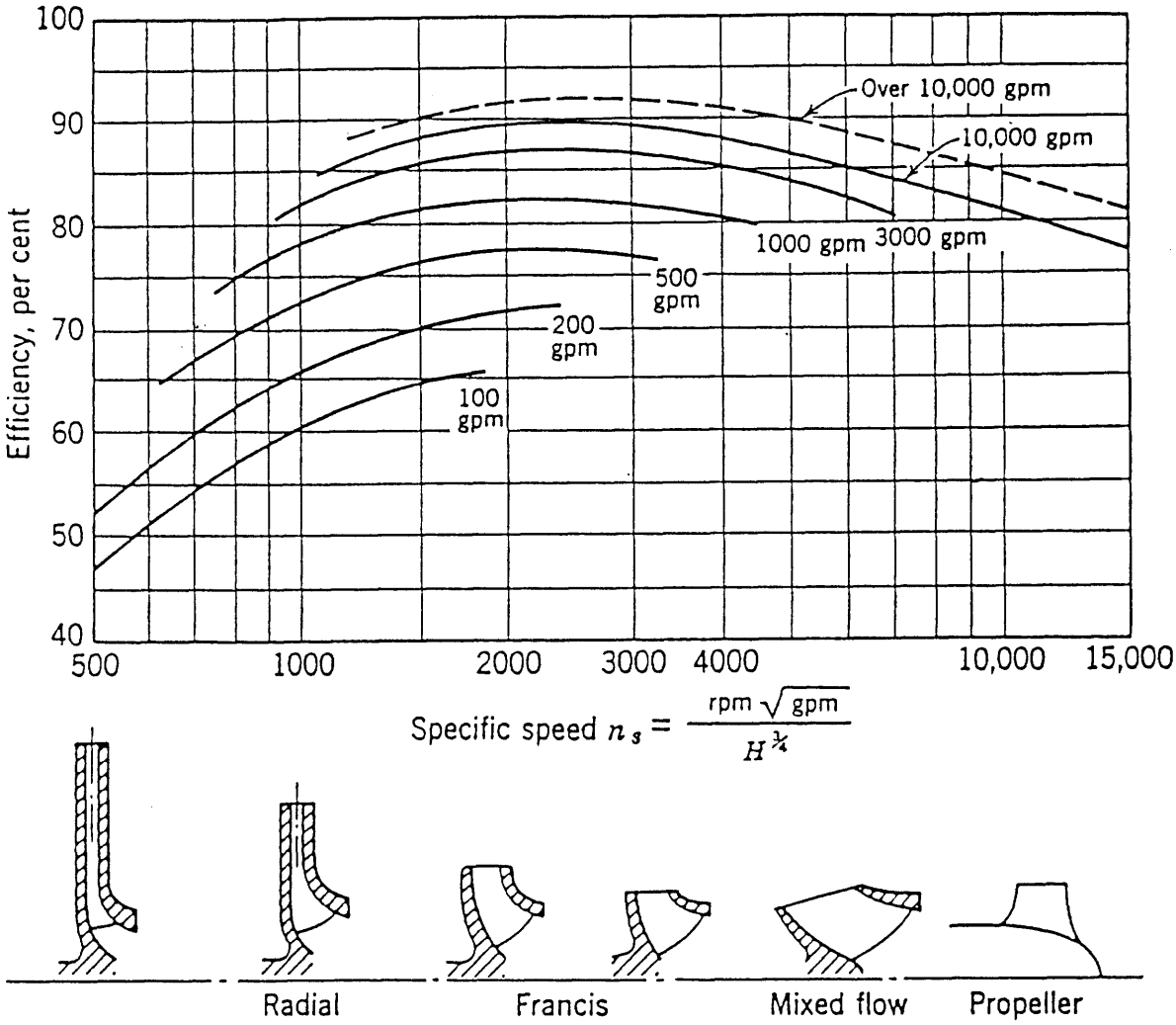

Figure 3.1: Pump impeller shape and performance vs N_S (from [24]).

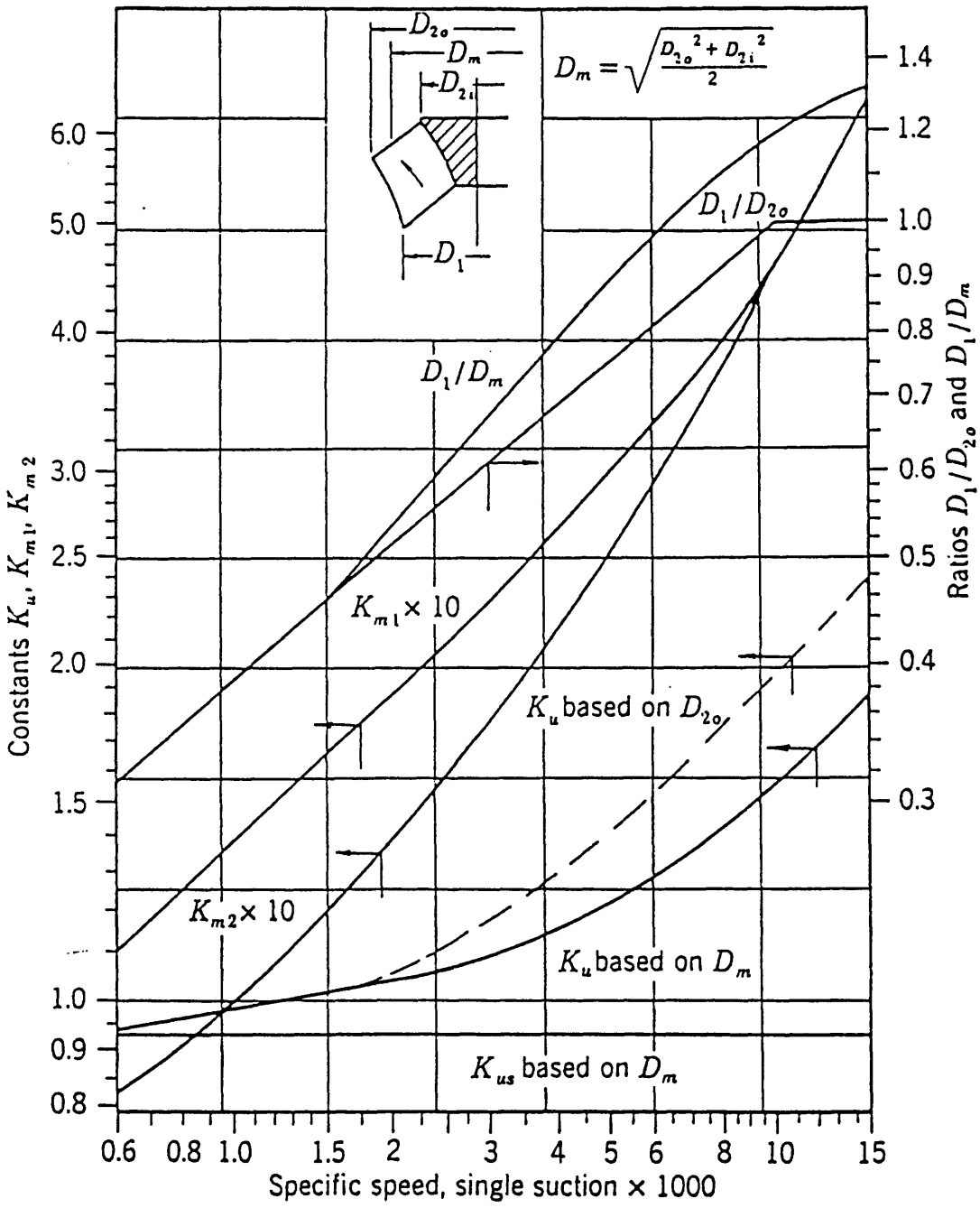

Figure 3.2: Impeller constants:
K_u, K_{m1}, K_{m2} dependence on N_s and geometric ratios (from [24]).

Parameter	HPU data	Scaled up data
N_s (SI/eng u.)	0.15/869	0.15/869
Φ/Q	/	0.1169/689 (gpm)
Ψ/H	/	0.974/13.5 (psi)
N	/	425 rpm
D_2	/	24"
b_2	/	0.566"
t	/	0.453"
Z	8	8
D_1	/	7.92"
N_{ss}	2000	3200
σ	0.01	1
R_e	10^6	$8\ 10^6$

Note: The numbers missing for the original HPU (high pressure unit) are not available for publication.

Figure 3.3: Summary of pump data.

	GE Lexan	DuPont Lucite	Rohm&H. Plexiglass
Ref. index	1.58	1.45	1.5
Transmittance	89 %	93 %	92 %
Young Mod.	1900 Mpa	2944 Mpa	3100 Mpa
Tensile str.	62 Mpa	74.5 Mpa	72 Mpa
Comp. Mod.	2400 Mpa	2944 Mpa	3100 Mpa
Comp. Str.	86 Mpa	123 Mpa	124 Mpa
Flexural Mod.	2300 Mpa	2944 Mpa	3100 Mpa
Flexural str.	97 Mpa	103 Mpa	110 Mpa
Rock. Hard.	M 70	M 100	M 102
Thermal exp	6.75 10^{-5} m/m/°C	7 10^{-5} m/m/°C	5 10^{-5} m/m/°C
W. abs. wgt.	0.58 %	0.3 %	1 %
W abs. vol.	0.0 %	0.0 %	0.0 %

Figure 3.4: Materials properties:
Comparison between Lexan™, Lucite™ and Plexiglass™.

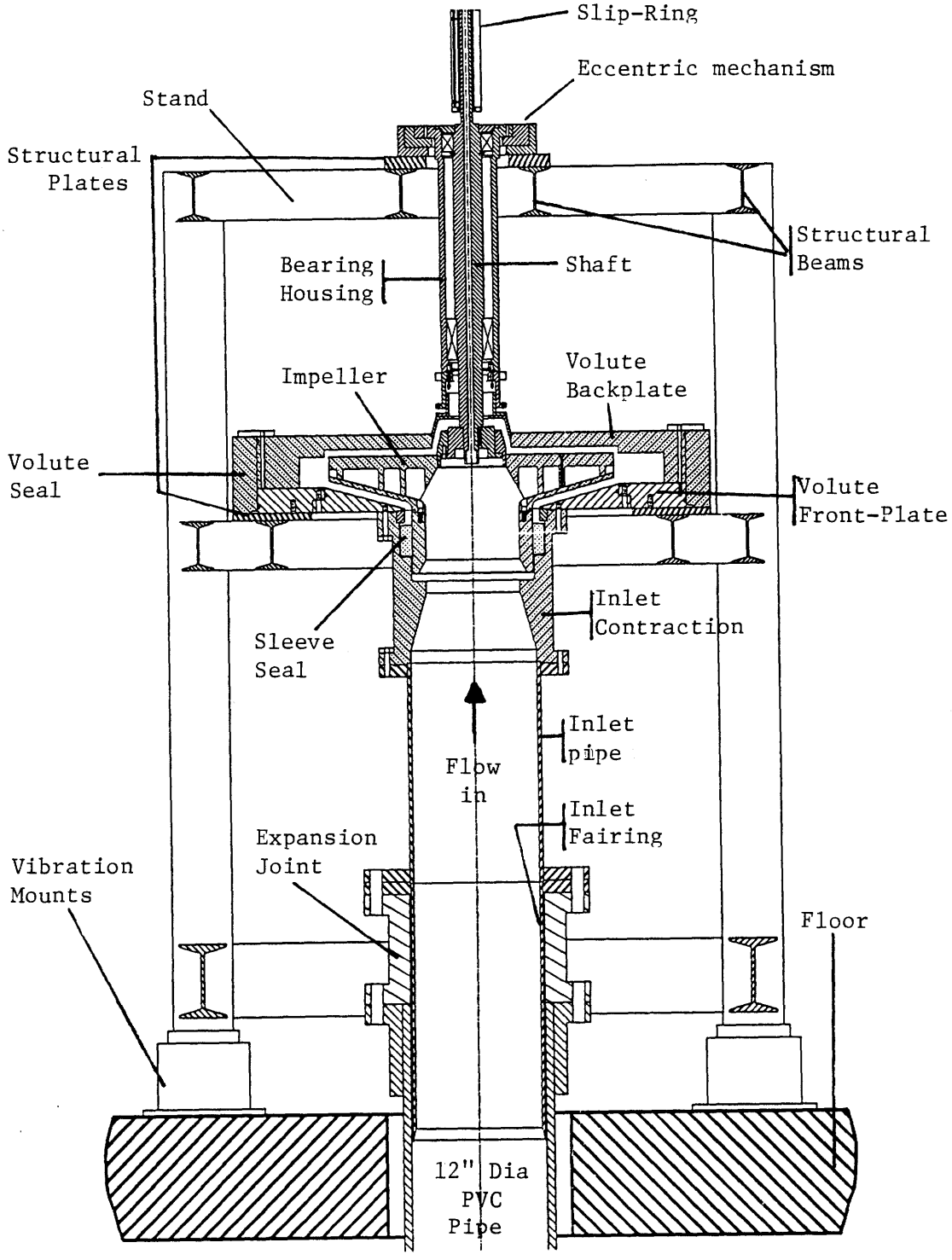

Figure 3.5: Elevation view: Test section assembly.

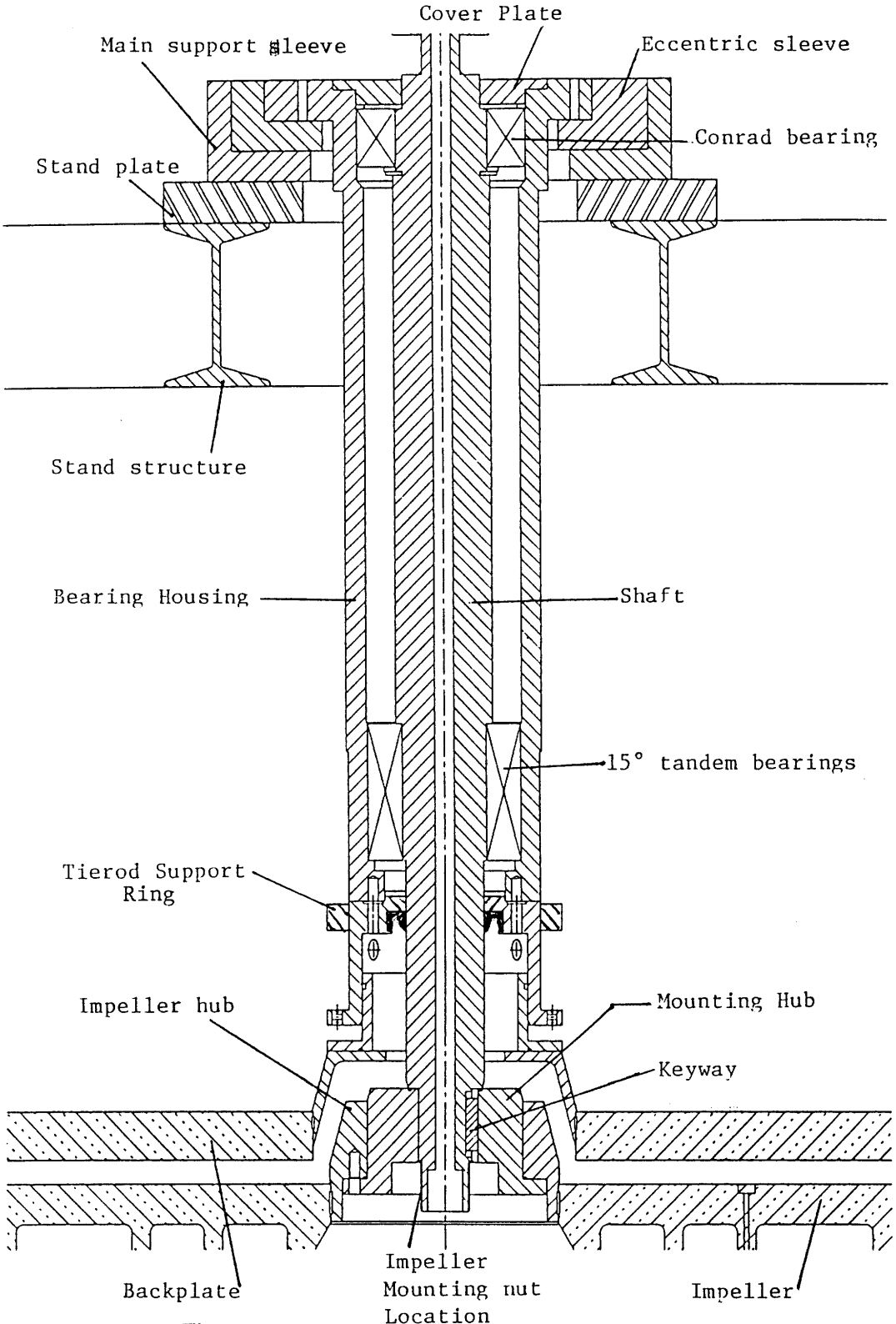

Figure 3.6: Shaft and bearing assembly detail.

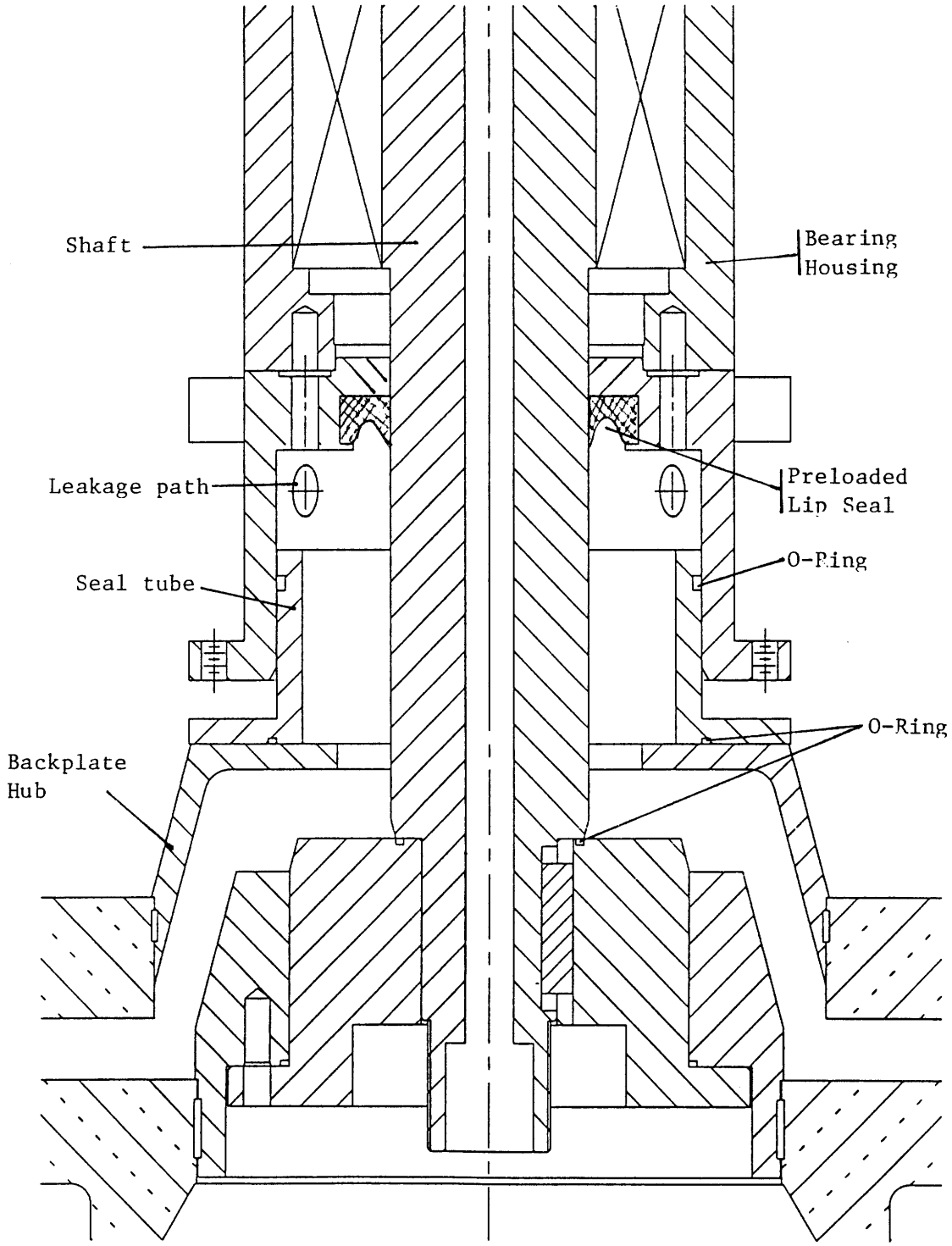

Figure 3.7: Seal detail.

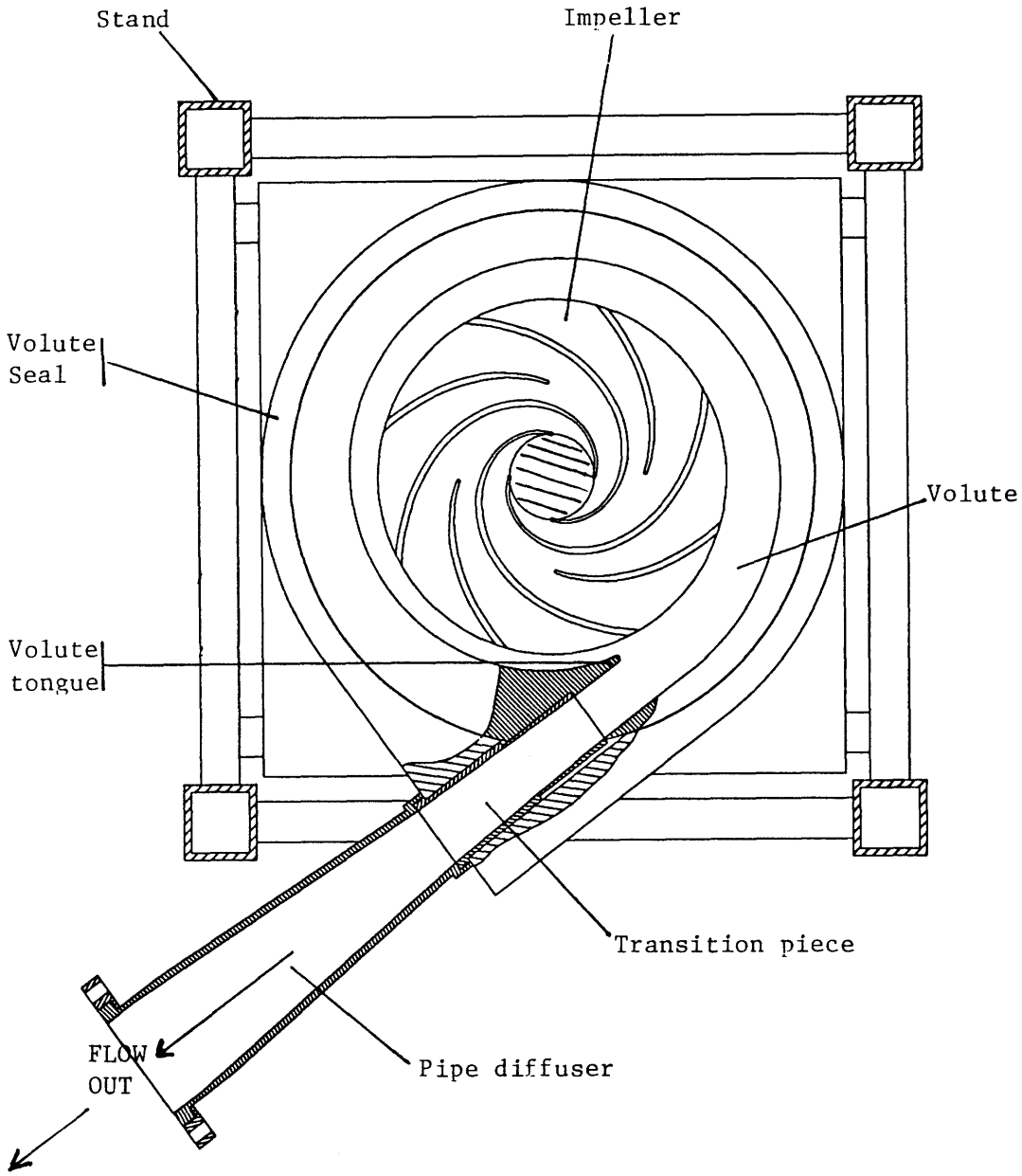

Figure 3.8: Top view: Test section assembly:
Horizontal layout and optical access.

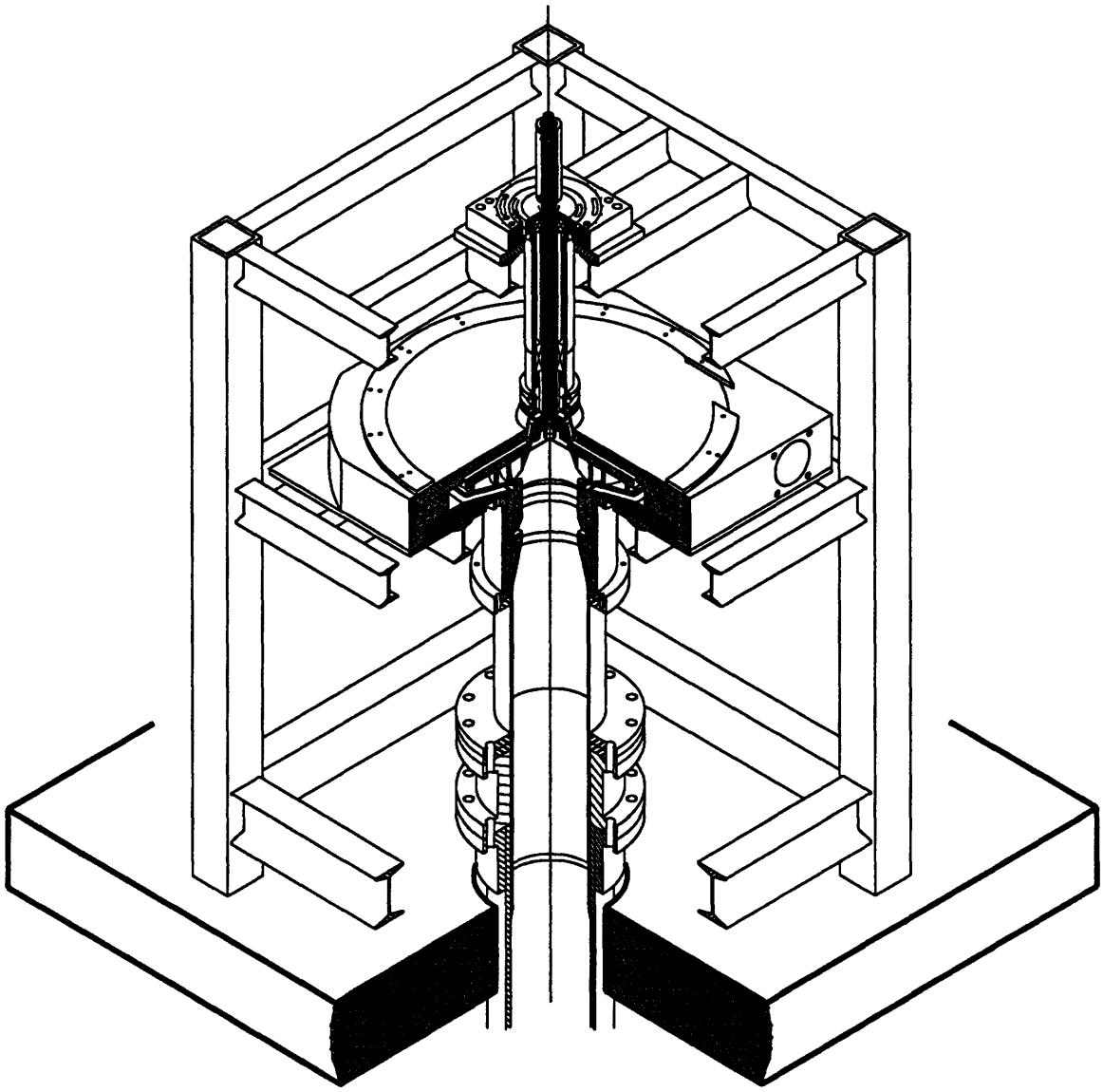

Figure 3.9: Isometric view of the test section

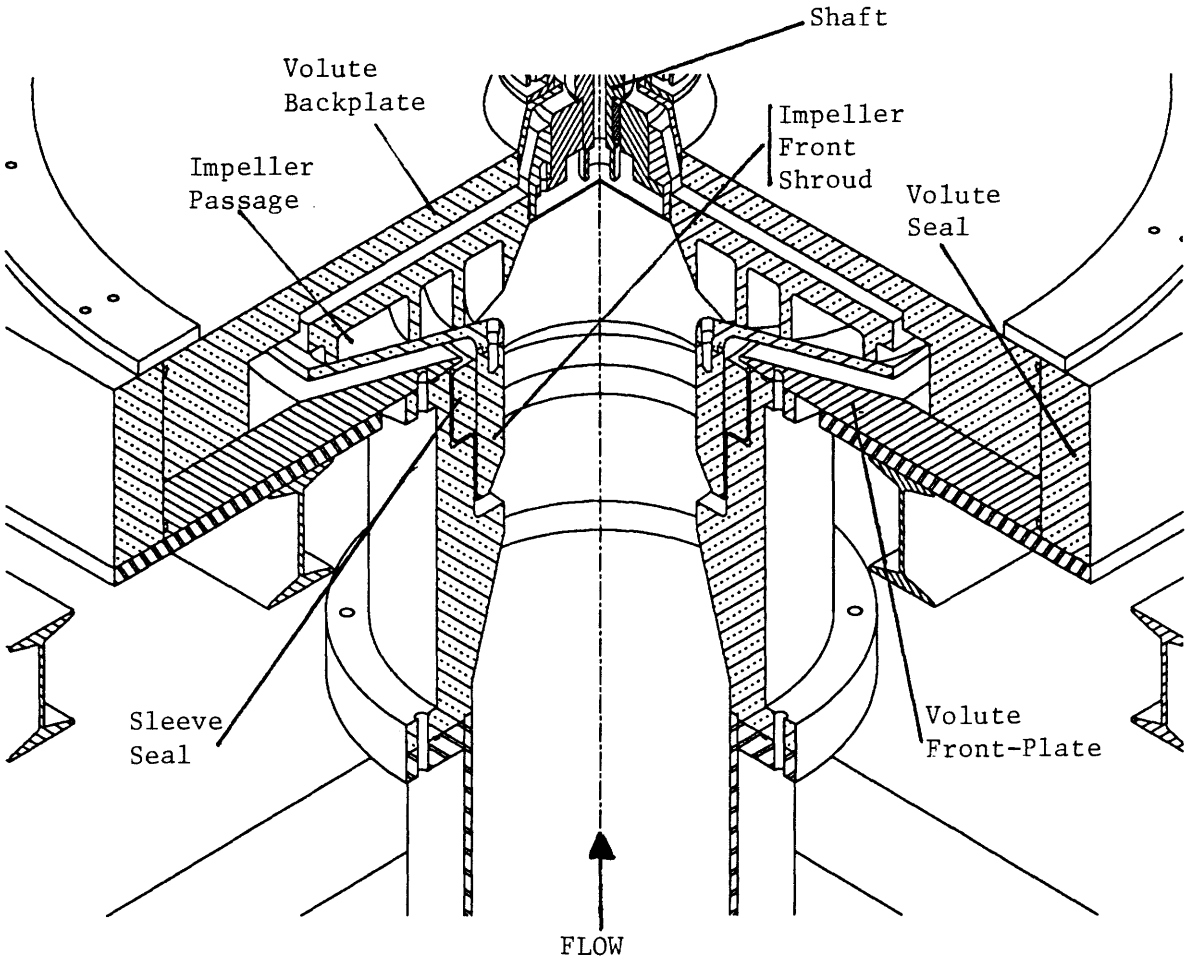

Figure 3.10: Detail of flow passage.

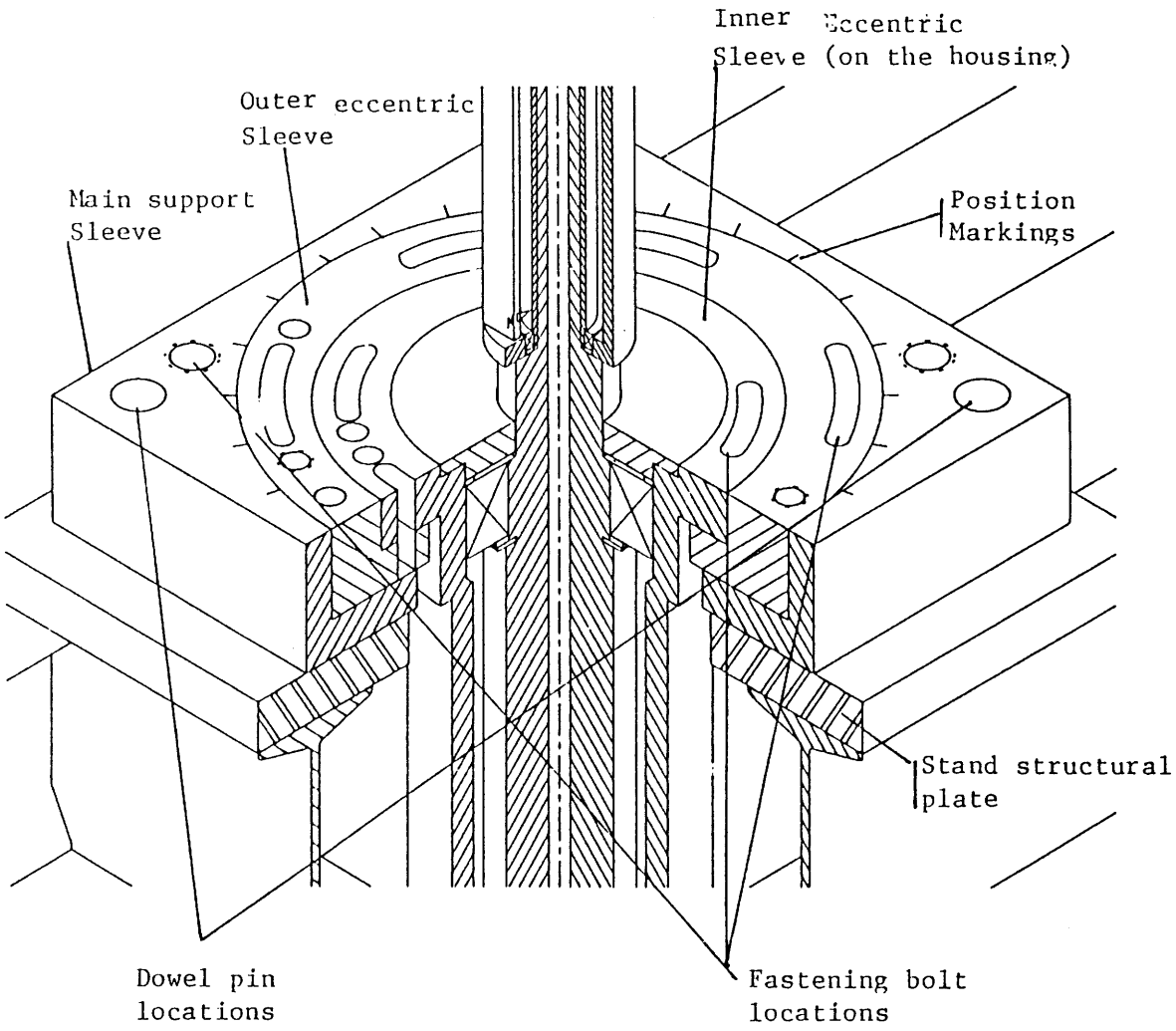

Figure 3.11: Eccentric mechanism.

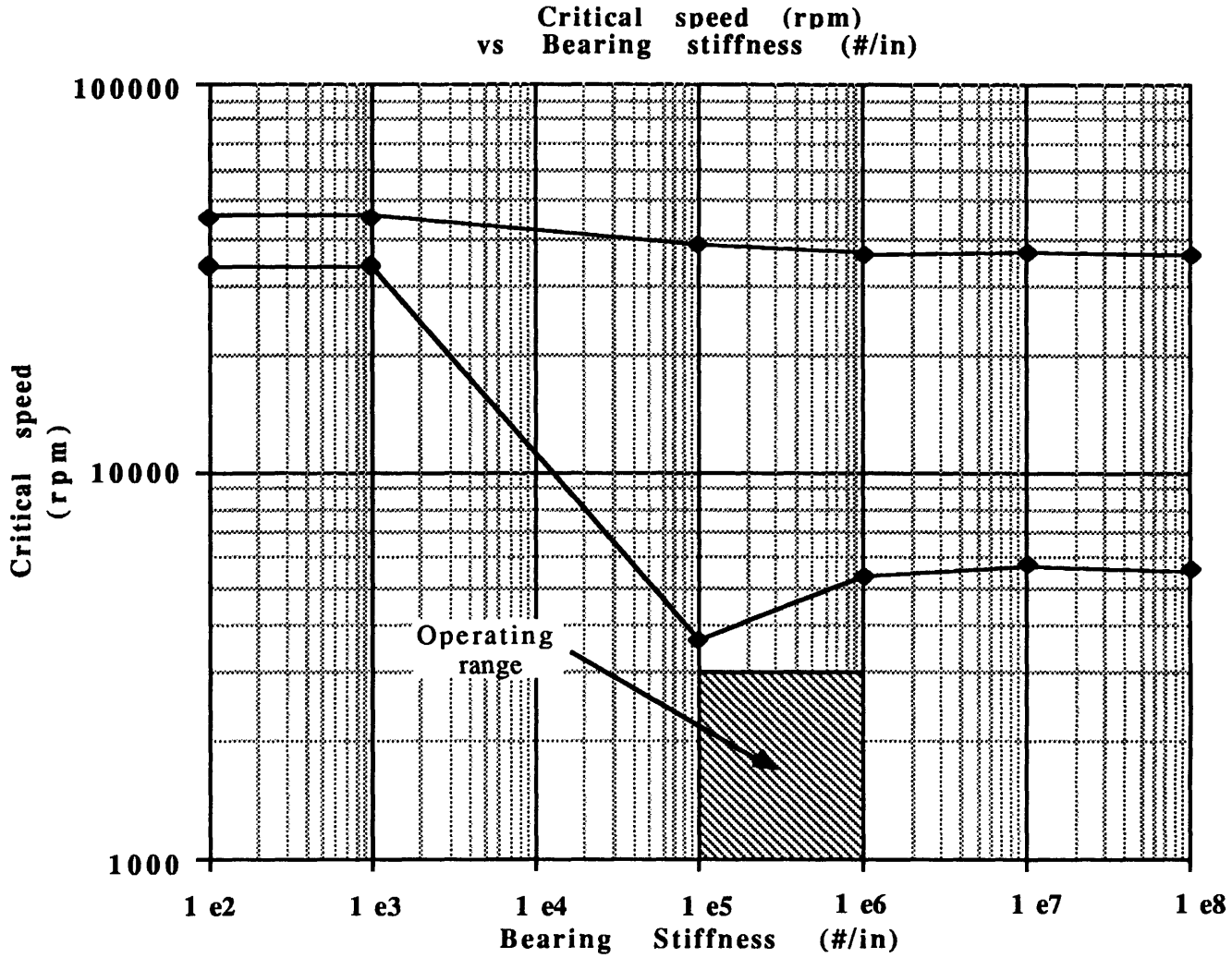

Figure 3.12: Critical speed vs bearing stiffness.

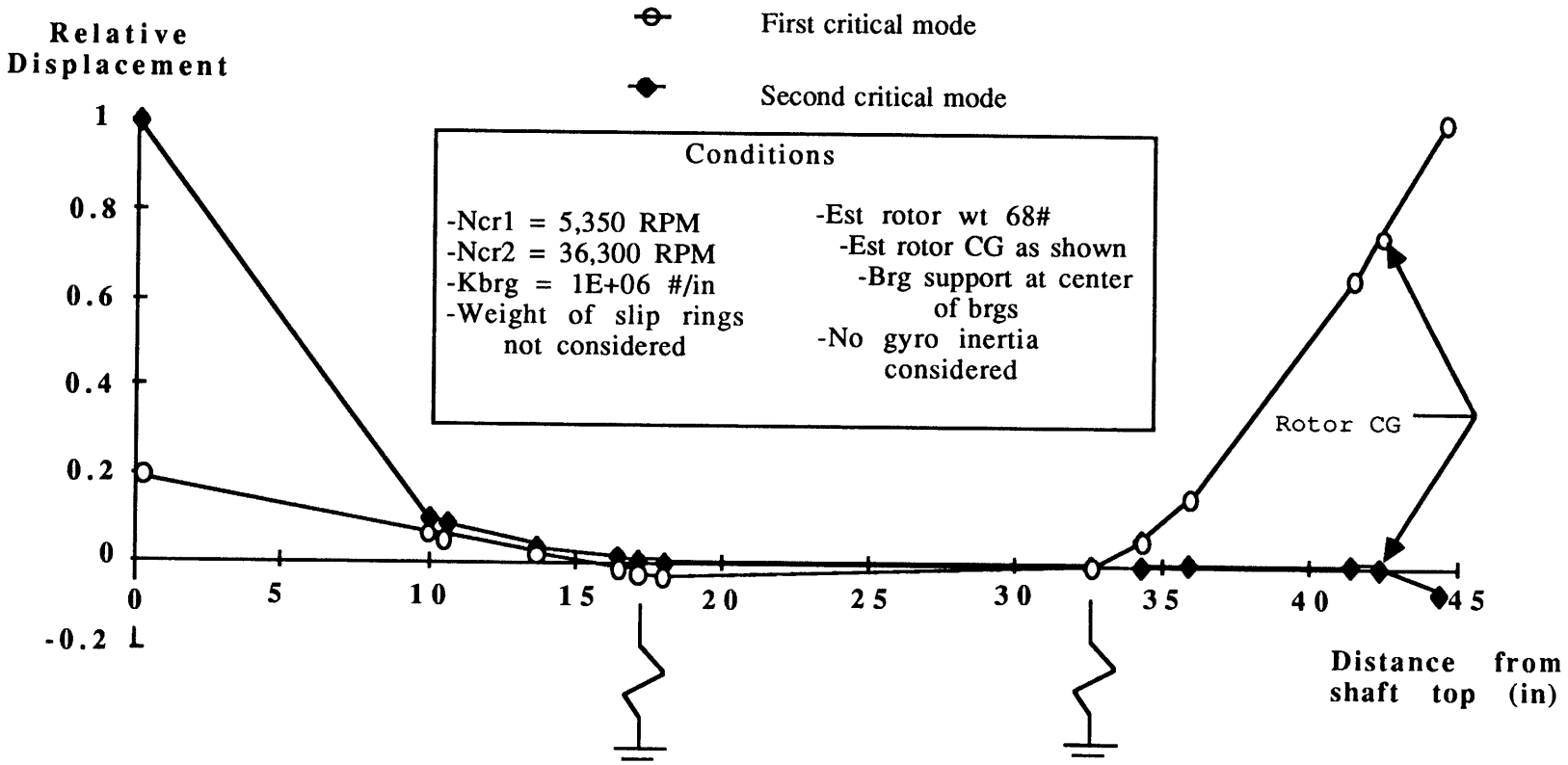

Figure 3.13: Critical mode shapes.

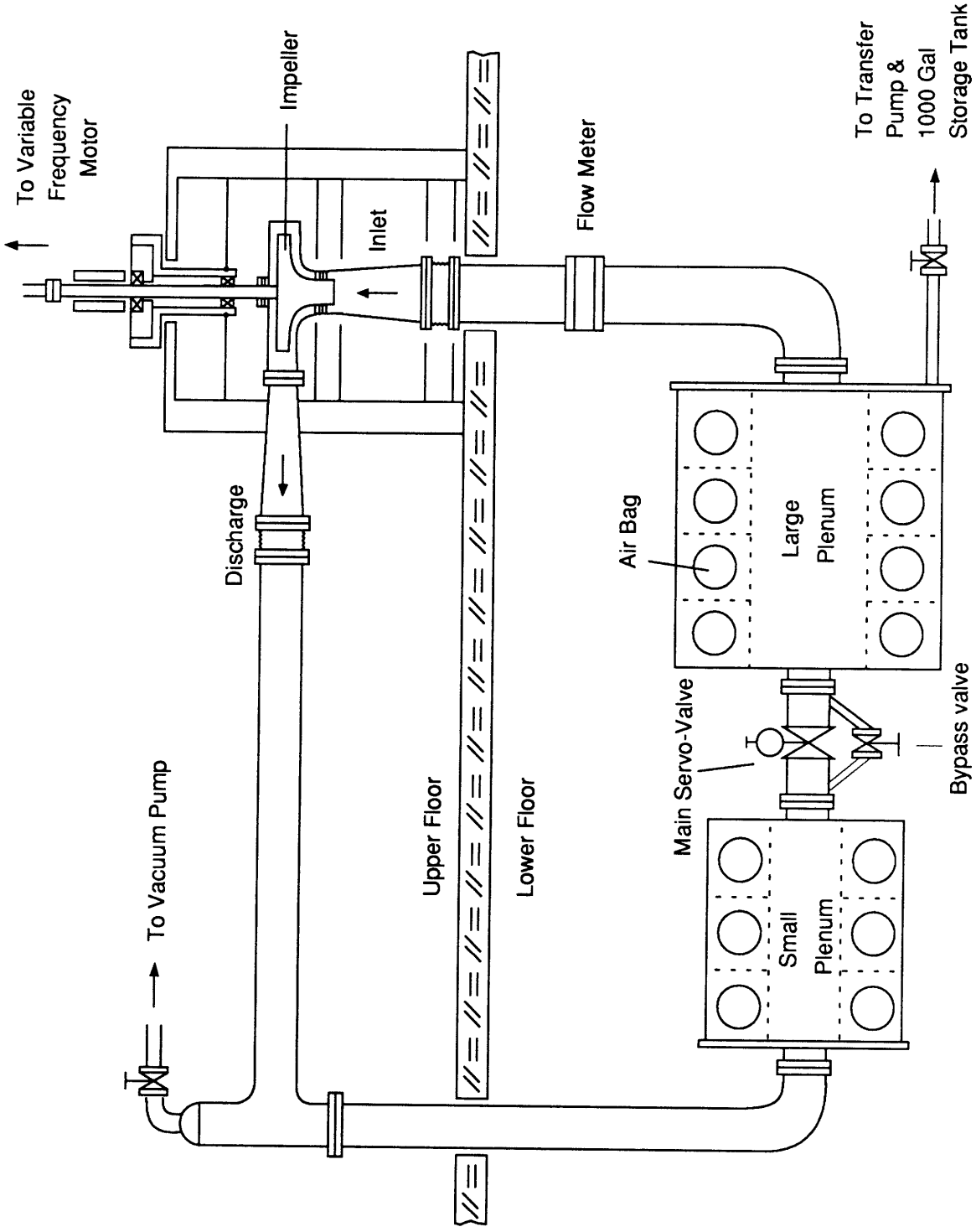

Figure 3.14: Sketch of the loop layout (not to scale).

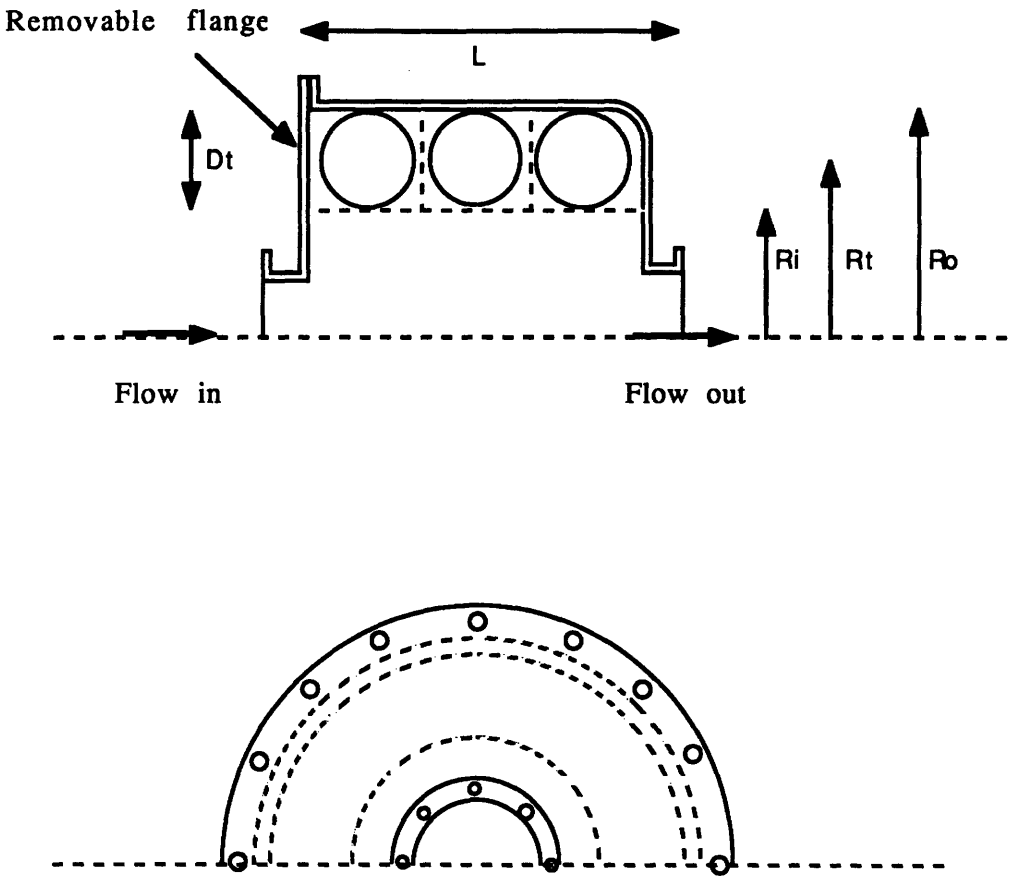

Figure 3.15: Plenum layout.

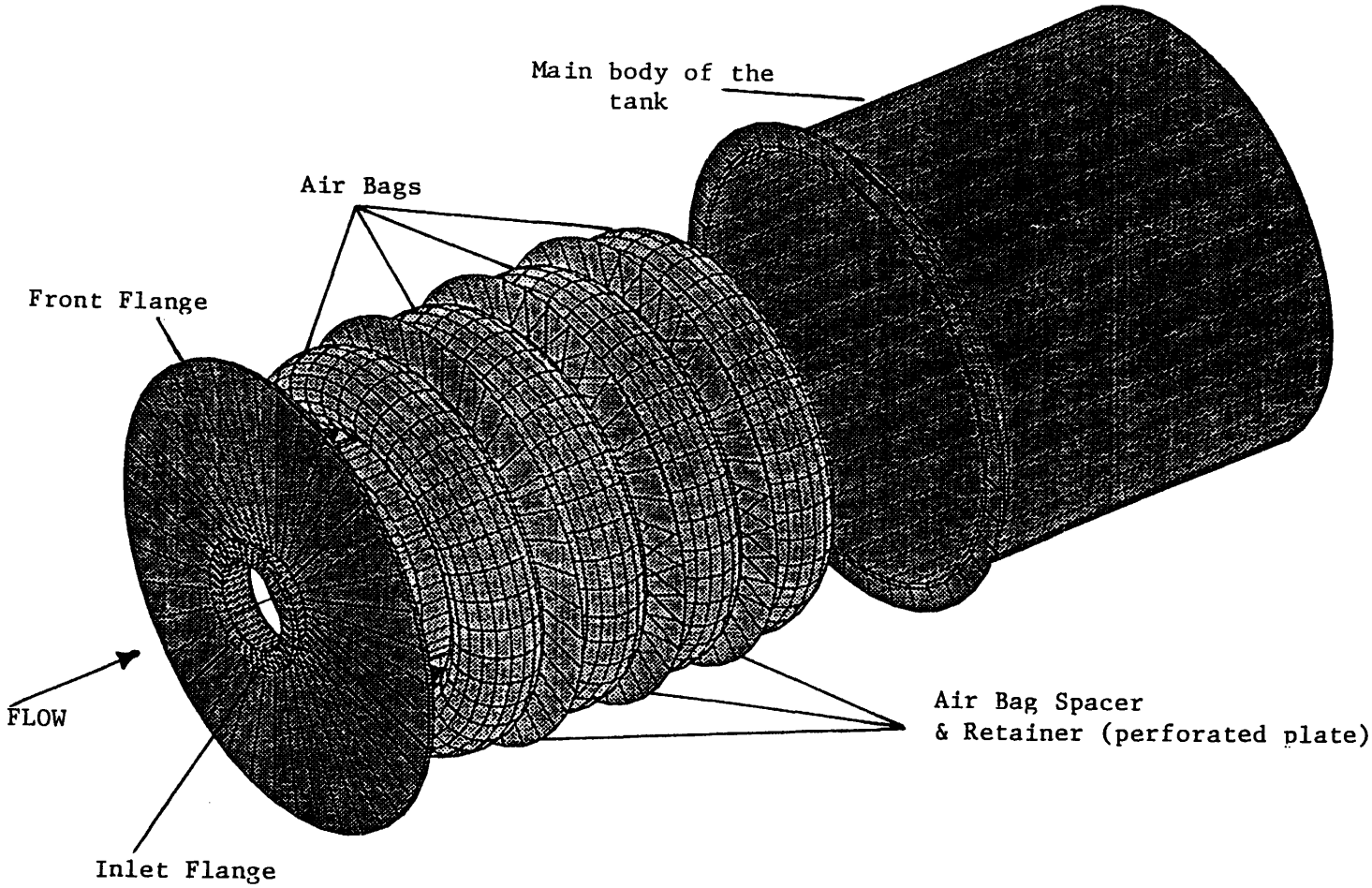

Figure 3.16: Exploded view of a plenum:
Detail of the air bag congfiguration and assembly.

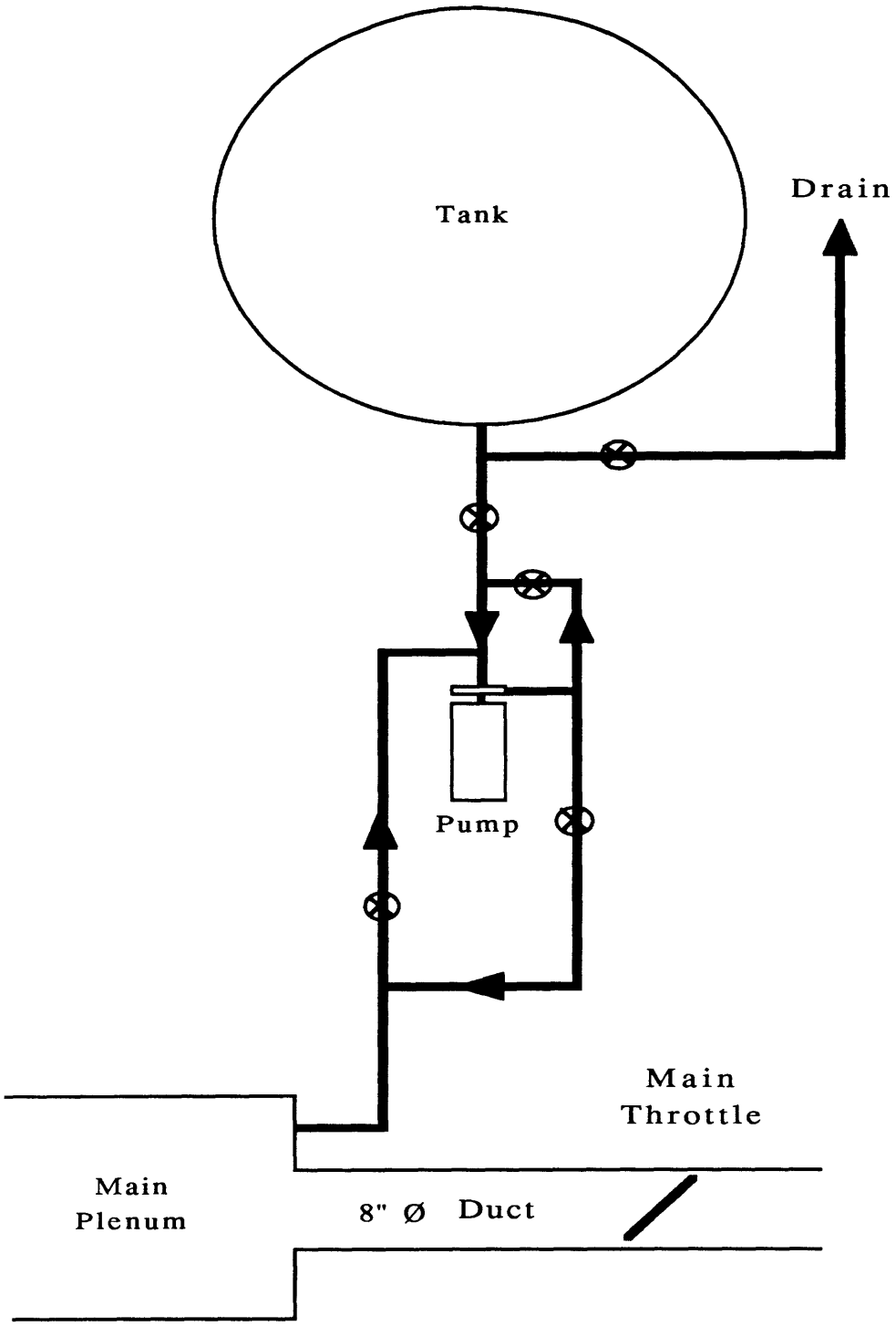

Figure 3.17: Transfer system.

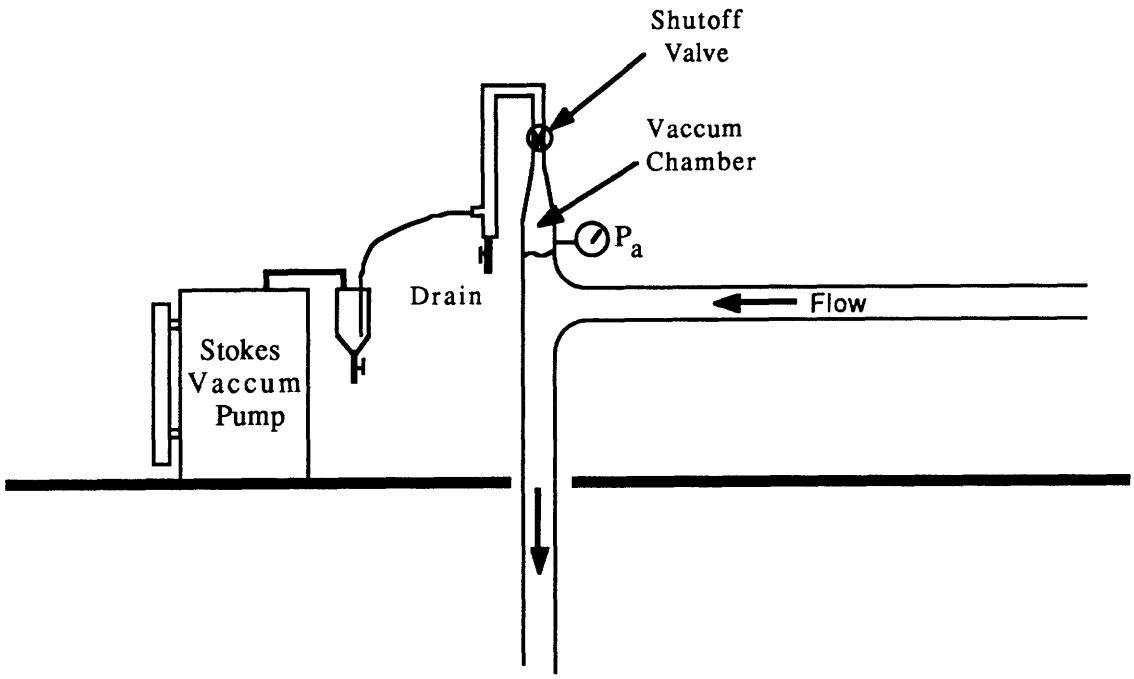

Figure 3.18: Deaeration system.

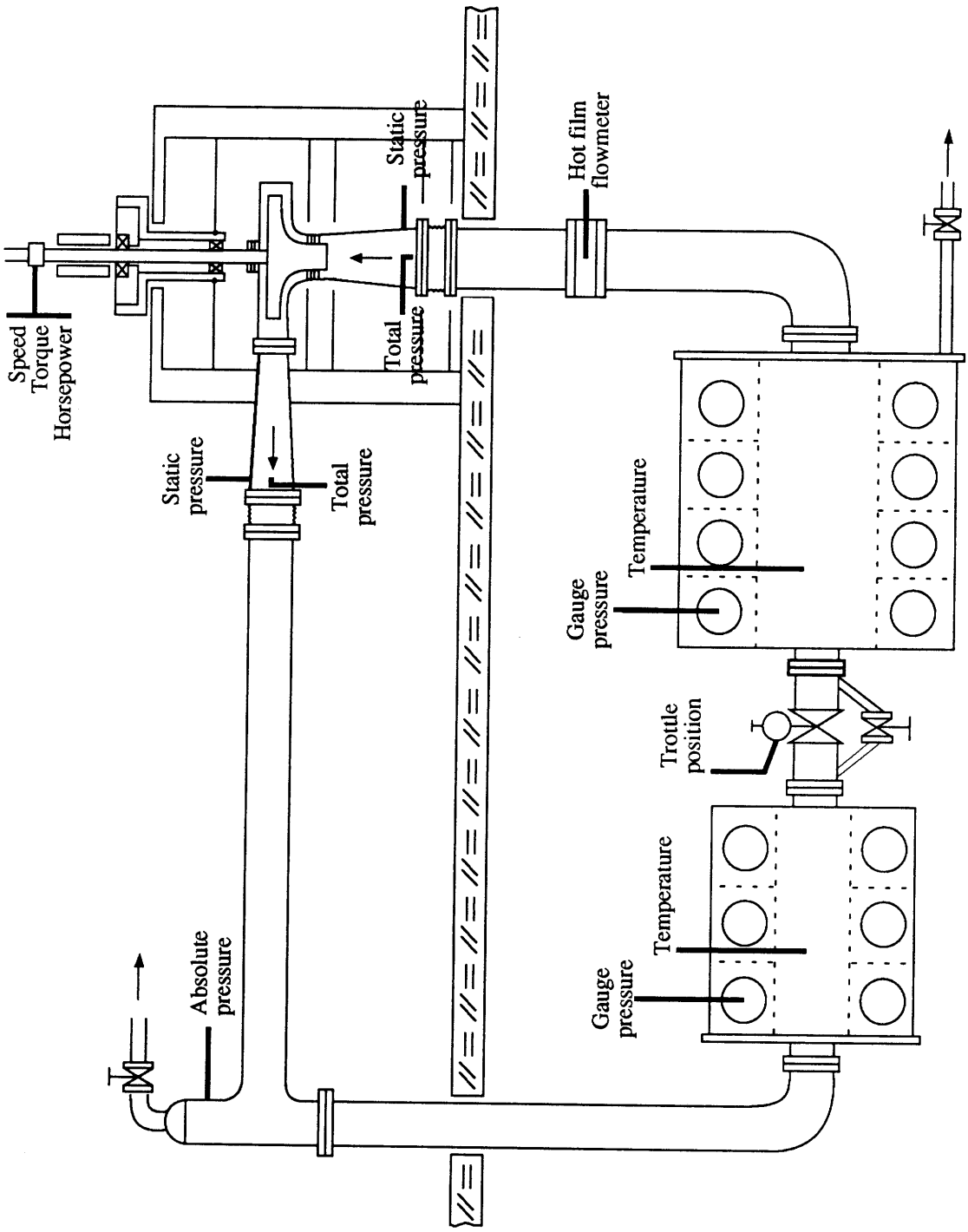

Figure 3.19: Overall instrumentation locations.

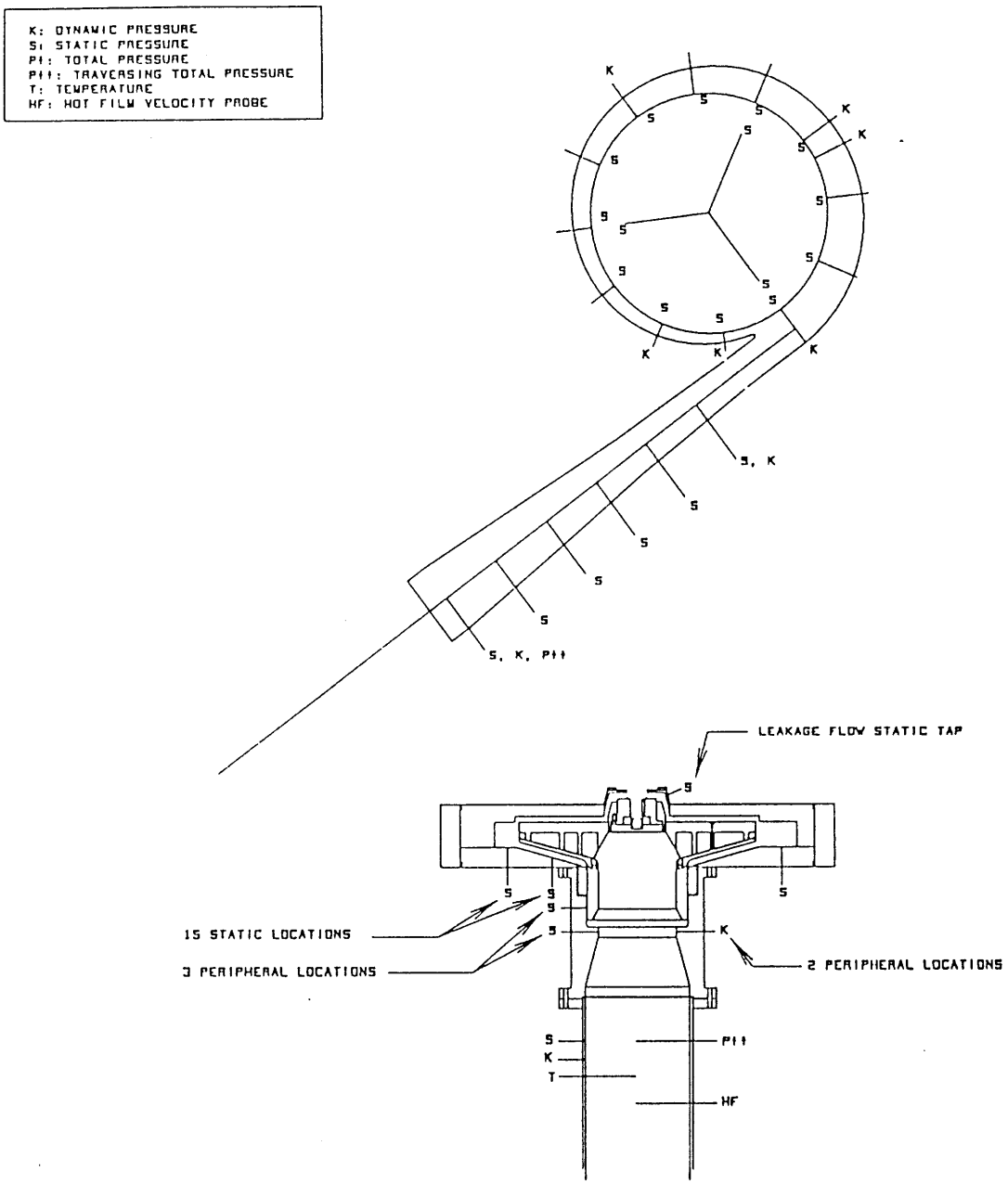

Figure 3.20: Detailed test section instrumentation locations.

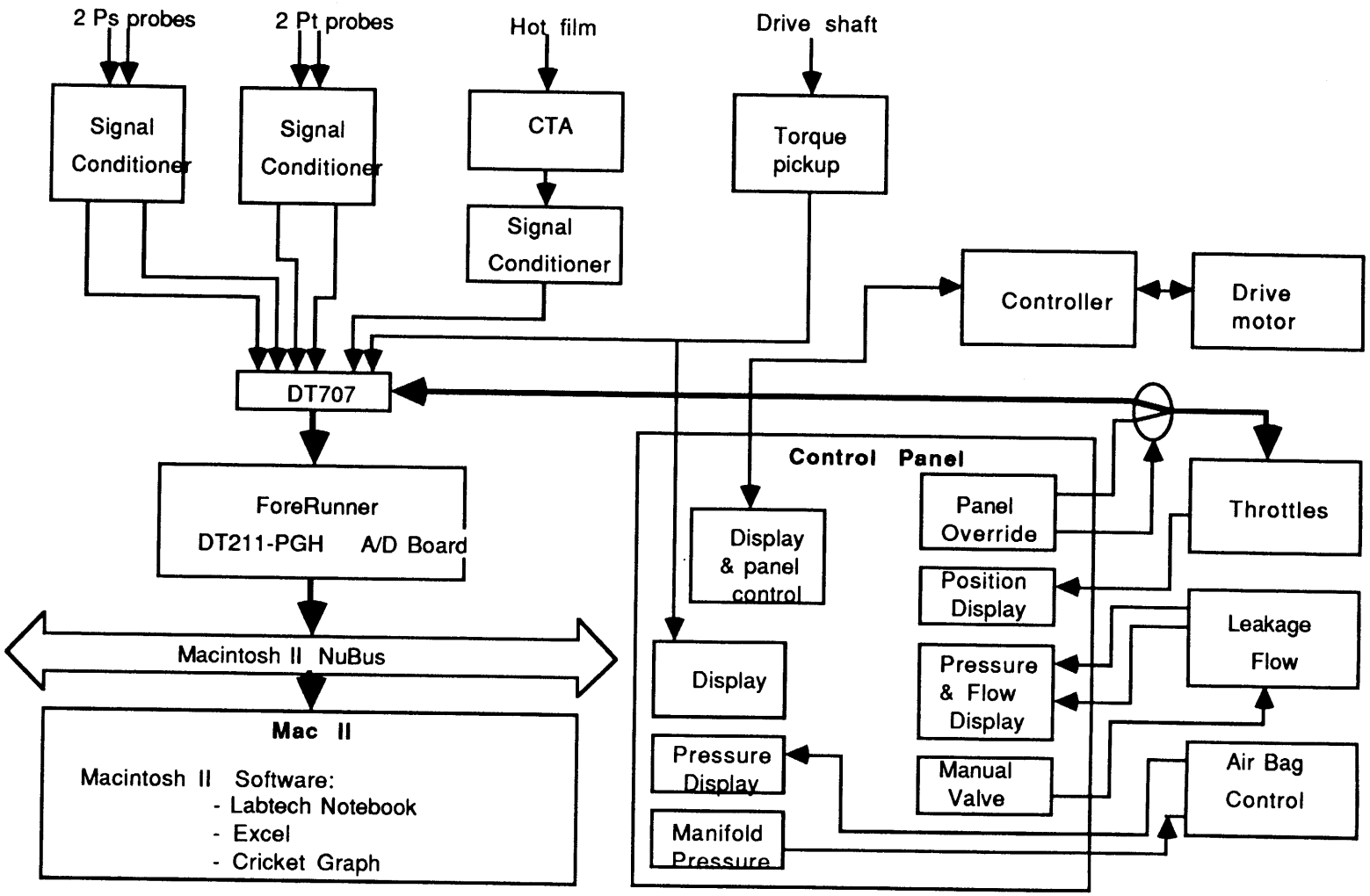

Figure 3.21: A/D signal flow chart.

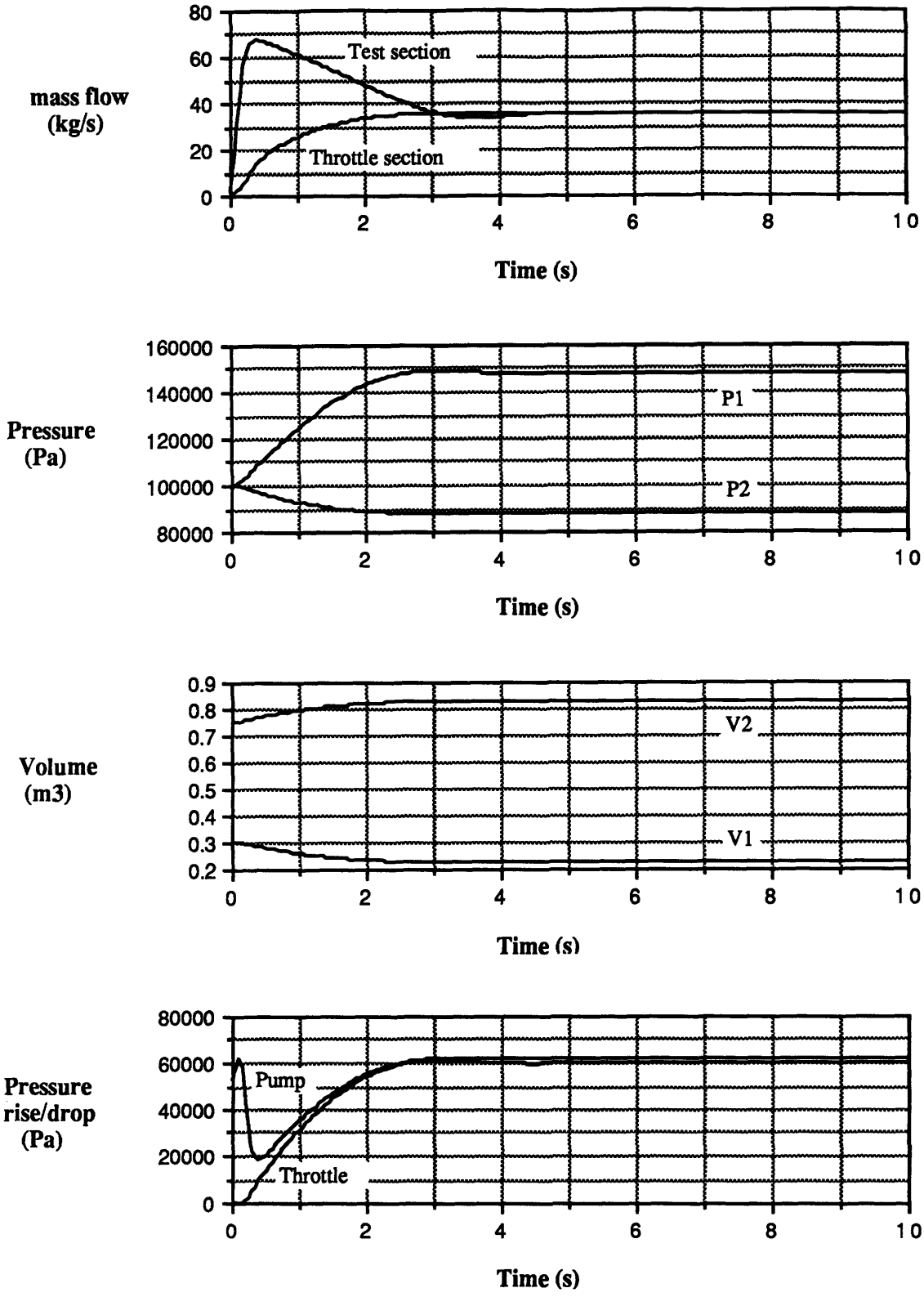

Figure 4.1: Transient response to an 'instant startup': Characterisitc time of the throttle ramp: 0.1s.

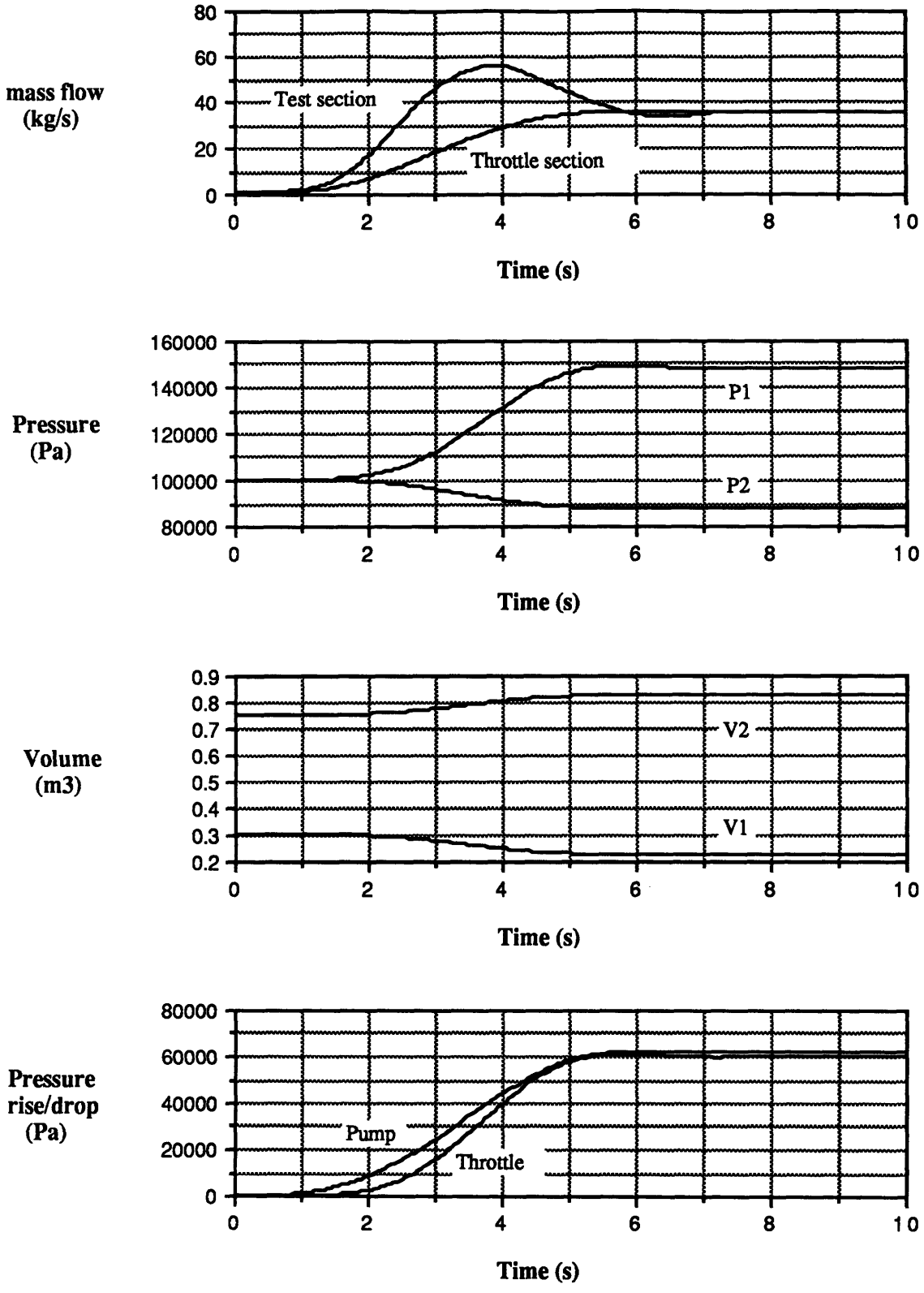

Figure 4.2: Transient response to a 'smooth startup': Characteristic time of the throttle ramp: 5s.

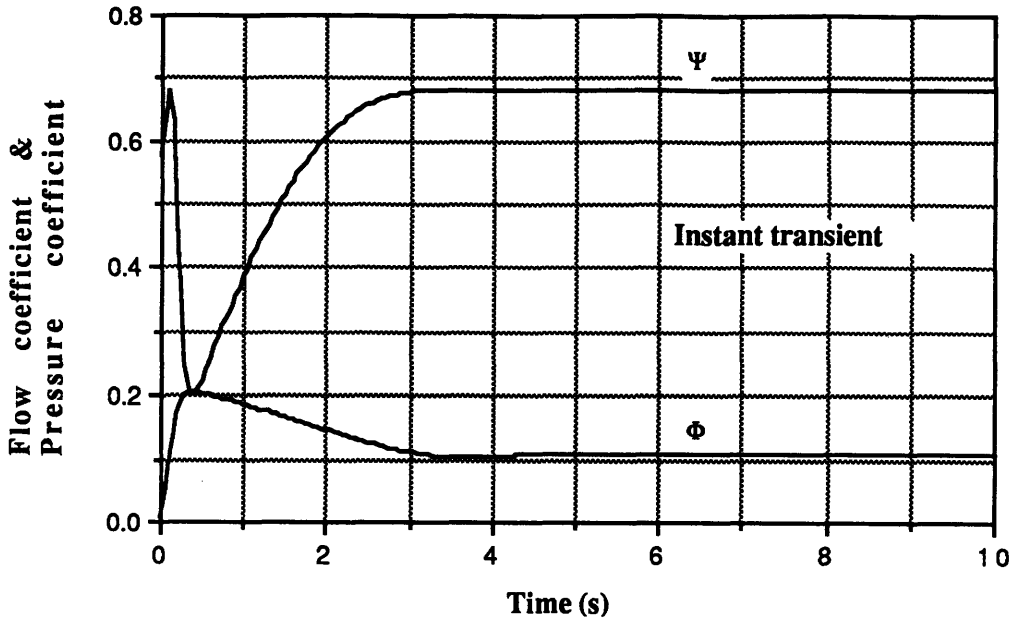

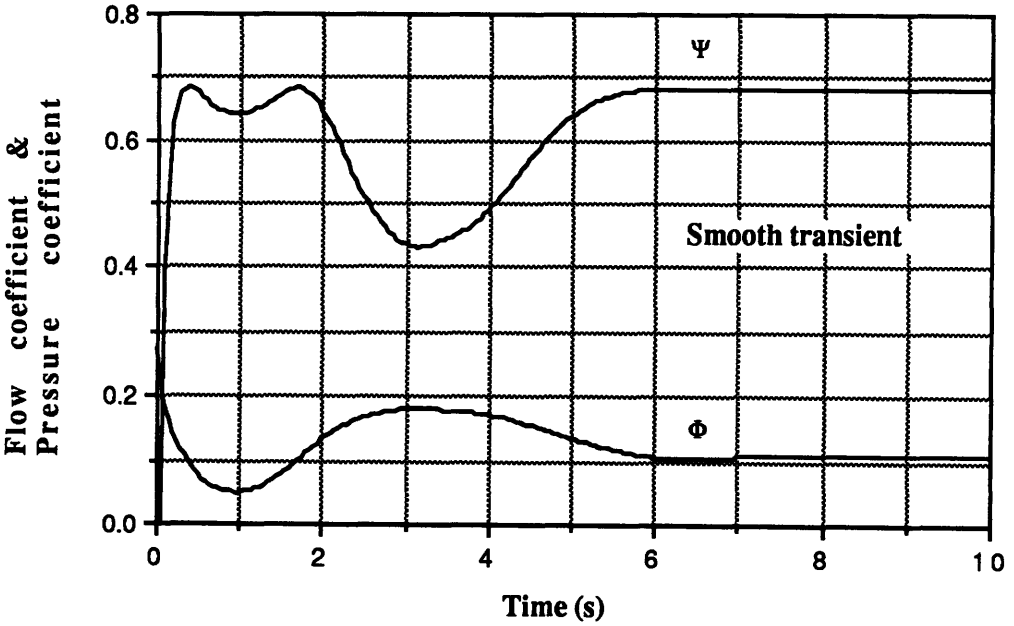

Figure 4.3: Transients in terms of flow coefficient Φ and pressure coefficient Ψ.

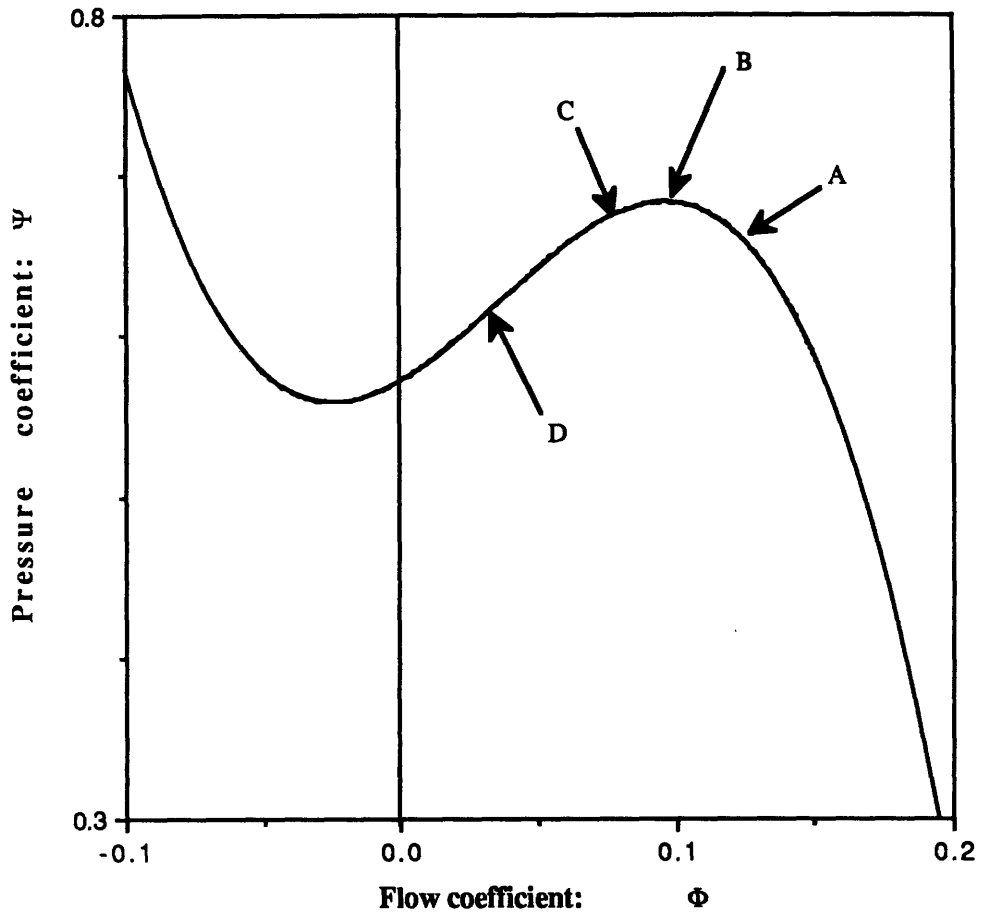

Figure 4.4: Location of the operating points on the characteristic.

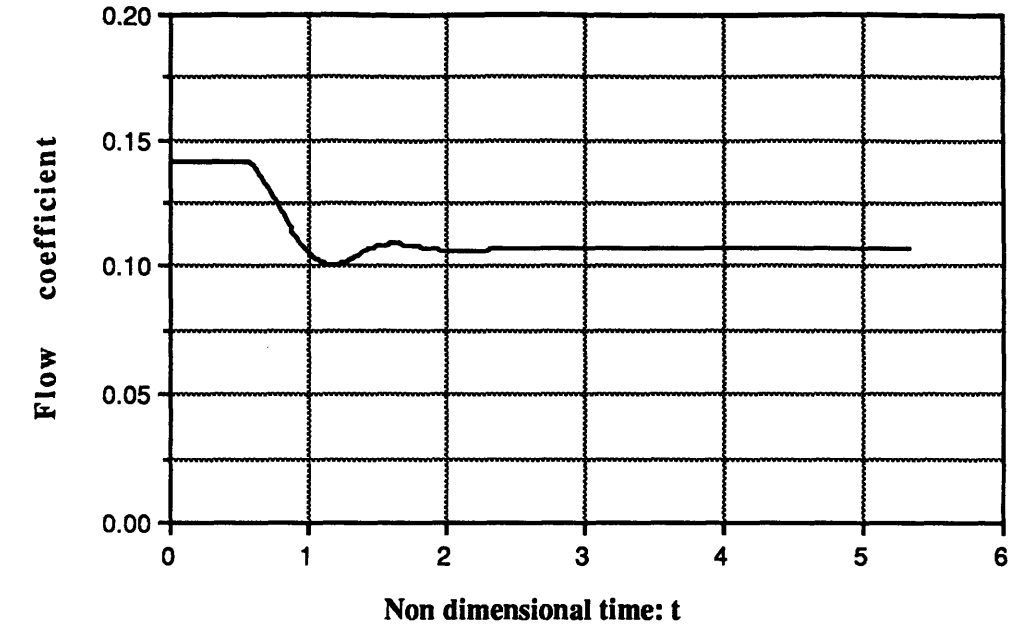

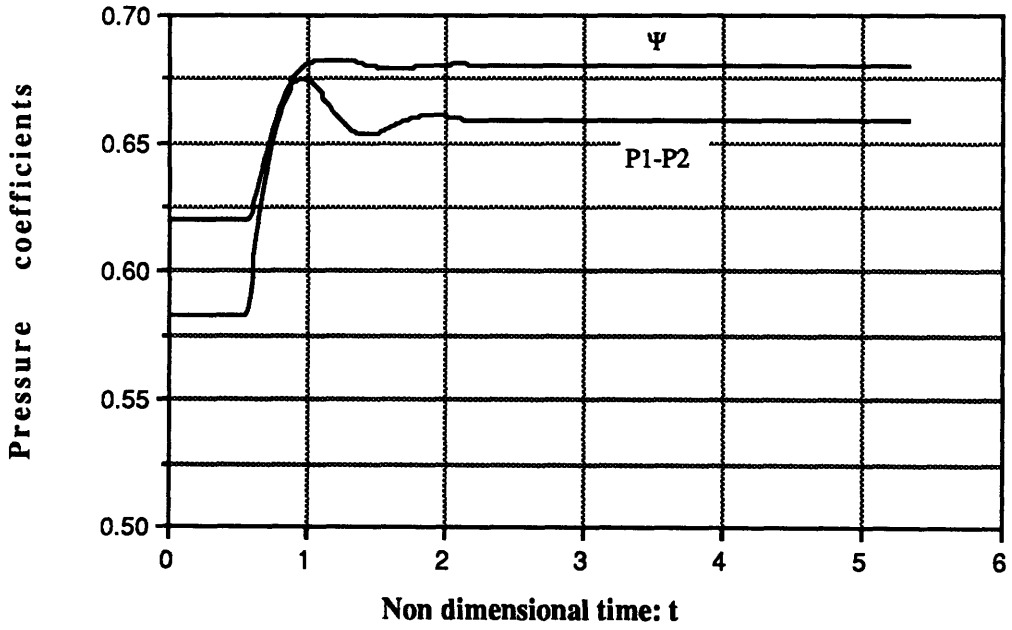

Figure 4.5: Response to point A: High damping:
Relaxation time is about one period.

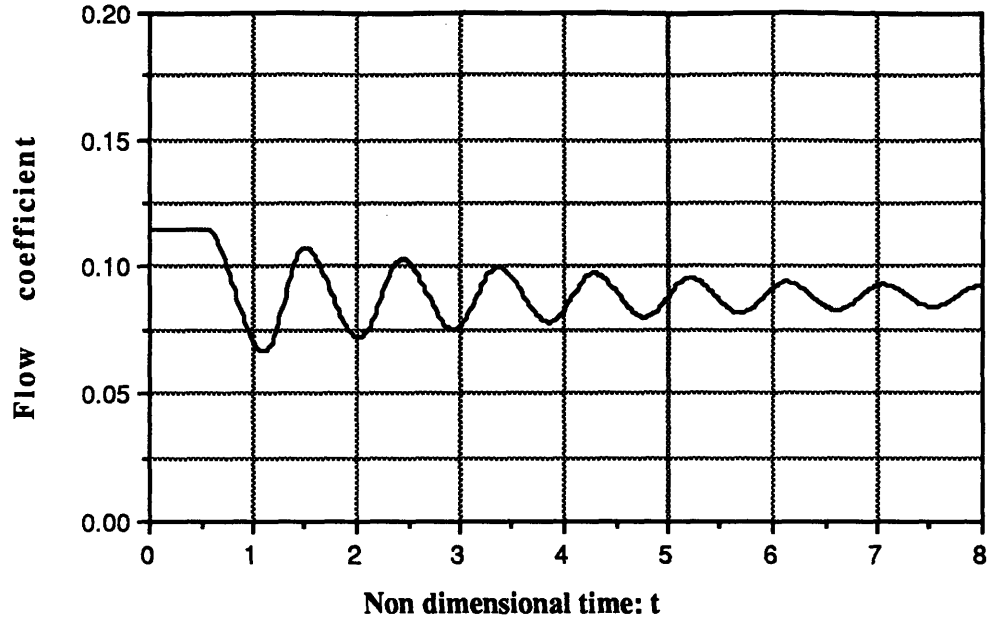

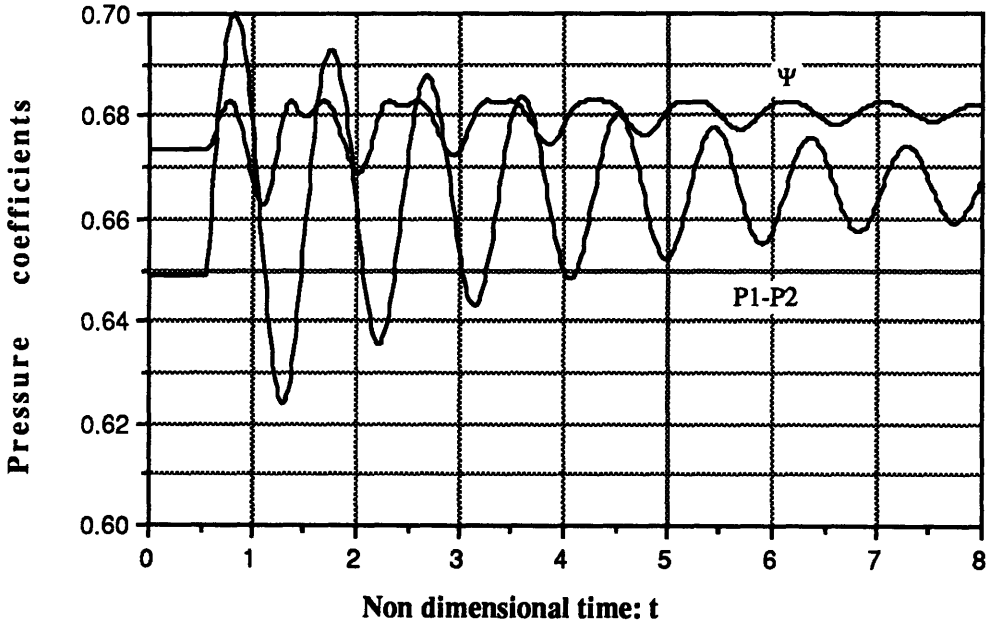

Figure 4.6: Response to point B: Low damping:
Relaxation time is about 14 periods.

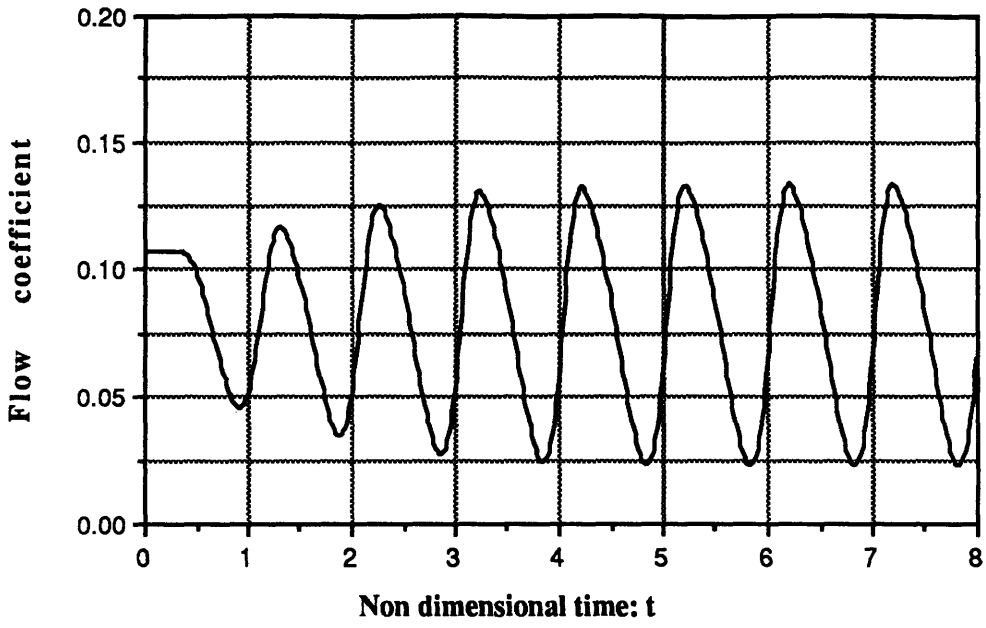

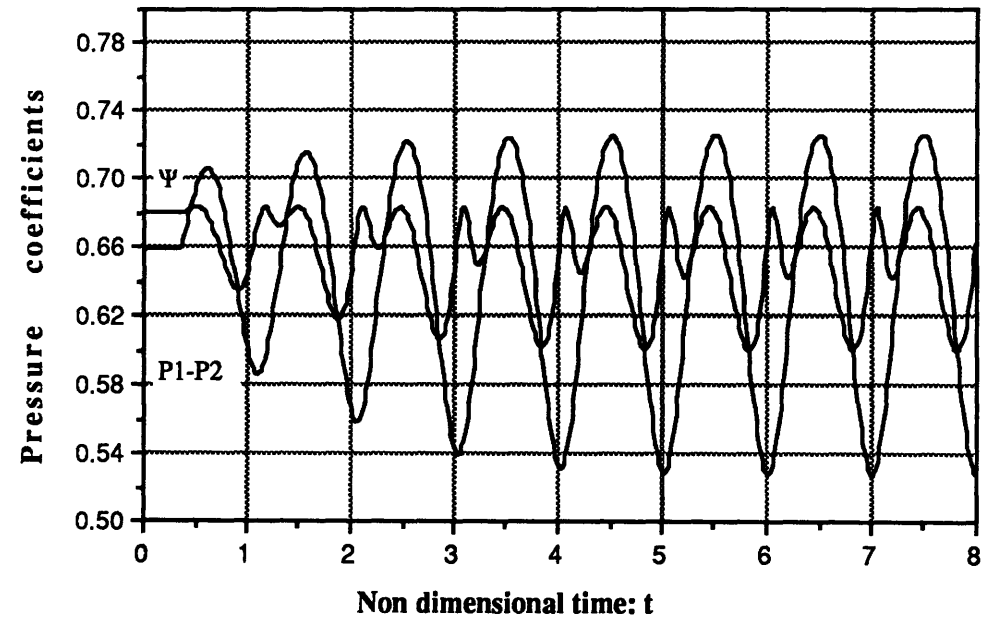

Figure 4.7: Response to point C: Mild surge:
Sustained oscillatory behavior without reverse flow.

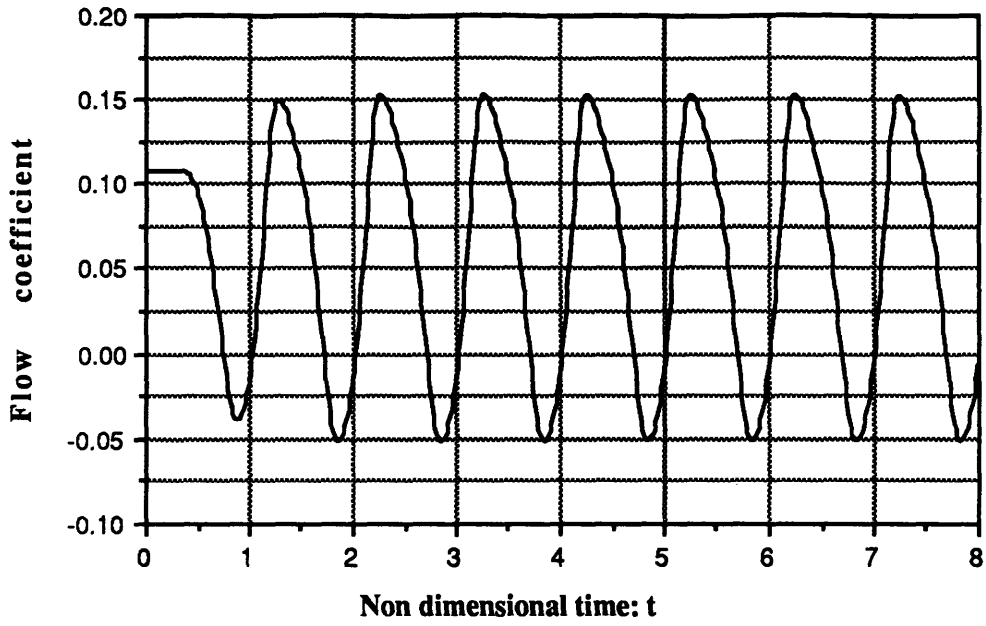

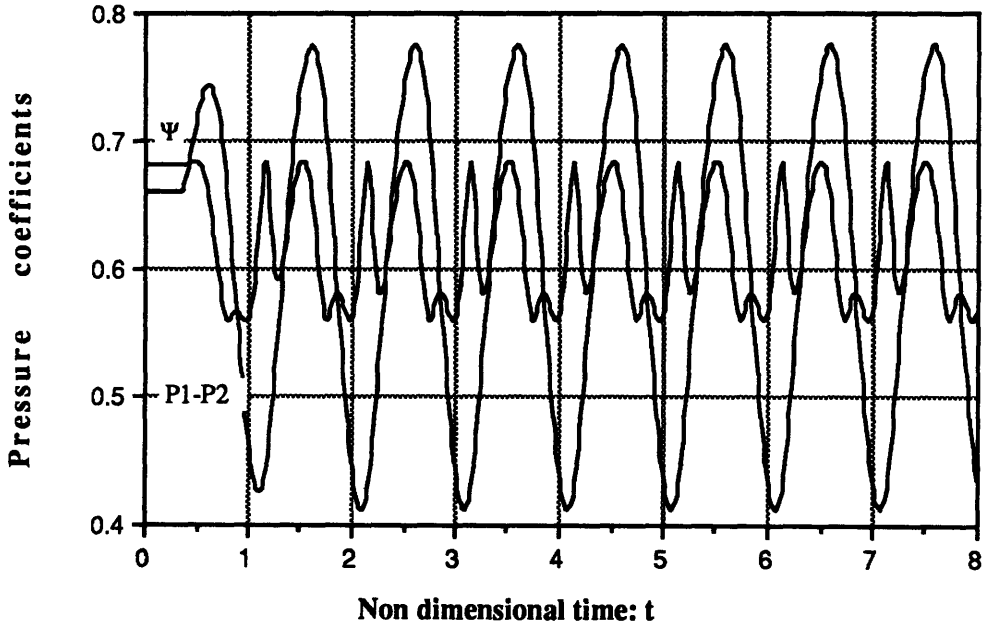

Figure 4.8: Response to point D: Deep surge:
Sustained oscillatory behavior with reverse flow.

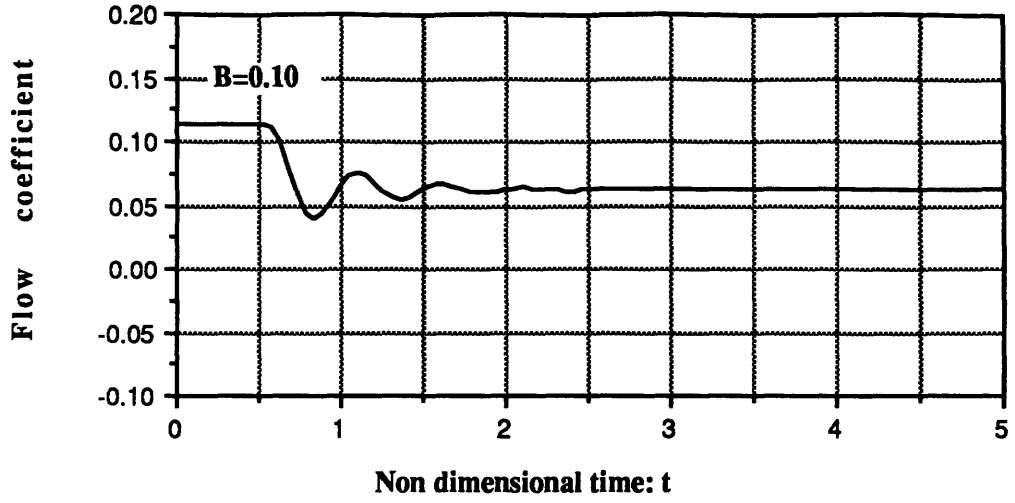

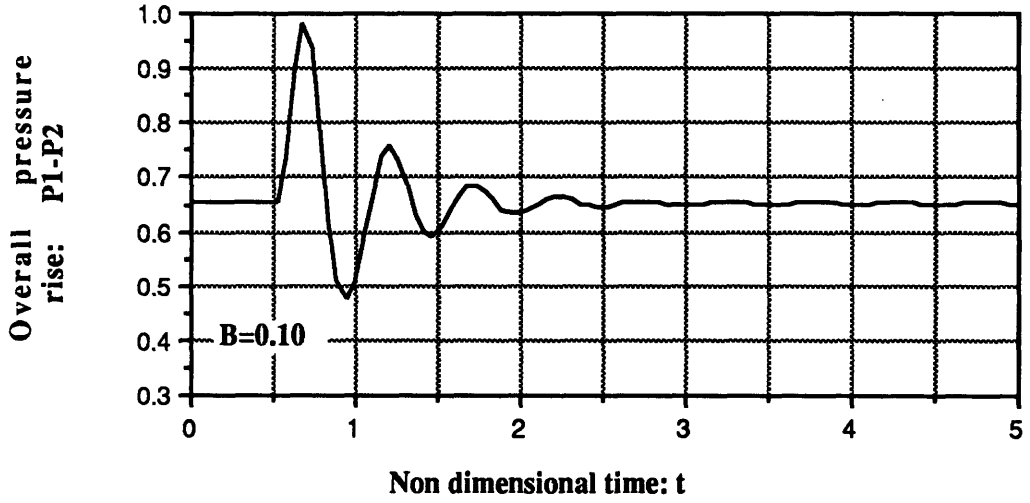

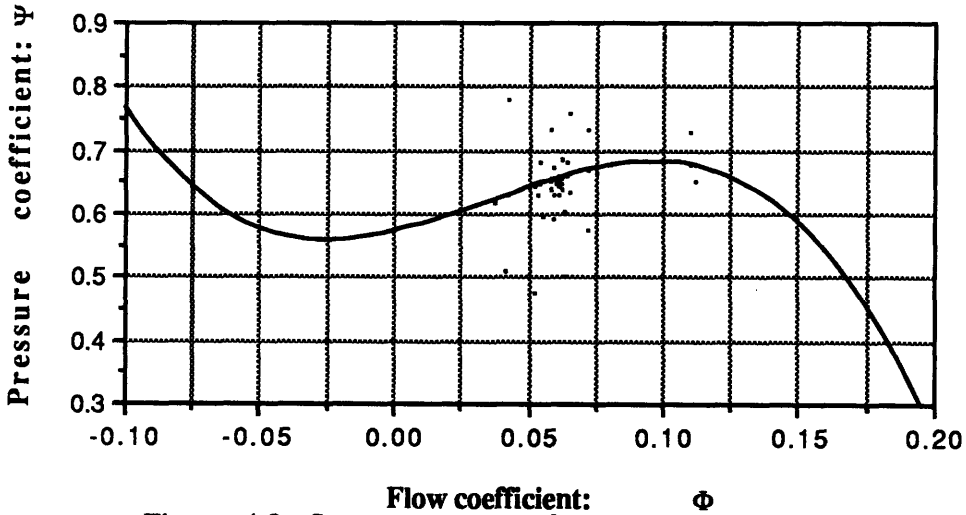

Figure 4.9: System response for B=0.10: Stabilized system.

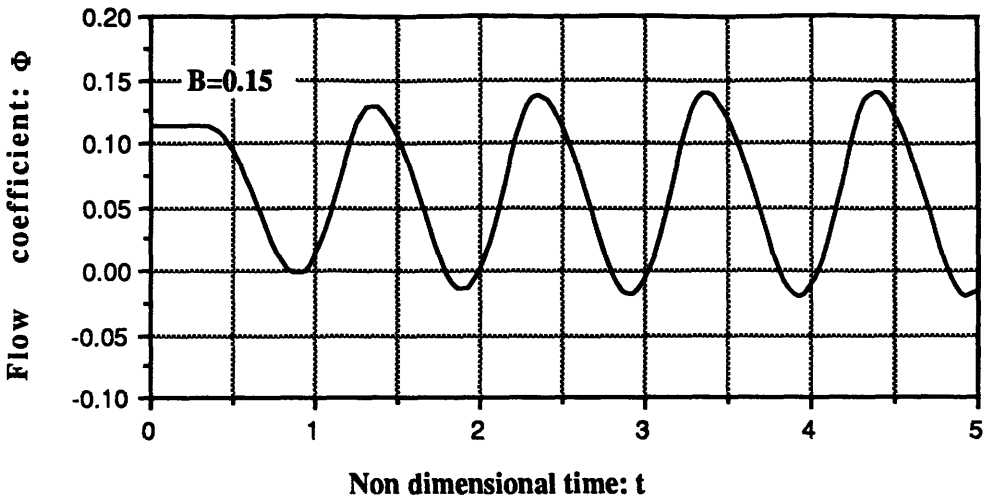

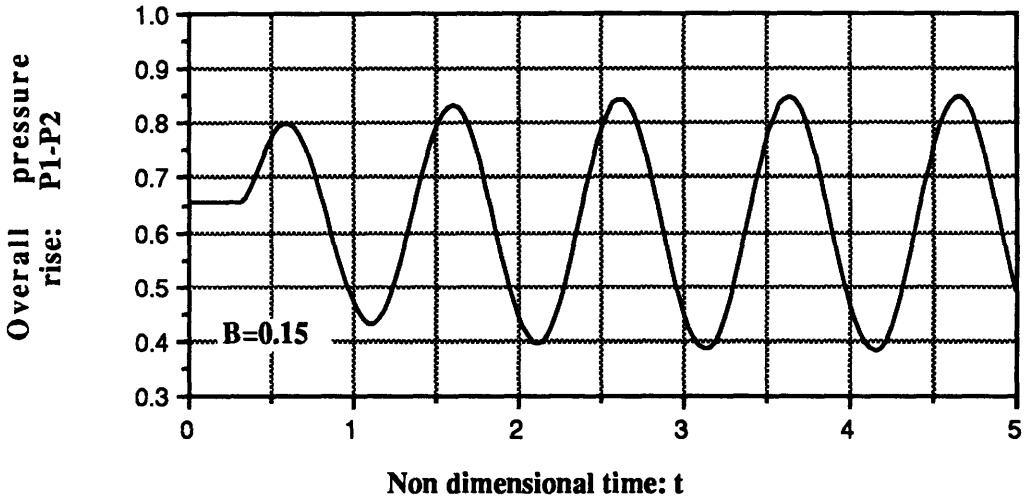

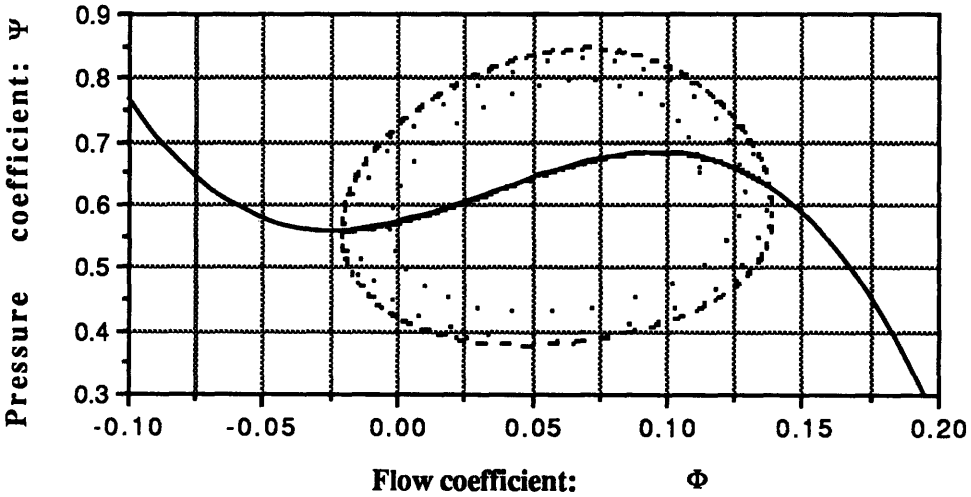

Figure 4.10: System response for B=0.15:
Quasi-circular limit cycle. Linearity is strong.

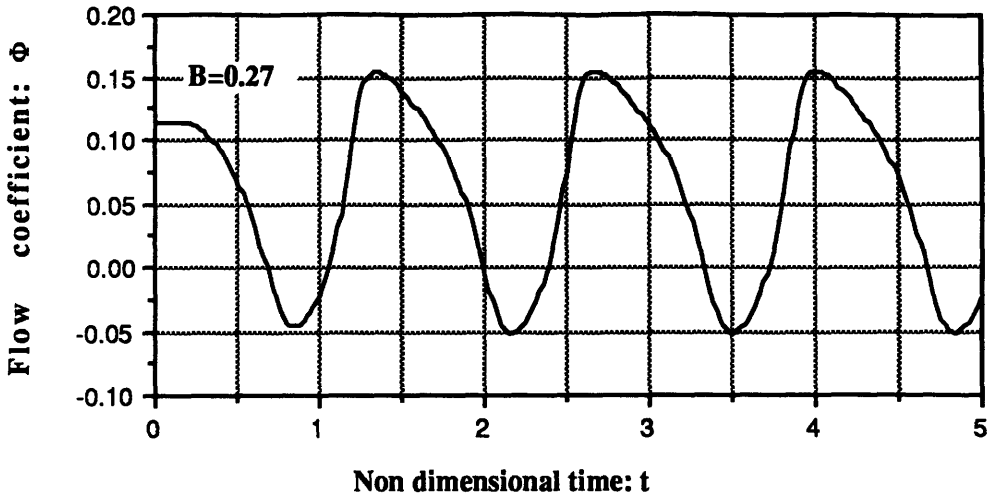

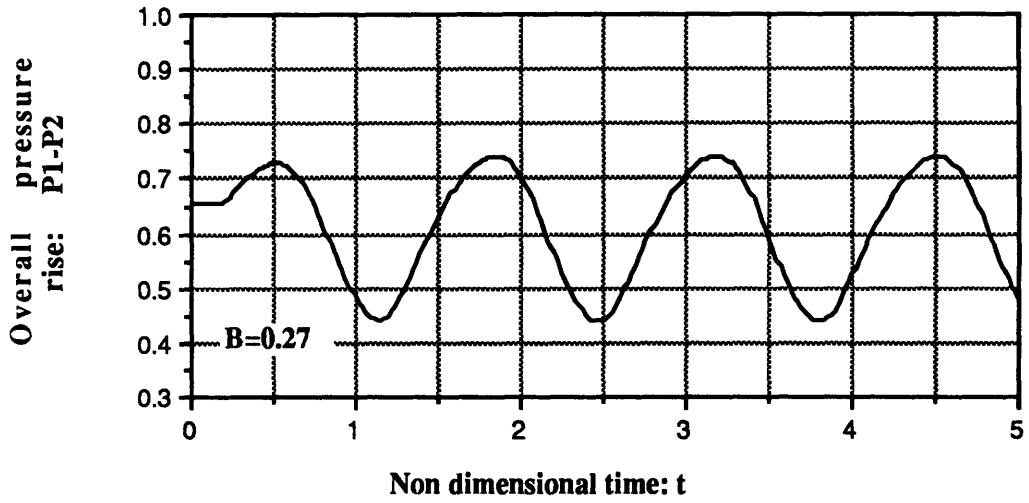

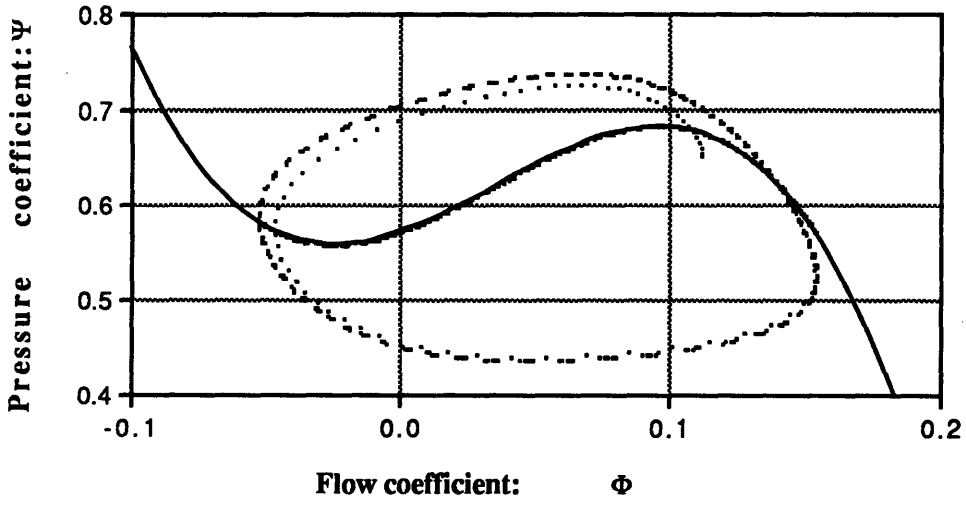

Figure 4.11: System response for B=0.27:
Distortion of the limit cycle. Non-linearity.

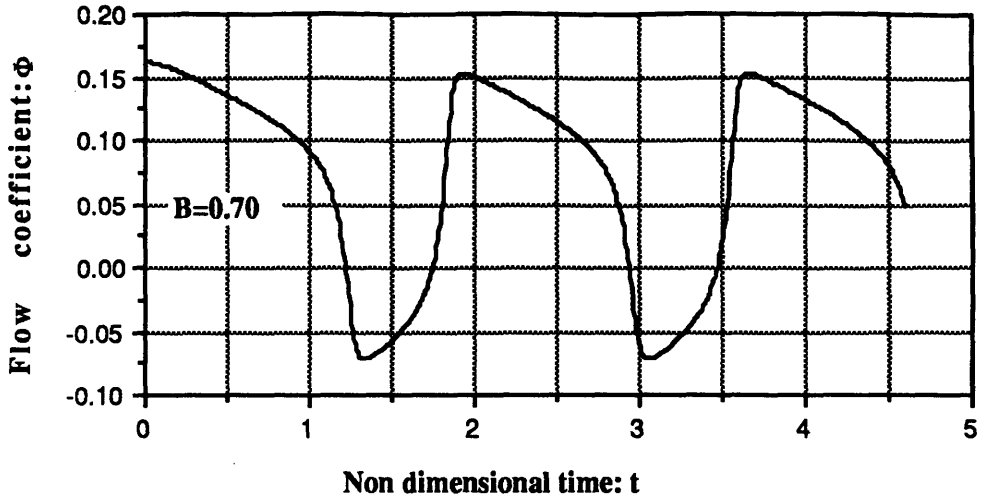

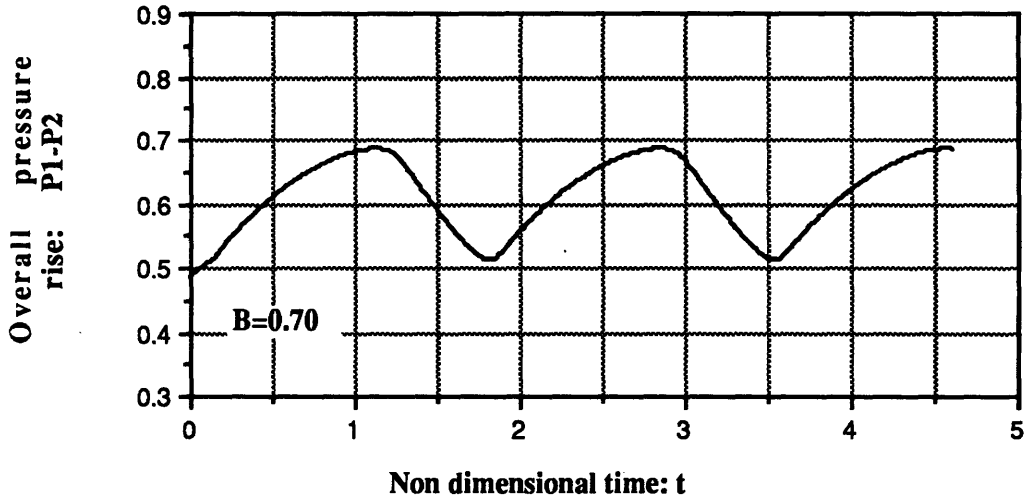

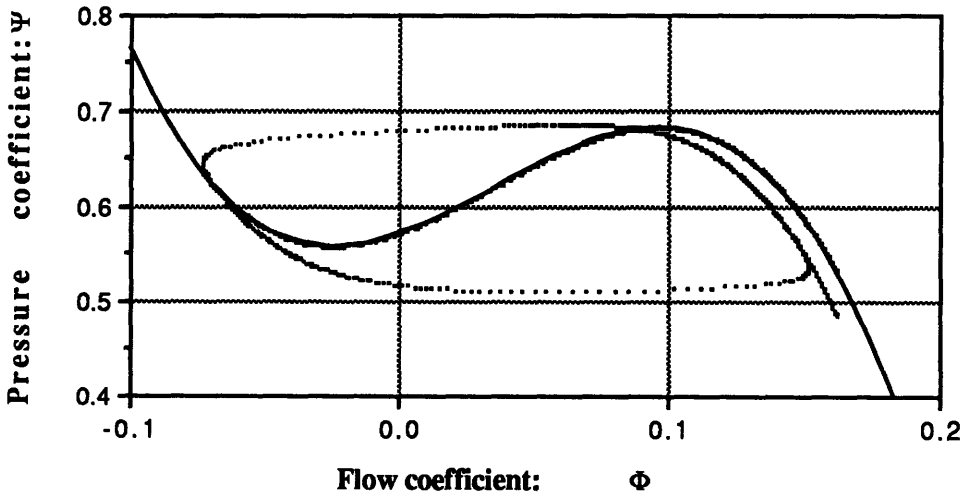

Figure 4.12: System response for B=0.7: Blowdown cycle. Non-linearity is dominant.

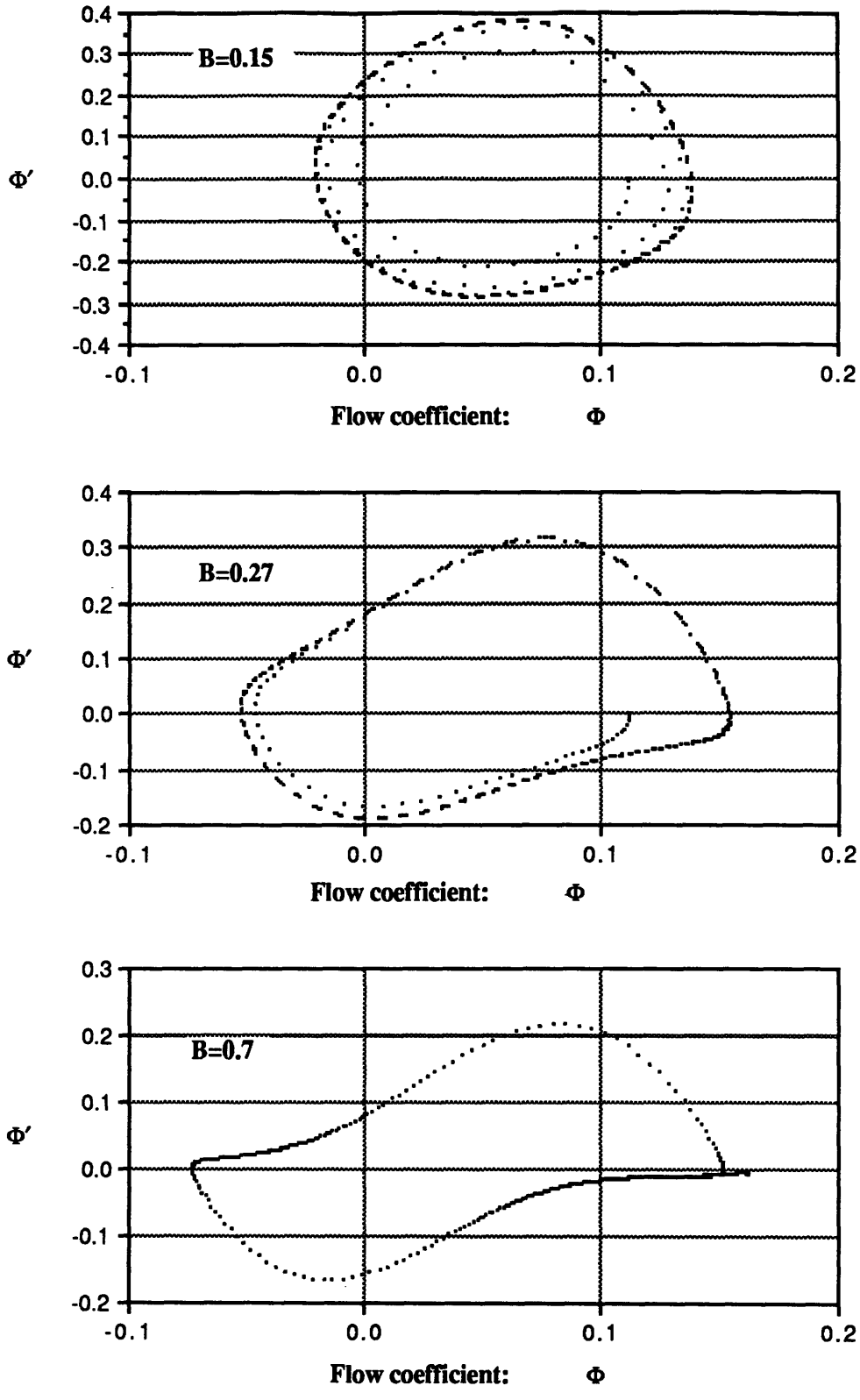

Figure 4.13: Phase plane portraits of Φ as a function of B: Effect of Non-linearity.

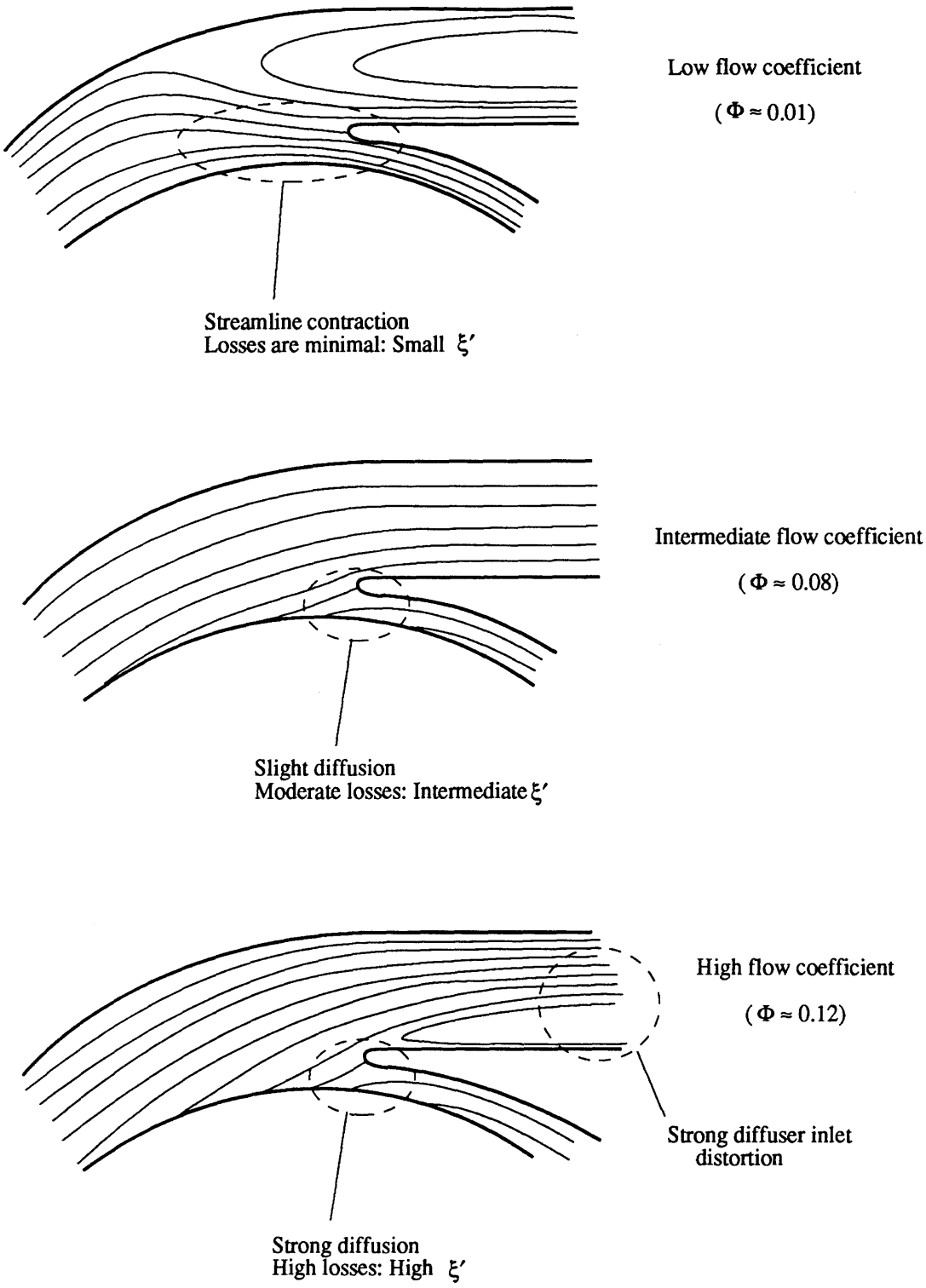

Figure 4.14: Volute tongue flow regimes and their effect on the tongue loss coefficient ξ'.

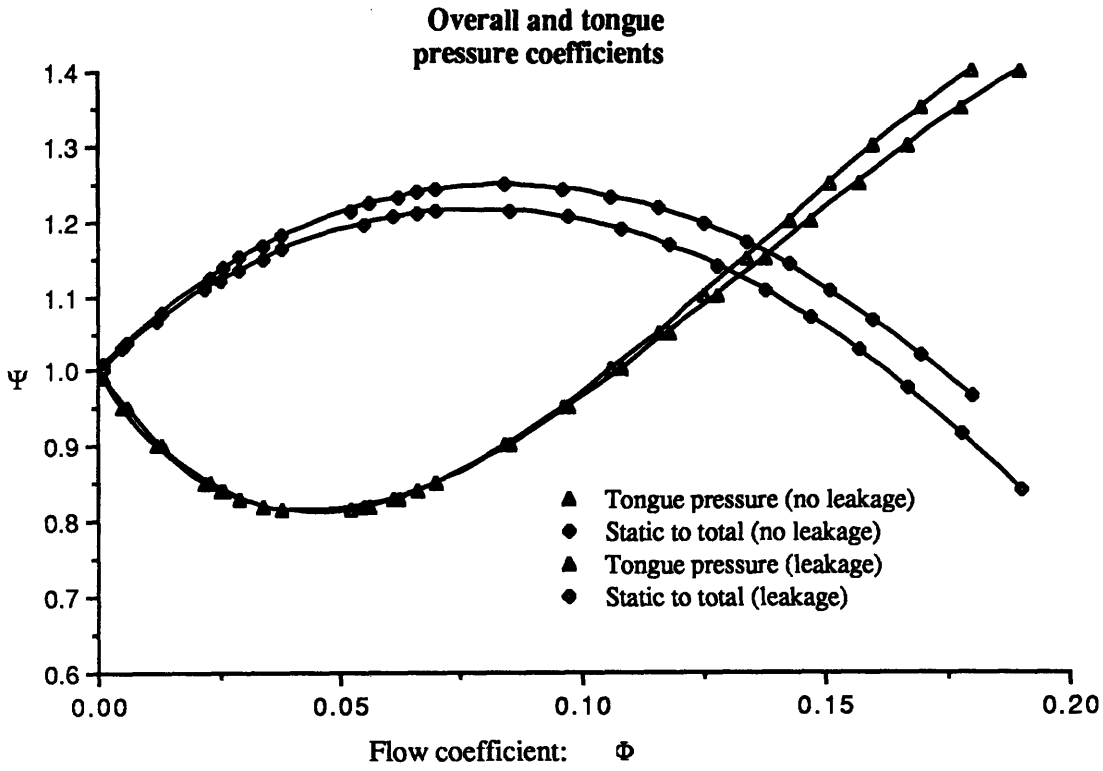

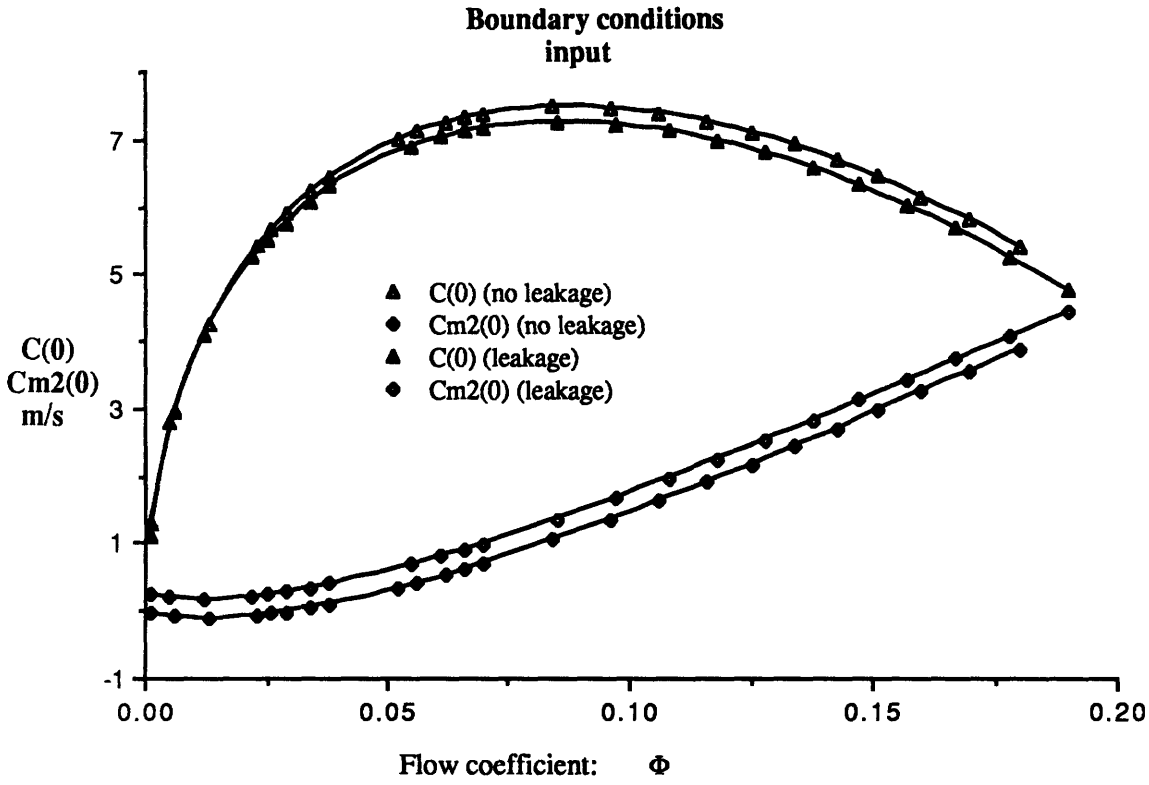

Figure 4.15: Boundary conditions for convergence: Choice of initial guesses as functions of flow rates.

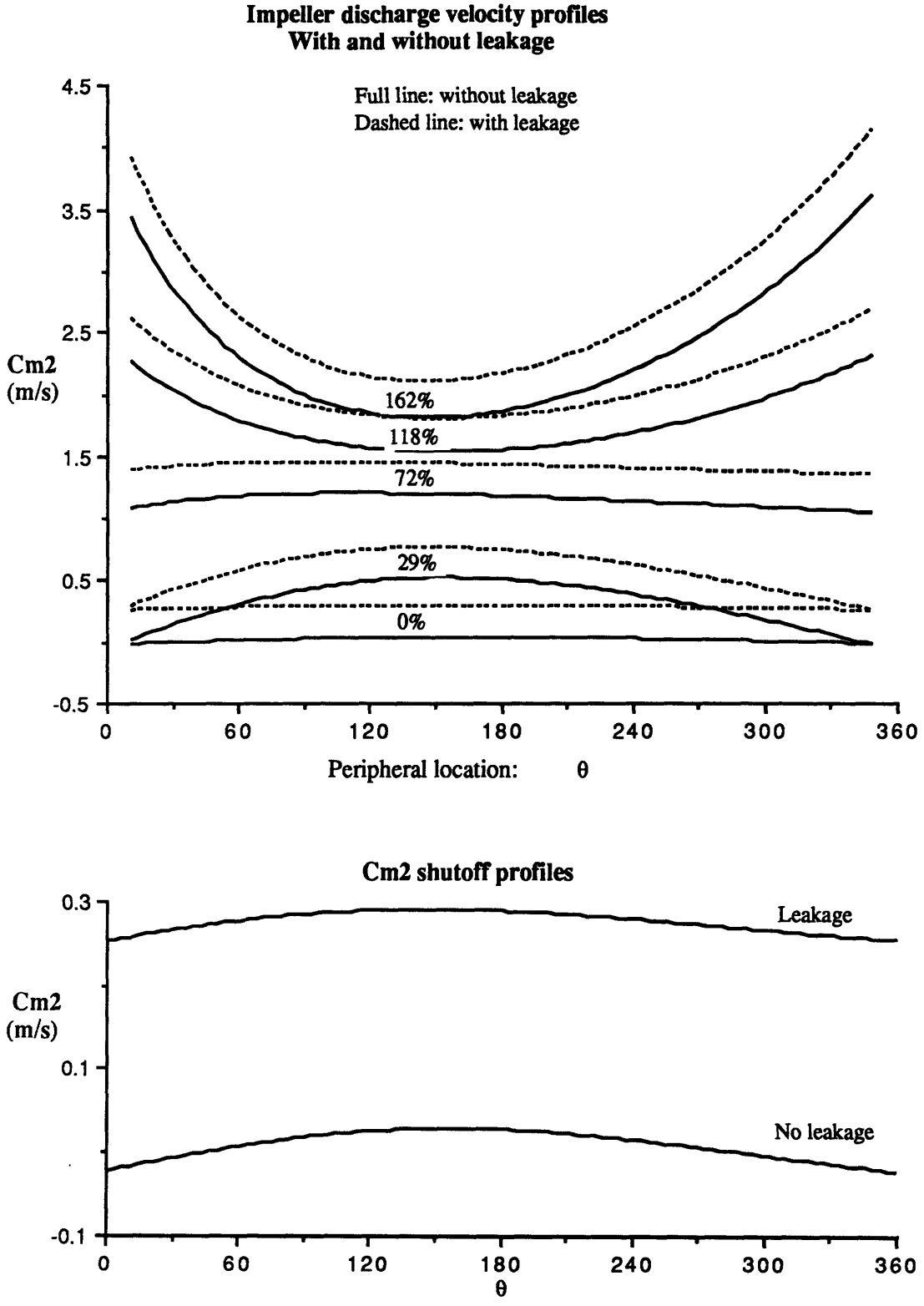

Figure 4.16: Impeller discharge velocity profiles.

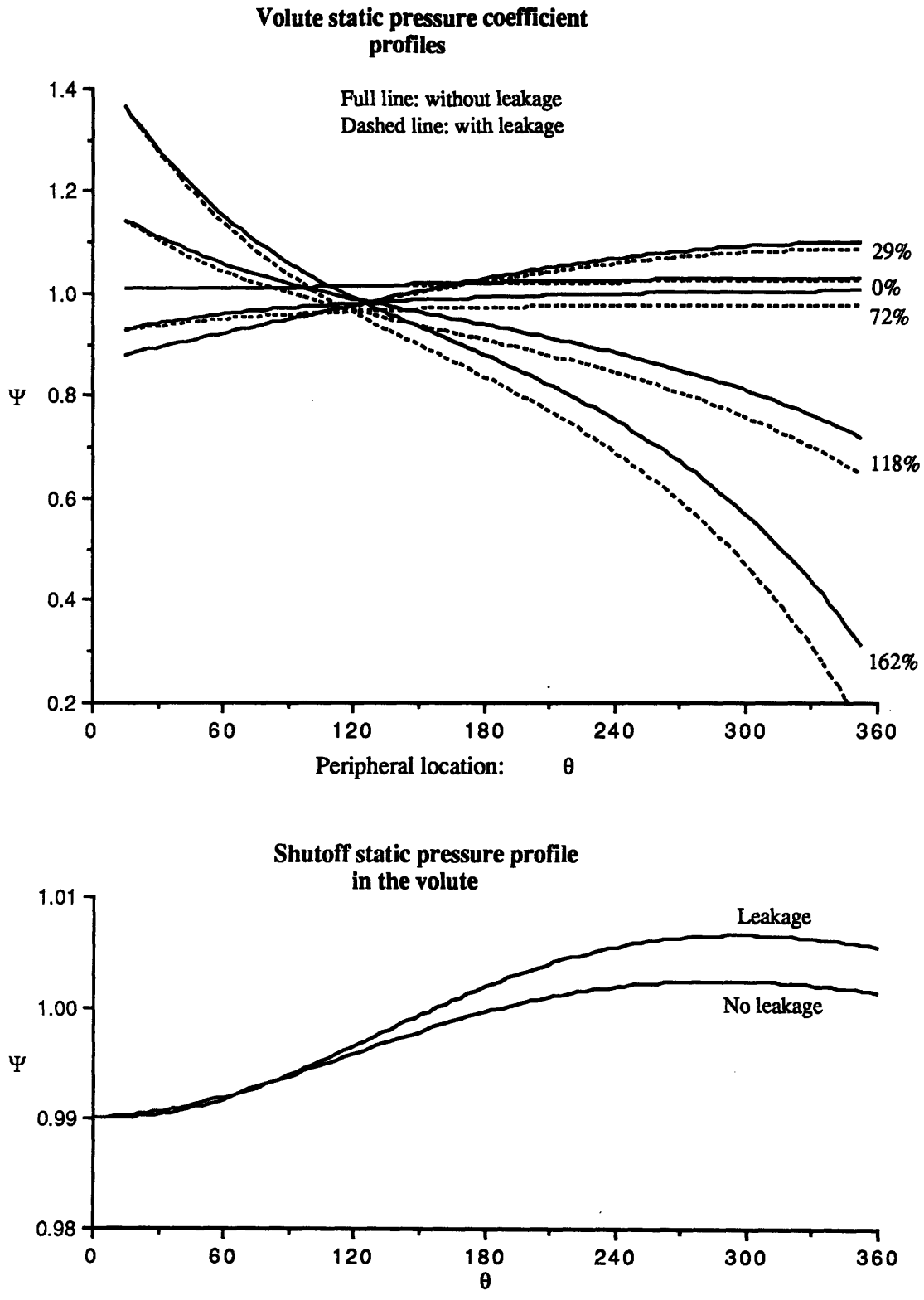

Figure 4.17: Volute static pressure profiles.

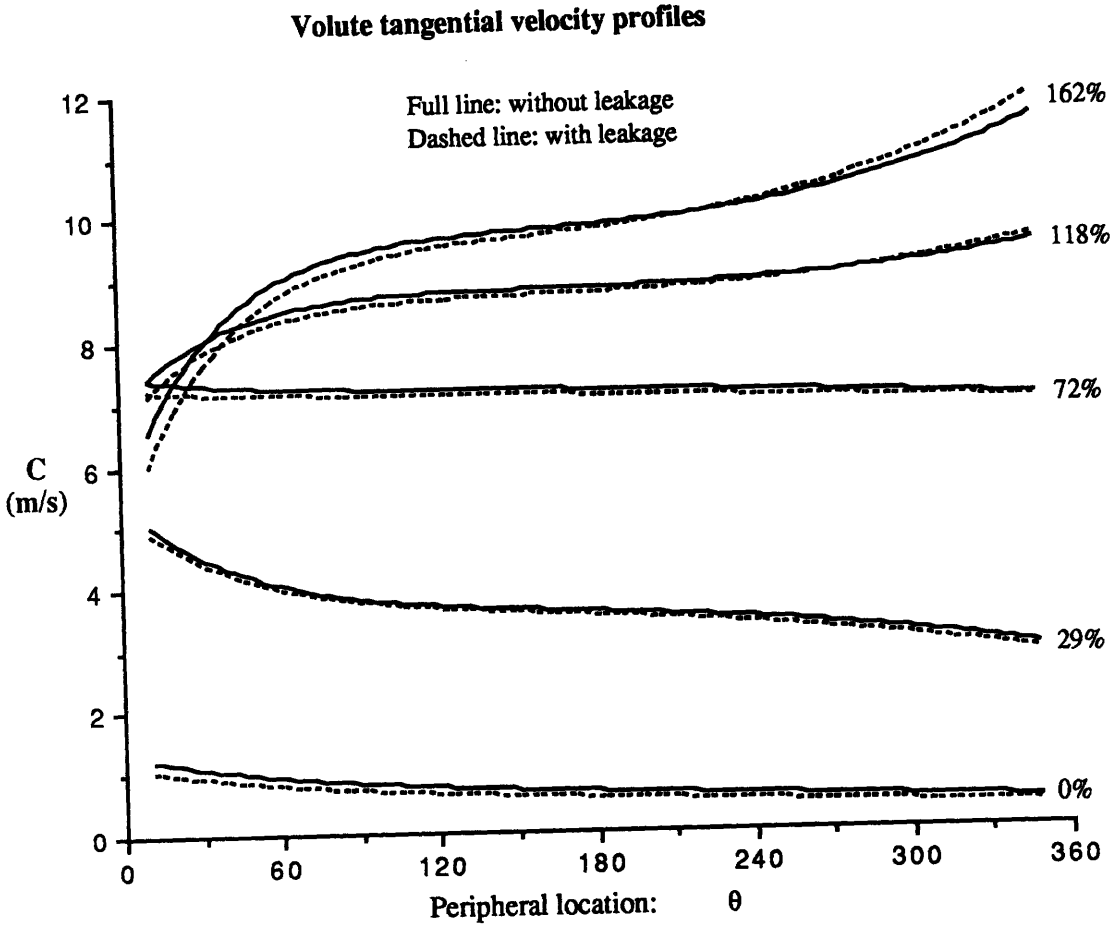

Figure 4.18: Volute tangential velocity profiles.

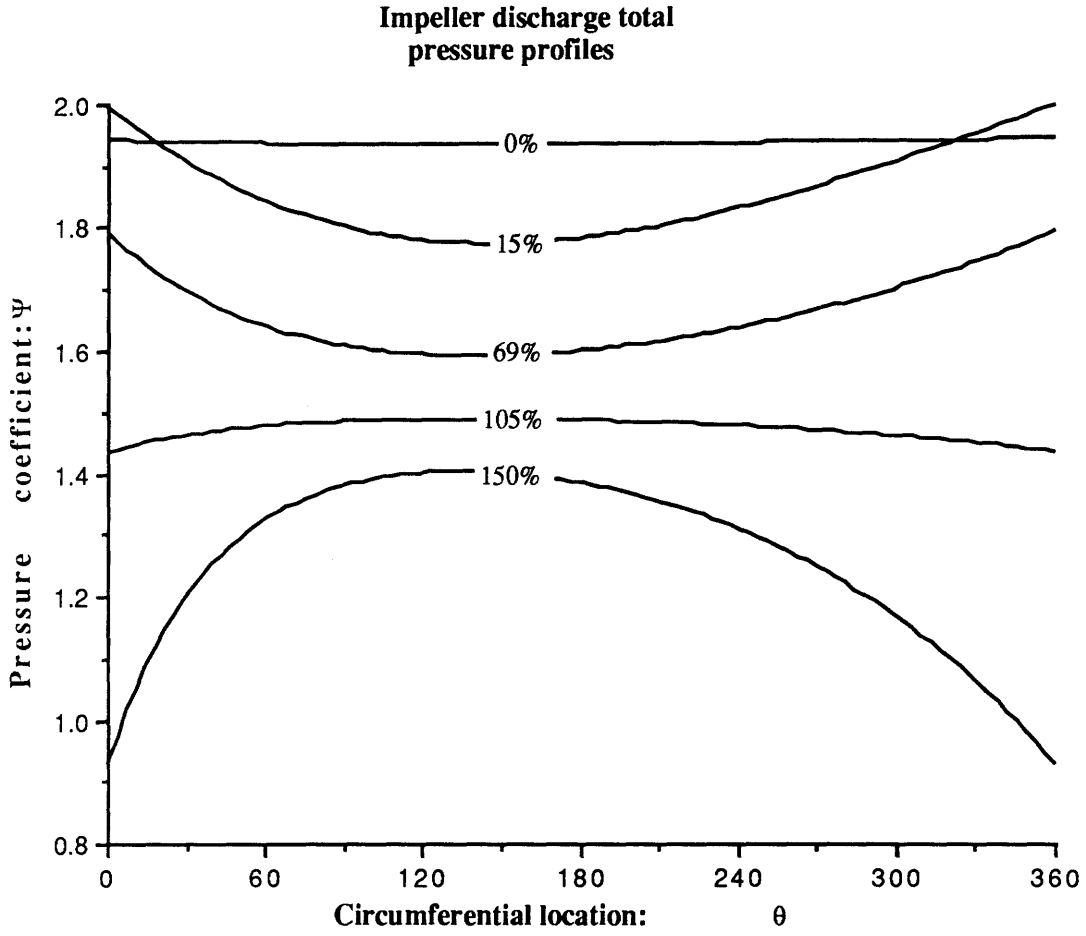

Figure 4.19: Impeller discharge absolute total pressure profiles.

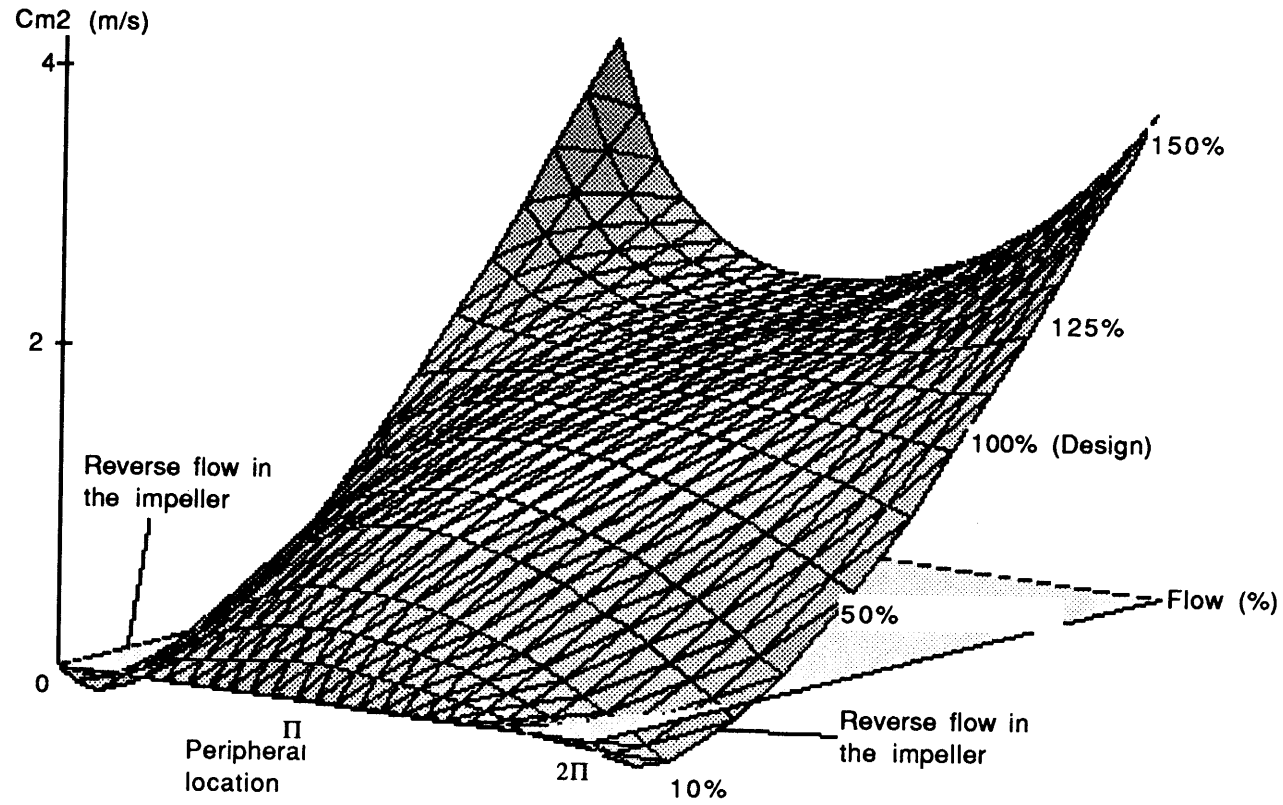

Figure 4.20: Impeller discharge velocity profiles in parameter space: Surface rendering of C_{m2} (θ,Φ).

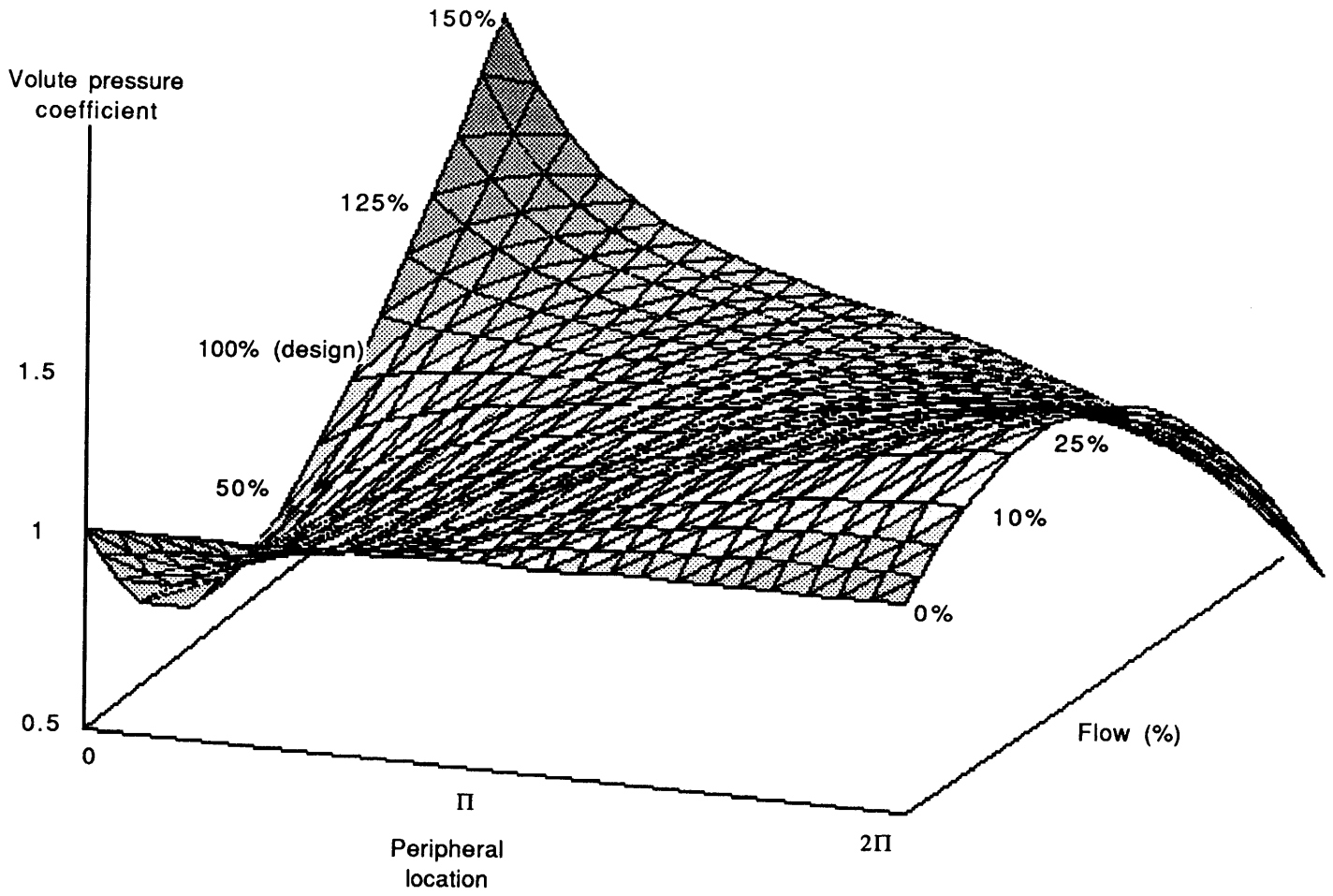

Figure 4.21: Volute static pressure profiles in parameter space: Surface rendering of Ψ_s (θ,Φ).

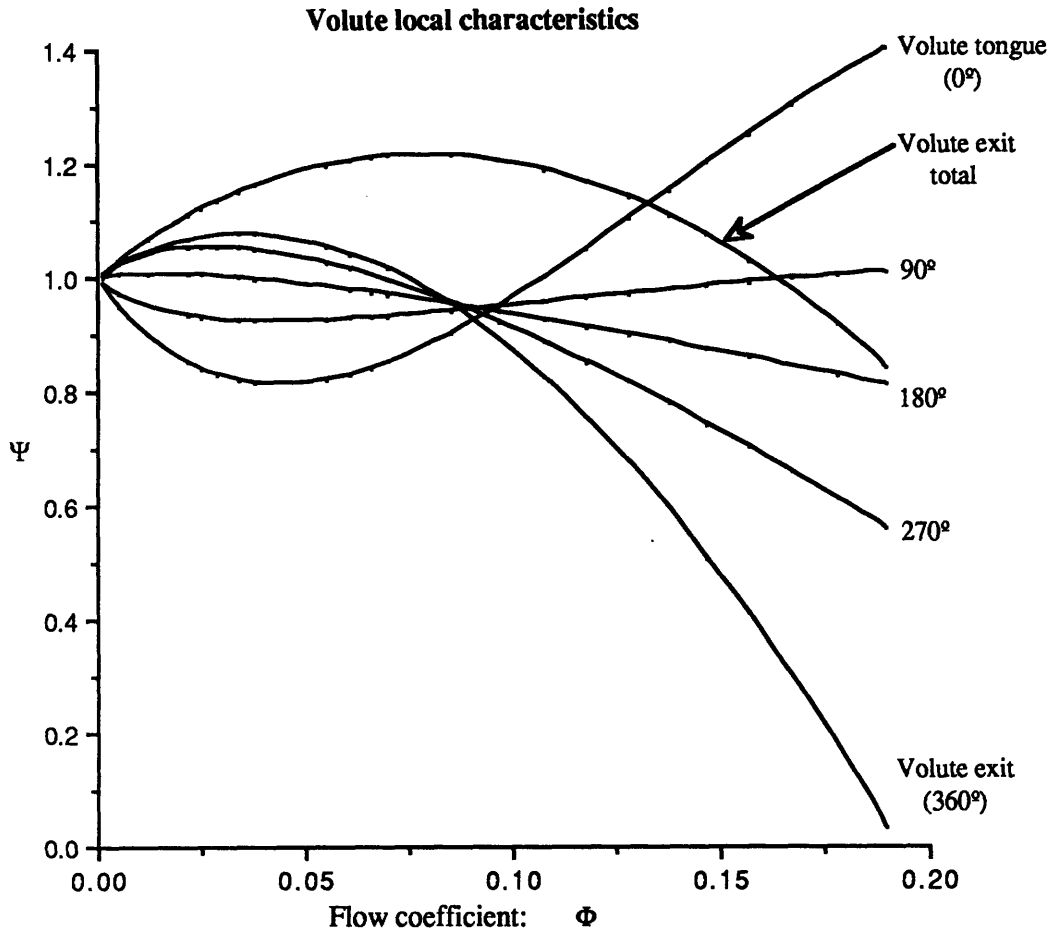

Figure 4.22: Volute local pumping characteristics at various circumferential locations.

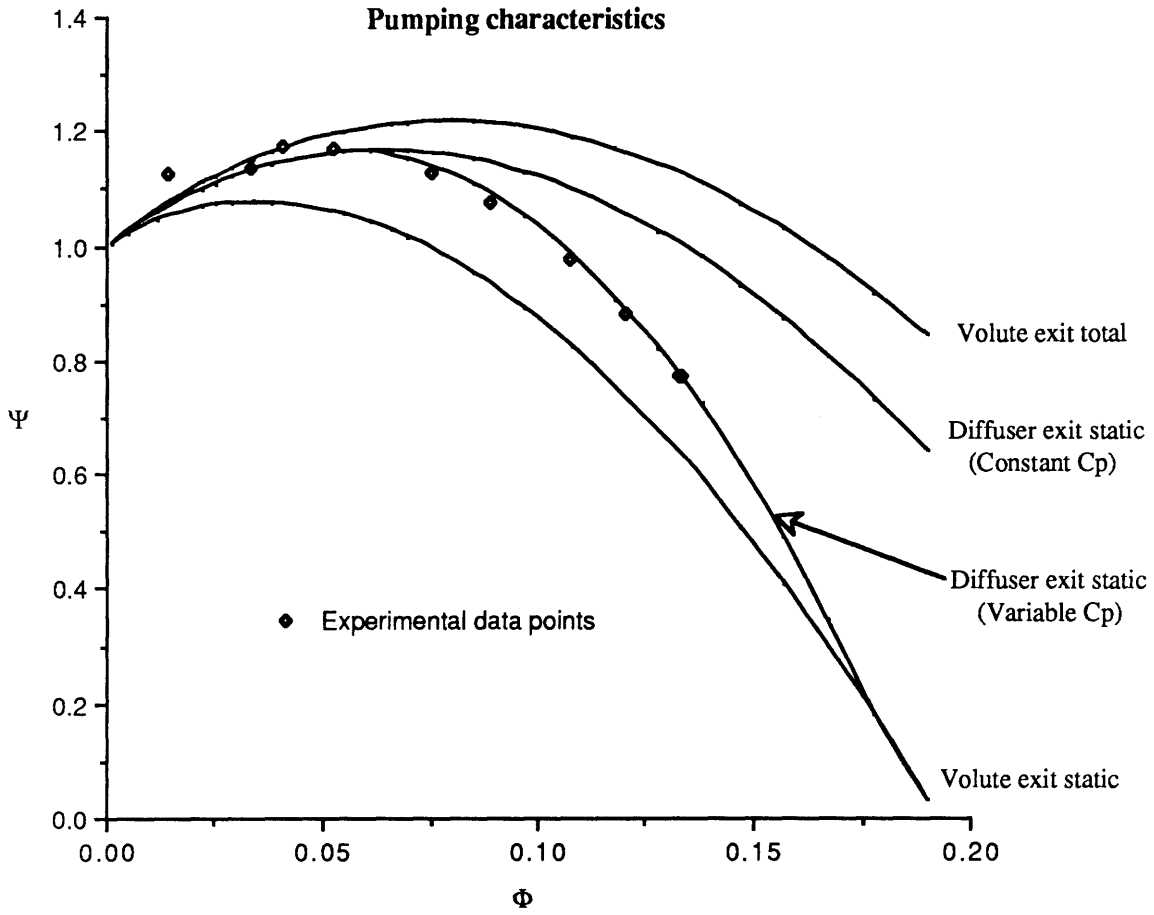

Figure 4.23: Diffuser operating characteristics.

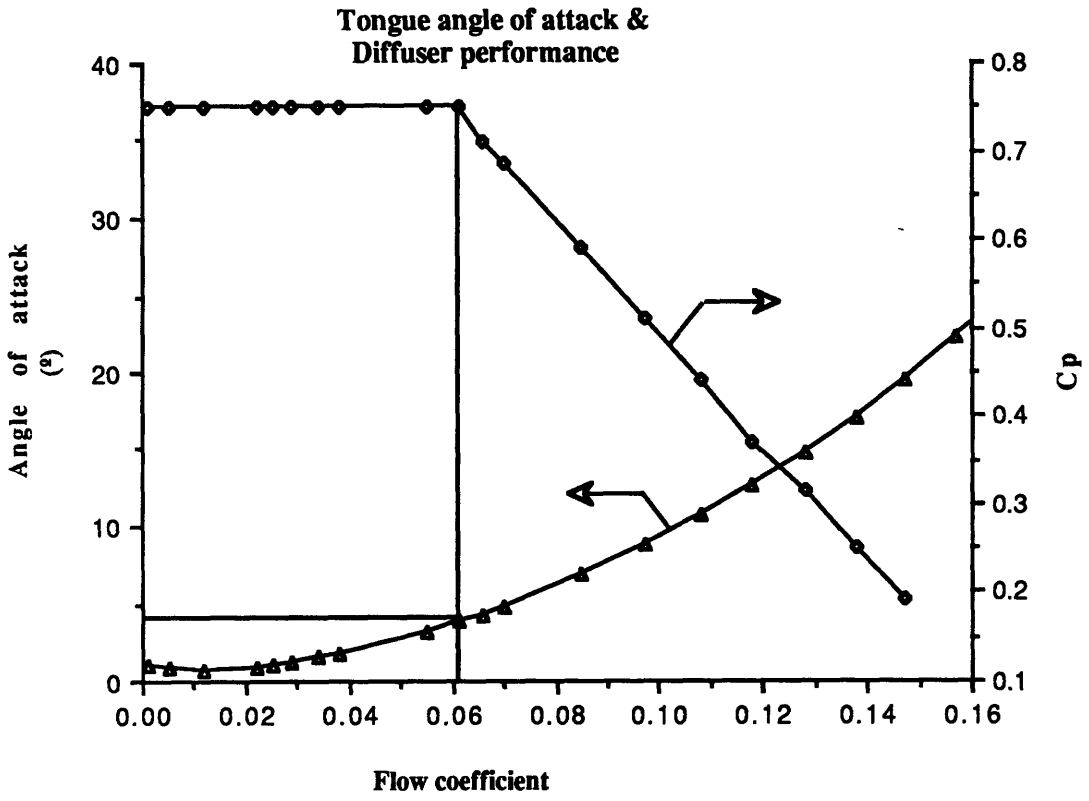

Figure 4.24: Volute tongue angle of attack and C_p modelling.

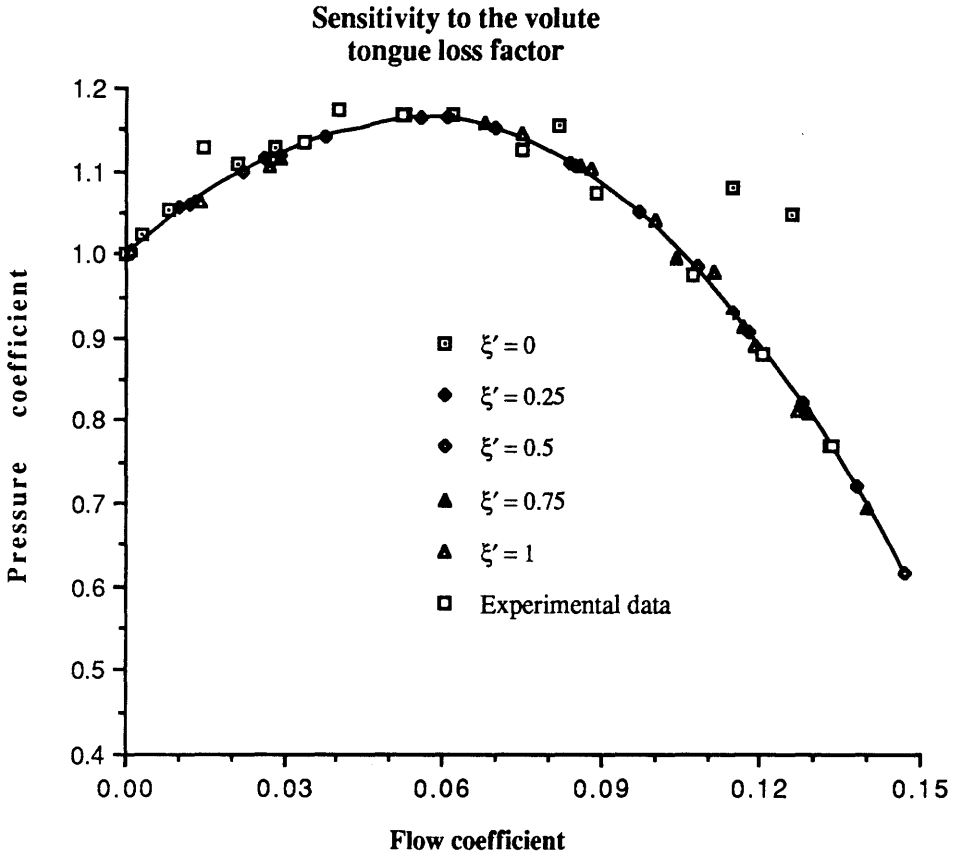

Figure 4.25: Sensitivity of the characteristic to ξ'.

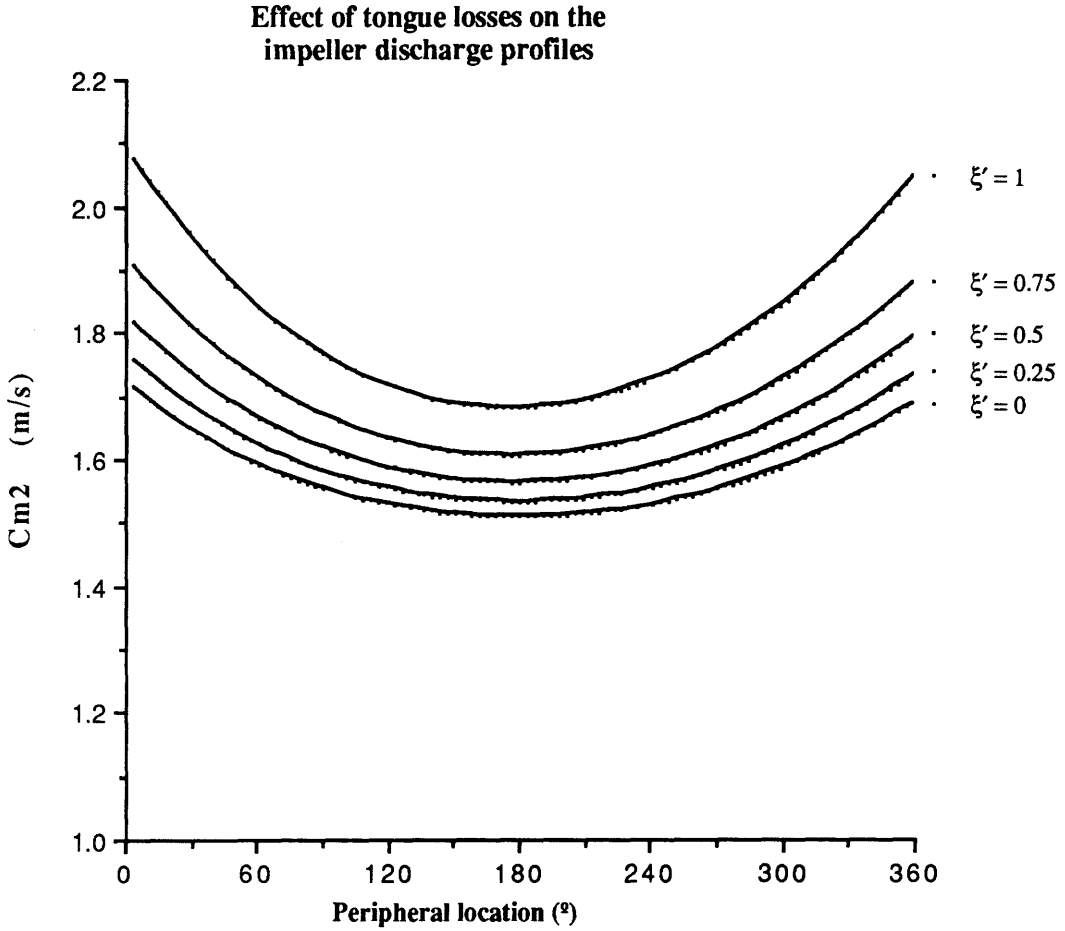

Figure 4.26: Sensitivity of the impeller dicharge velocity profiles to ξ'.

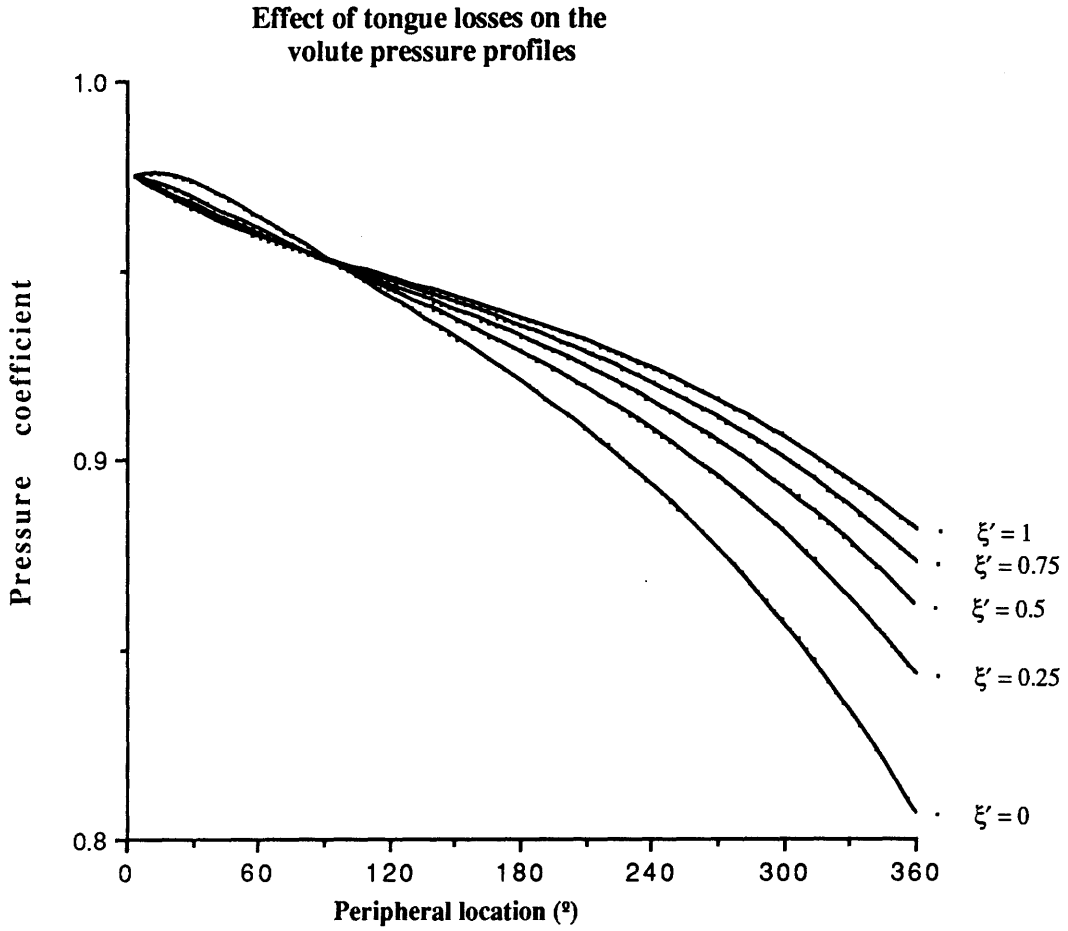

Figure 4.27: Sensitivity of the volute pressure profiles to ξ'.

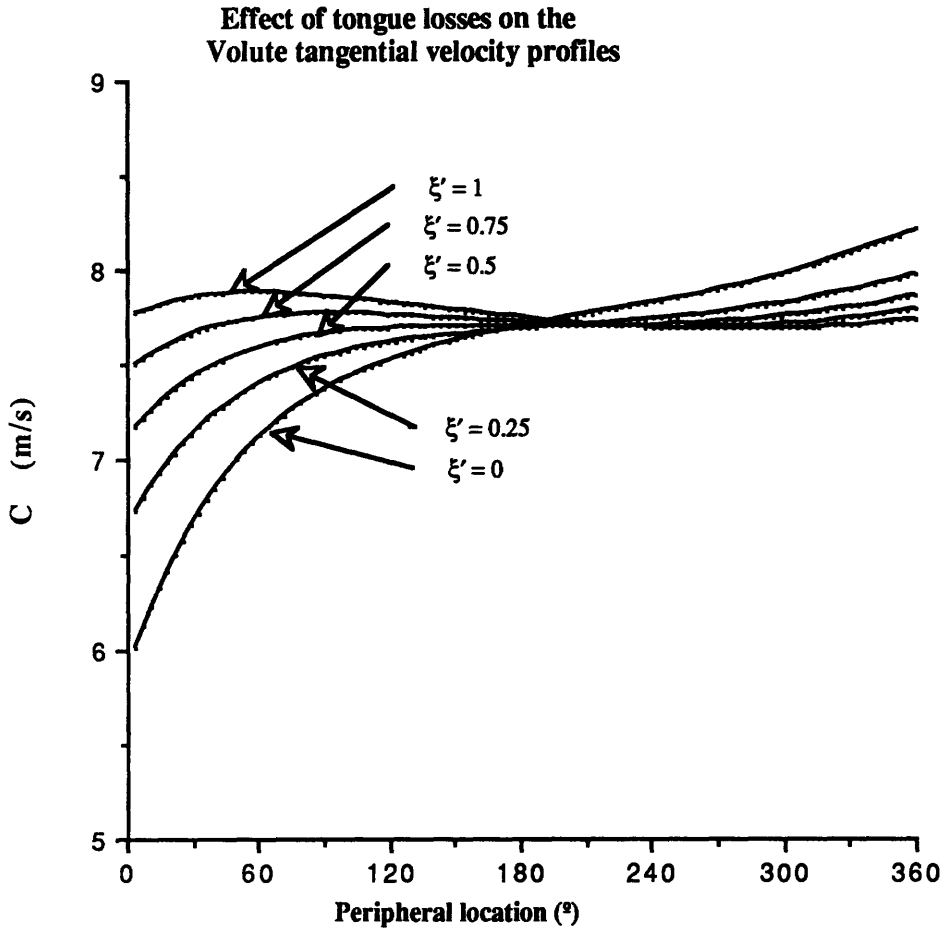

Figure 4.28: Sensitivity of the volute tangential velocity profiles to ξ'.

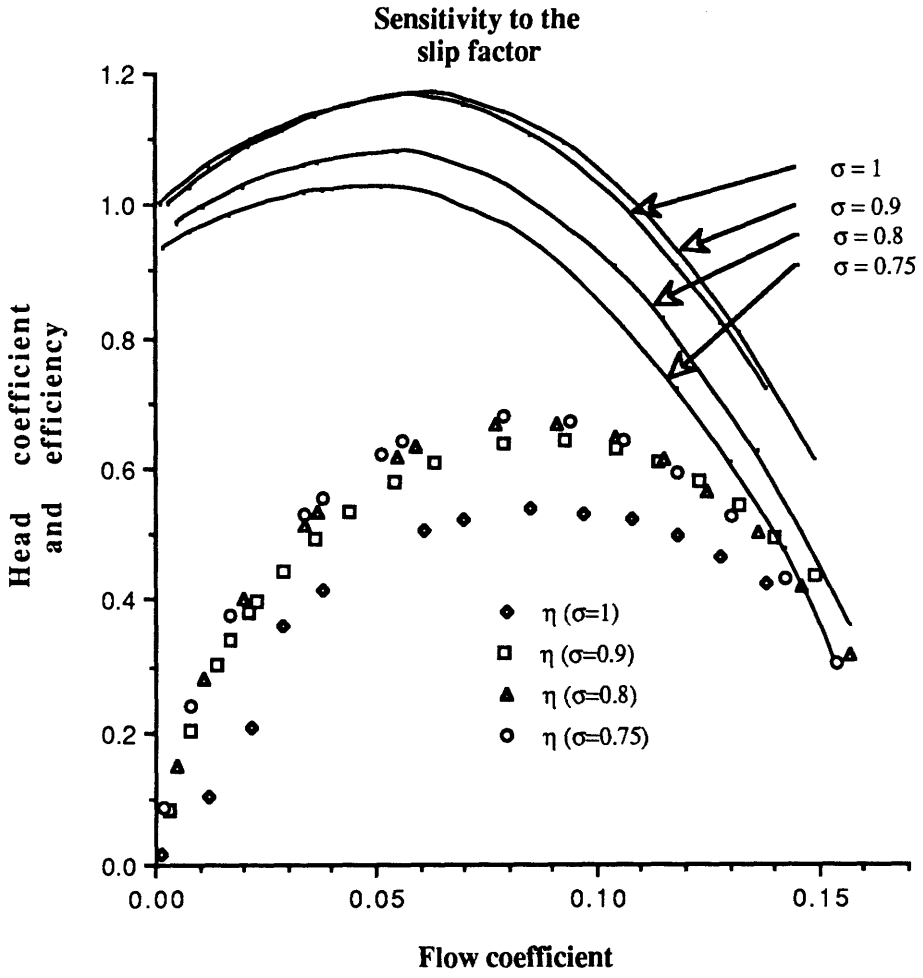

Figure 4.29: Sensitivity of the characteristic to σ: Head and efficiency curves for s=1, 0.9, 0.8, 0.75.

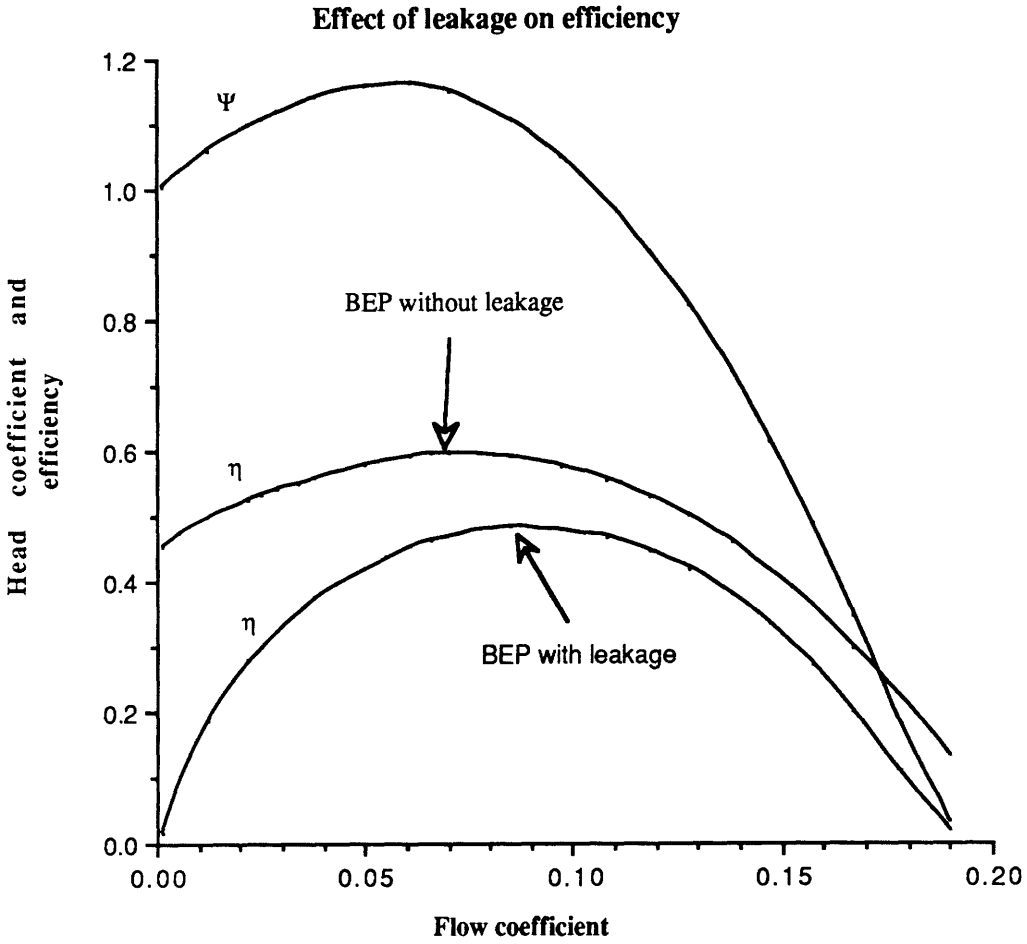

Figure 4.30: Effect of the leakage flows on the efficiency η.

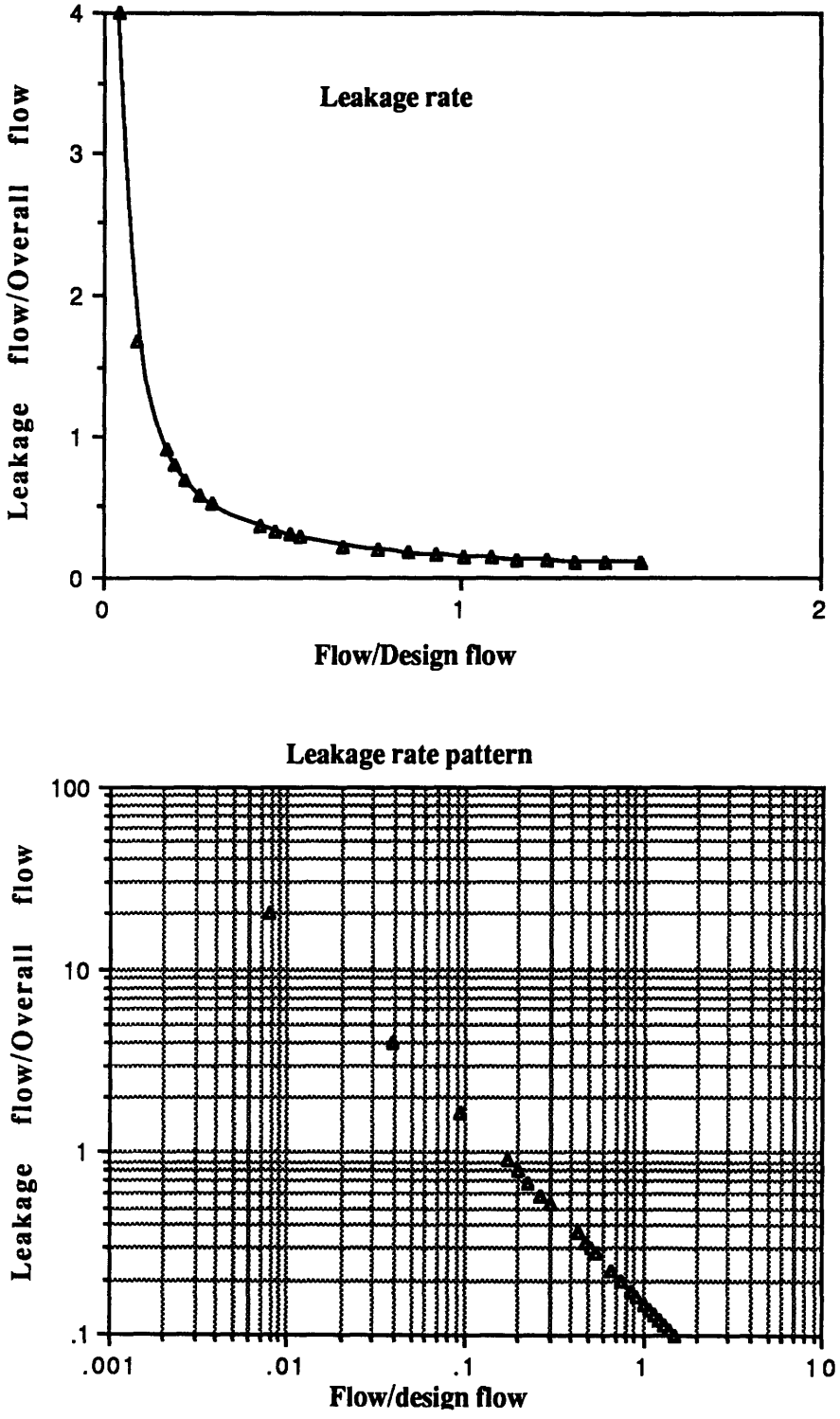

Figure 4.31: Leakage flow correlations.

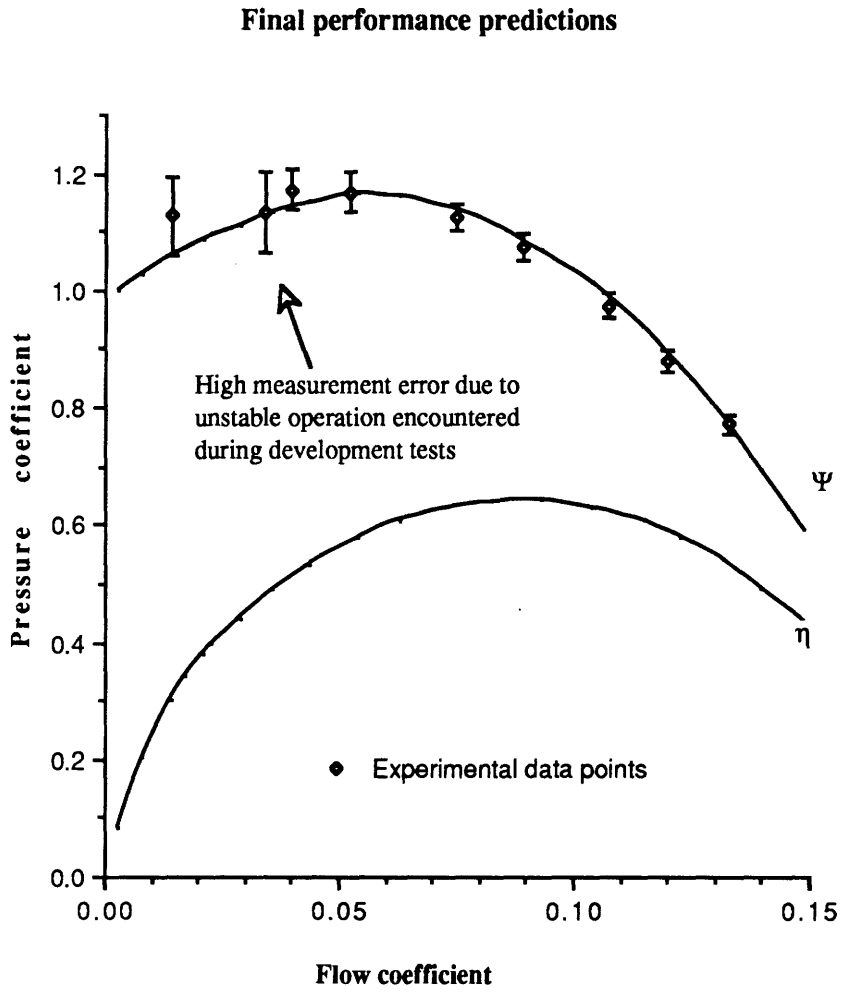

Figure 4.32: Final performance predictions.

APPENDIX A

Thrust loading calculations

The object here is to calculate the net thrust loads induced by the asymmetry in pressure distributions along the front and back shrouds. This force will be in the downward direction, trying to 'pull' the impeller off the shaft, since the backplate of the impeller has a much larger area. The following hypotheses are made during this calculation:

- The static pressure rise in the impeller is known and shall be assumed to be the only driver of the leakage flows.
- The pressure drop along the front shroud will be considered linear. This is obviously wrong as the major part of that pressure drop takes place in the labyrinth seal, but in doing so the pressure forces that counteract the overall load are overestimated. The result will therefore be conservative.
- The incoming dynamic head on the impeller eye will be neglected (it amounts to about 50 N at 700 gpm).
- Two extreme cases will be considered for the back shroud. One with no leakage and another where there is full leakage with a pressure drop equal to the static pressure rise in the impeller. The first is obviously the worst case as the whole pressure rise is transmitted to the back plate.
- The cross-sectional area of the blades will be neglected in the evaluation of the internal pressure forces.

For the calculation one can simply integrate the pressure loads along the front and back shrouds and inside the impeller blade passages. For the back shroud this can be written:

$$F_b = 2\pi \int_{R_i}^{R_o} P_b(r) r\,dr - 2\pi \int_{R_i}^{R_o} P(r) r\,dr - \pi R_i^2 P_i \qquad (A.1)$$

And in case of no back shroud leak the pressure along the back shroud passage is constant:

$$P_b(r) = \text{const.} = P_i + \Delta P_s \qquad (A.2)$$

So:

$$F_b=\pi\left(R_o^2 - R_s^2\right)\left(P_i+\Delta P_s\right) - 2\pi\int_{R_i}^{R_s} P(r)\,r\,dr - \pi R_i^2 P_i \tag{A.3}$$

The expression is similar for the front shroud:

$$F_f=-2\pi\int_{R_i}^{R_s} P_f(r)\,r\,dr + 2\pi\int_{R_i}^{R_s} P(r)\,r\,dr \tag{A.4}$$

By assuming a linear profile for P_f one can write:

$$P_f(r)=P_i+\frac{(R - R_i)}{(R_o - R_i)}\Delta P_s \tag{A.5}$$

And therefore:

$$F_f=-\pi\left(R_o^2 - R_i^2\right)P_i - \frac{2\pi\,\Delta P_s}{(R_o - R_i)}\cdot\left[r^2\left(\frac{r}{3} - \frac{R_i}{2}\right)\right]_{R_i}^{R_o} + 2\pi\int_{R_i}^{R_s} P(r)\,r\,dr \tag{A.6}$$

So finally, in this case of no back shroud leakage the total thrust can be written:

$$F = F_b + F_f \tag{A.7}$$

In other words:

$$F=-\pi R_s^2 P_i + \pi\Delta P_s\left[R_o^2 - R_s^2 - \frac{2}{(R_o - R_i)}\left(\frac{R_o^3}{3} - \frac{R_i R_o^2}{2} + \frac{R_i^3}{6}\right)\right] \tag{A.8}$$

Now, in the case of a full back shroud leak, the following pressure distribution is assumed along the back shroud:

$$P_b(r)=P_i+\frac{(R - R_s)}{(R_o - R_s)}\Delta P_s \tag{A.9}$$

So, in this case:

$$F_b = \pi\left(R_0^2 - R_s^2\right)P_i + \frac{2\pi\,\Delta P_s}{\left(R_o - R_s\right)}\left[r^2\left(\frac{r}{3} - \frac{R_s}{2}\right)\right]_{R_s}^{R_o} - 2\pi\int_{R_i}^{R_0} P(r)\,r\,dr - \pi R_i^2 P_i \tag{A.10}$$

And the total thrust becomes:

$$F = -\pi R_s^2 P_i + \pi\Delta P_s\left[\frac{2}{\left(R_o - R_\alpha\right)}\left(\frac{R_o^3}{3} - \frac{R_\alpha R_o^2}{2} + \frac{R_\alpha^3}{6}\right)\right]_i^s \tag{A.11}$$

Numerically:

- P_i = 7 psi.
- ΔP_S = 6 psi.

So for no back shroud leak:

F = 6 KN = 1200 lb.

And for full back shroud leakage:

F = 1.5 KN = 300 lb.

APPENDIX B

Effect of the piping compliance

The object here is to determine the effect of piping expansion and make sure it is negligible with respect to the variation of volume in the compliant air bags. For this one calculates the volume variation per unit length of the piping and compares it to the volume variation in the bags.

Considering the hoop stress in the pipe one can write:

$$\sigma = \frac{\delta P.R}{t} \qquad \text{(B.1)}$$

Where:

- σ: Perturbation stress in the pipe wall (per unit length).
- δP: Perturbation of the internal pressure.
- t: Pipe wall thickness.
- R: Pipe median radius.

So the relative elongation ε can be written:

$$\varepsilon = \frac{\delta P.R}{E.t} \qquad \text{(B.2)}$$

Where E is the Young modulus for PVC.

The relative volume increase can be written:

$$\frac{\delta V}{V} = (1+\varepsilon)^2 - 1 \qquad \text{(B.3)}$$

For the gas compliances the relative volume increase is:

$$\frac{\delta V}{V} = \frac{\delta P}{\gamma . P} \qquad \text{(B.4)}$$

Numerically the radius of the 8" pipe is 0.1016 m and the radius of the 12" pipe is 0.1524 m. There is a total of 0.65 m^3 of 8" pipe and 0.180 m^3 of 12" pipe. The Young modulus of PVC is 2.4 10^8 Pa/m^2 and the thickness of the piping can be estimated at 7 mm in both cases. An operating pressure of 1 atm, a volume of 1 m^3 in the air bags (total) and a pressure perturbation of 0.5 atm, will be considered. With these numbers the ratio of volumetric variation turns out to be:

$$\frac{\Delta V_{pipe}}{\Delta V_{compl}} = 1\% \qquad \text{(B.5)}$$

This is negligible, especially if one considers that the pressure differentials will be much less than 1 Atm.

APPENDIX C

Evaluation of the leakage factor, k

The leakage factor k is defined by the following equation:

$$\Psi = k \left(\frac{C_{1m}}{U} \right)^2 \tag{C.1}$$

So, explicitly:

$$k = \Psi \left(\frac{U}{C_{1m}} \right)^2 \tag{C.2}$$

To estimate k, the main hypothesis is that the flow through the shroud passage is axysimmetric and radial. Moreover, in the real case, where swirl can be quite strong, the local value of k is considered the same as if the whole flow were axysimmetric with the same characteristics as the local flow. The pressure drop takes place mainly in the seal passage, so one only has to consider the losses due to the floating labyrinth seal. The configuration is described on the following sketch:

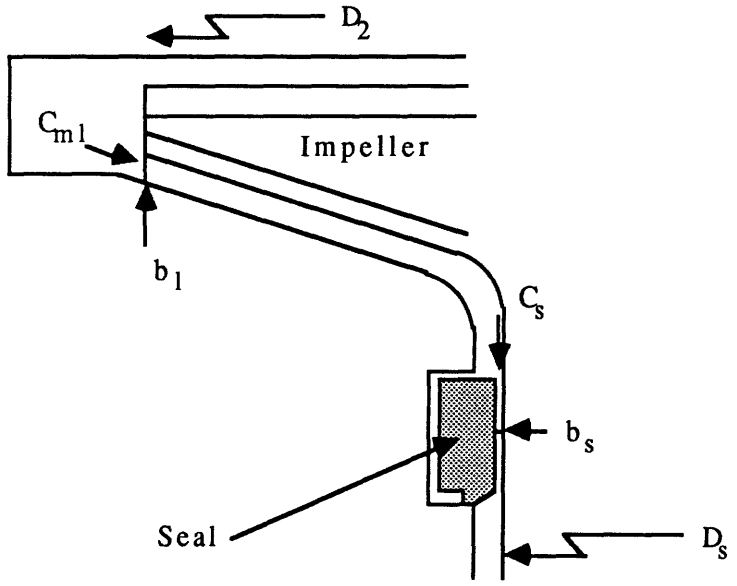

Continuity implies that:

$$\pi D_2 b_1 C_{1m} = \pi D_s b_s C_s \tag{C.3}$$

And therefore:

$$C_s = C_{lm}\frac{D_2\, b_1}{D_s\, b_s} \tag{C.4}$$

The flow in the seal passage is turbulent (R_e of the order of 5.10^6) so the pressure drop in terms of the average dynamic head is:

$$\Delta P = \left(\lambda_s \frac{L}{D_h} + \frac{3}{2}\right)\rho\frac{C_s^2}{2} \tag{C.5}$$

Where λ_s is the friction factor once again determined from the Moody diagram for smooth pipe flow. The term $\frac{3}{2}$ accounts for the losses at the inlet to the seal and at its discharge into the shroud passage (discharge into an infinite reservoir: one dynamic head is lost). So, given the definition of the hydraulic diameter D_h:

$$\Delta P = \lambda_s \frac{L}{4\, b_s}\rho\, C_s^2 \tag{C.6}$$

In terms of the local volute pressure coefficient:

$$\tfrac{1}{2}\rho\frac{U^2}{C_{lm}^2}\Psi = \left(\lambda_s\frac{L}{2\, b_s} + \frac{3}{2}\right)\frac{\rho}{2}\left(\frac{D_2\, b_1}{D_s\, b_s}\right)^2 \tag{C.7}$$

And finally:

$$k = \left(\lambda_s\frac{L}{2\, b_s} + \frac{3}{2}\right).\left(\frac{D_2\, b_1}{D_s\, b_s}\right)^2 \tag{C.8}$$

Numerically:

$$\boxed{k \approx 1.5\ 10^4}$$

This leakage factor corresponds to a very simplified case of the flow between the shroud and the casing. The real flow is really a circular Couette flow whose evaluation is much more involved. However, since the sensitivity of the model to this factor is not very important, an order of magnitude estimation is sufficient to yield acceptable results.

APPENDIX D

Numerical solver for system (2.7)

with

Output sample

```
*************************************************************************
* Dynamic simulation of a closed loop. Resonant frequencies and B
* parameters.
*        Version 5: automatic scan of the Head curve of the pump
*                   results are spooled to the printer
*************************************************************************
*       We consider a closed loop consisting of N legs, one main plenum and
* N-1 "secondary" plenums or compliances. All the characteristics are
* interactively prompted so the user specifies the system. The operating
* range from 0.001 to 0.1 is scanned.
*       The program calculates the perturbation growth rates as well as
* the natural frequencies for values of the flow coefficient in the above
* interval spaced by INC.
*       The system is solved for the eigen values of the first order
*  differential equations of mass flow and pressure.
*************************************************************************

      PARAMETER (NMAX=10,NMAX2=20,GAMMA=1.4)
      PARAMETER (RO=1000,PI=3.14159)
      INTEGER N,Z
      REAL VOLPL,PPL,PSLOPE,TSLOPE,SPEED,PHI,PSI,INC
      REAL AREA(NMAX),VCOM(NMAX),PCOM(NMAX),LEN(NMAX),DYN(NMAX)
      REAL MATRIX(NMAX2,NMAX2),WR(NMAX2),WI(NMAX2),DAMP(NMAX)
      REAL B(NMAX2),FREQ(NMAX2),UPAR(NMAX2),ZAPR(NMAX2),ZAPI(NMAX2)
      CHARACTER*1 CONF
      COMMON  LEN(NMAX),AREA(NMAX),VCOM(NMAX),
     /          PCOM(NMAX),MATRIX(NMAX2,NMAX2),
     /          DYN(NMAX),DAMP(NMAX)
      CALL SPLOWN ('  ')
*************************************************************************
****                          DATA   ACQUISITON
*************************************************************************
****         The loop characteristics are read in the file SYSPAR4
*************************************************************************
      OPEN (UNIT=1,FILE='SYSPAR4')
      READ (1,*)N

      IF (N.GT.NMAX) THEN
            WRITE (9,1008)
            GOTO2
      ENDIF

      READ (1,*) VOLPL,PPL

      DO 3 I=1,N
            READ (1,*) LEN(I),AREA(I),DYN(I),VCOM(I),PCOM(I)
3     CONTINUE

      READ (1,*) SPEED
      READ (1,*) NP
      READ (1,*) NT

      GOTO 10
*************************************************************************
****          DATA  ENTRY IN CASE OF NON CONFIRM.  OR N>NMAX
*************************************************************************
*     If user does not confirm the data or the number of legs exceeds nmax
* the whole ste of parameters is read at the keyboard. The user only needs
```

```
* to reenter the changes.
*************************************************************************
2     WRITE (9,1000)
      READ (9,*)N

      IF (N.GT.NMAX) THEN
            WRITE (9,1008)
            GOTO 2
      ENDIF


      WRITE (9,1001)
      READ (9,*)VOLPL
      WRITE (9,1002)
      READ (9,*)PPL

      DO 5 I=1,N-1
            WRITE(9,1015) I
            READ(9,*) LEN(I)
            WRITE (9,1005) I
            READ (9,*) AREA(I)
            WRITE (9,1016) I
            READ (9,*) DYN(I)
            WRITE (9,1006) I
            READ (9,*) VCOM(I)
            WRITE (9,1007) I
            READ (9,*) PCOM(I)
5     CONTINUE

      WRITE (9,1015) N
      READ (9,*) LEN(N)
      WRITE (9,1005) N
      READ (9,*) AREA(N)
      WRITE (9,1009)
      READ (9,*) SPEED
      WRITE (9,1013)
      READ (9,*)NP
      WRITE (9,1014)
      READ (9,*)NT
*************************************************************************
****                          DATA CONFIRM
*************************************************************************
*      Display of the current parameters and request of confirmation.
*************************************************************************
10    CALL TESTPRINT (N,VOLPL,PPL,SPEED,NP,NT)
      WRITE (9,1012)
      READ (9,1011) CONF

      IF (CONF='N') THEN
            GOTO 2
      ENDIF
      CALL HEADER (N,VOLPL,PPL,SPEED,NP,NT)
      WRITE (6,*) '  '
      WRITE (6,1028)
*************************************************************************
****                          TREATEMENT
*************************************************************************
      WRITE (9,1017)
```

```
      READ (9,*) INC
      DO 600 PHI=0.01,0.05,INC
*****************************************************************************
      WRITE (9,1027) PHI
*****************************************************************************
      CALL SLOPE(N,PHI,PSI,PSLOPE,TSLOPE,NP,NT,SPEED)
*****************************************************************************
      CALL STIFMATRIX(N,VOLPL,PPL,NP,NT,PSLOPE,TSLOPE,SPEED)
*****************************************************************************

      N=2*N
      CALL ELMHES(MATRIX,N,NMAX2)
      CALL HQR(MATRIX,N,NMAX2,WR,WI)
      N=N/2
*****************************************************************************
*         Calculate the relevant variables and spool the results.
*****************************************************************************
*                The frequency is the reduced frequency
*****************************************************************************
      DO 12 I=1,2*N
            IF (WI(I).NE.0) THEN
                  B(I)=SPEED/ABS(2*WI(I)*LEN(NP))
                  FREQ(I)=ABS(WI(I))/(2*PI*7)
                  UPAR(I)=(B(I)**2)*PSLOPE*TSLOPE
            ELSE
                  B(I)=0
                  FREQ(I)=0
                  UPAR(I)=0
            ENDIF
12    CONTINUE

      DO 15 Z=1,NMAX2
            ZAPI(Z)=0
            ZAPR(Z)=0
15    CONTINUE

      Z=1
      DO 13 I=1,2*N
            IF (((WI(I).EQ.0).AND.(WR(I).EQ.0)).OR.
     /                (ABS(WR(I)).LE.1E-8)) GOTO 13
            DO 16 J=1,Z
                  IF ((ABS(WI(I)).EQ.ABS(ZAPI(J)))
     /                        .AND.(WR(I).EQ.ZAPR(J))) GOTO 13
16          CONTINUE

            WRITE (6,1026)PHI,PSI,WI(I),WR(I),FREQ(I),B(I),UPAR(I)
            Z=Z+1
            ZAPI(Z)=WI(I)
            ZAPR(Z)=WR(I)
13    CONTINUE

600   CONTINUE

      CALL SPLNOW
*****************************************************************************
*          Program exit and current configuration save if desired.
*****************************************************************************
      WRITE (9,1023)
```

```
      READ (9,1024) CONF
      REWIND 2
      IF (CONF='Y') GO TO 100
      GO TO 2
100   WRITE (9,*) 'DO YOU WANT TO SAVE CURRENT CONFIGURATION (Y/N)?'
      READ (9,1024) CONF
      IF (CONF='N') GO TO 200
      REWIND 1

      WRITE (1,*) N
      WRITE (1,*) VOLPL,PPL
      DO 150 I=1,N
            WRITE (1,*) LEN(I),AREA(I),DYN(I),VCOM(I),PCOM(I)
150   CONTINUE
      WRITE (1,*) SPEED
      WRITE (1,*) NP
      WRITE (1,*) NT

*************************************************************************
****                        FORMATS
*************************************************************************
1000  FORMAT ('ENTER NUMBER OF LEGS:')
1001  FORMAT ('ENTER PLENUM VOLUME:')
1002  FORMAT ('ENTER PLENUM PRESSURE:')
1005    FORMAT ('ENTER THE REFERENCE AREA OF LEG:',I2)
1006  FORMAT ('ENTER THE VOLUME OF COMPLIANCE No:',I2)
1007  FORMAT ('ENTER THE PRESSURE OF COMPLIANCE No:',I2)
1008  FORMAT ('TOO MANY LEGS.10 MAX PLEASE!!')
1009  FORMAT ('ENTER THE WHEEL SPEED:')
1010  FORMAT ('END')
1011  FORMAT (A1)
1012  FORMAT ('PLEASE CONFIRM YOUR DATA(Y/N).')
1013  FORMAT ('ENTER THE No. OF THE LEG CONT. THE PUMP:')
1014  FORMAT ('ENTER THE No. OF THE LEG CONTAINING THE THROTTLE:')
1015  FORMAT ('ENTER THE LENGTH OF LEG:',I2)
1016    FORMAT ('ENTER THE NO. OF DYNAMIC HEADS LOST IN LEG:',I2)
1017  FORMAT ('ENTER THE DESIRED FLOW COEF. INCREMENT:')
1022  FORMAT (I2,5X,1PE10.3,4X,1PE10.3,5X,1PE10.3,5X
     /                       ,1PE10.3,5X,1PE10.3)
1023  FORMAT (/,'DO YOU WANT TO END (Y/N)?:')
1024  FORMAT (A)
1025    FORMAT (I2,5X,1PE10.3,4X,1PE10.3)
1026  FORMAT (F4.3,X,F4.3,X,1PE10.3,X,1PE10.3,X,1PE10.3
     /          ,X,1PE10.3,X,1PE10.3)
1027  FORMAT ('COMPUTING FOR PHI=',F5.3)
1028  FORMAT (' PHI  PSI     WI          WR
     /    FREQ       B PAR      UPAR  ')
*************************************************************************
      CALL SPLEND
200   END
      INCLUDE SPLOWN.INC
*************************************************************************
****                            SUBROUTINES
*************************************************************************
*              Screen display of current loop configuration
*************************************************************************
      SUBROUTINE TESTPRINT (N,VOLPL,PPL,SPEED,NP,NT)
      PARAMETER (NMAX=10,NMAX2=20)
```

```
      REAL VOLPL,PPL,PSLOPE,TSLOPE
      REAL AREA(NMAX),VCOM(NMAX),PCOM(NMAX)
      REAL MATRIX(NMAX,NMAX),DYN(NMAX)
      COMMON LEN(NMAX),AREA(NMAX),VCOM(NMAX),
     /         PCOM(NMAX),MATRIX(NMAX2,NMAX2),
     /         DYN(NMAX),DAMP(NMAX)

      WRITE (9,2002)
      WRITE (9,3001)N
      WRITE (9,2003)
      WRITE (9,3002)VOLPL,PPL
      WRITE (9,2005)

      DO 15 I=1,N-1
            WRITE(9,3004) I,LEN(I),AREA(I),DYN(I),
     /                        VCOM(I),PCOM(I)
15    CONTINUE

      WRITE (9,3005) N,LEN(N),AREA(N),DYN(N)
      WRITE (9,2006)
      WRITE (9,3006) SPEED,NP,NT
*-----------------------------------------------------------------------

2002  FORMAT ('THE NUMBER OF LEGS YOU CHOSE:')
2003  FORMAT ('   PLENUM  VOLUME        PLENUM PRESSURE')
2005  FORMAT (' N      LENGTH      REF. AREA        LOSS
     /         COMPL.VOL.        COMPL.PR.')
2006  FORMAT ('   SPEED    PUMP LEG      THROTTLE LEG')
3001  FORMAT (6X,I2)
3002  FORMAT (3X,1PE10.3,13X,1PE10.3)
3003  FORMAT (4X,1PE10.3)
3004  FORMAT (I2,3X,1PE10.3,4X,1PE10.3,4X,1PE10.3,
     /                  6X,1PE10.3,8X,1PE10.3)
3005  FORMAT (I2,3X,1PE10.3,4X,1PE10.3,4X,1PE10.3)
3006  FORMAT (1PE10.3,4X,I2,14X,I2)
*-----------------------------------------------------------------------
      RETURN
      END
*************************************************************************
*         write the header for the configuration in the result file
*************************************************************************
      SUBROUTINE HEADER (N,VOLPL,PPL,SPEED,NP,NT)
      PARAMETER (NMAX=10,NMAX2=20)
      REAL VOLPL,PPL,PSLOPE,TSLOPE
      REAL AREA(NMAX),VCOM(NMAX),PCOM(NMAX)
      REAL MATRIX(NMAX,NMAX),DYN(NMAX)
      COMMON LEN(NMAX),AREA(NMAX),VCOM(NMAX),
     /         PCOM(NMAX),MATRIX(NMAX2,NMAX2),
     /         DYN(NMAX),DAMP(NMAX)

      WRITE (6,2002)
      WRITE (6,3001)N
      WRITE (6,2003)
      WRITE (6,3002)VOLPL,PPL
      WRITE (6,2005)

      DO 15 I=1,N-1
            WRITE(6,3004) I,LEN(I),AREA(I),DYN(I),
```

```
     /                          VCOM(I),PCOM(I)
15    CONTINUE

      WRITE (6,3005) N,LEN(N),AREA(N),DYN(N)
      WRITE (6,2006)
      WRITE (6,3006) SPEED,NP,NT
*-----------------------------------------------------------------------

2002  FORMAT ('THE NUMBER OF LEGS YOU CHOSE:')
2003  FORMAT ('   PLENUM  VOLUME         PLENUM PRESSURE')
2005  FORMAT (' N      LENGTH      REF. AREA        LOSS
     /         COMPL.VOL.         COMPL.PR.')
2006  FORMAT ('   SPEED    PUMP LEG      THROTTLE LEG')
3001  FORMAT (6X,I2)
3002  FORMAT (3X,1PE10.3,13X,1PE10.3)
3003  FORMAT (4X,1PE10.3)
3004  FORMAT (I2,3X,1PE10.3,4X,1PE10.3,4X,1PE10.3,
     /                  6X,1PE10.3,8X,1PE10.3)
3005  FORMAT (I2,3X,1PE10.3,4X,1PE10.3,4X,1PE10.3)
3006  FORMAT (1PE10.3,4X,I2,14X,I2)
*-----------------------------------------------------------------------
      RETURN
      END
*************************************************************************
*    Calculation of the system matrix for the eigen value extraction.
*************************************************************************
      SUBROUTINE STIFMATRIX(N,VOLPL,PPL,NP,NT,PSLOPE,TSLOPE,SPEED)
      PARAMETER (NMAX=10,NMAX2=20,GAMMA=1.4,RO=1000)
      REAL VOLPL,PPL
      REAL AREA(NMAX),VCOM(NMAX),PCOM(NMAX),LEN(NMAX)
      REAL MATRIX(NMAX2,NMAX2),DAMP(NMAX)
      COMMON  LEN(NMAX),AREA(NMAX),VCOM(NMAX),
     /          PCOM(NMAX),MATRIX(NMAX2,NMAX2),
     /          DYN(NMAX),DAMP(NMAX)

      DO 6 I=1,N+N
            DO 7 J=1,N+N
                  MATRIX(I,J)=0
6           CONTINUE
7     CONTINUE


      MATRIX(1,N+1)=-AREA(1)/LEN(1)
      MATRIX(1,N+N)=AREA(1)/LEN(1)

      DO 8 I=2,N
            MATRIX(I,N+I)=-AREA(I)/LEN(I)
            MATRIX(I,N+I-1)=AREA(I)/LEN(I)
8     CONTINUE

      DO 11 I=1,N-1
            MATRIX(N+I,I)=(GAMMA*PCOM(I))/(RO*VCOM(I))
            MATRIX(N+I,I+1)=-MATRIX(N+I,I)
11    CONTINUE

      MATRIX(N+N,N)=(GAMMA*PPL)/(RO*VOLPL)
      MATRIX(N+N,1)=-(GAMMA*PPL)/(RO*VOLPL)
```

```
      DO 12 I=1,N
            MATRIX(I,I)=DAMP(I)*(AREA(I)/LEN(I))
12    CONTINUE

      RETURN
      END
*************************************************************************
* Calculation of the steady state operating point and the various damping
* coefficients. The pump and throttle slopes are also computed at the
* state operating point.
*************************************************************************
      SUBROUTINE SLOPE(N,PHI,PSI,PSLOPE,TSLOPE,NP,NT,SPEED)
      REAL PHI,PSI,PSLOPE,TSLOPE,SPEED
      PARAMETER (NMAX=10,NMAX2=20,RO=1000,PI=3.1415926)
      PARAMETER (D2=0.609,B2=1.27E-2)
      REAL LEN(NMAX),AREA(NMAX),DYN(NMAX),DAMP(NMAX)
      COMMON  LEN(NMAX),AREA(NMAX),VCOM(NMAX),
     /          PCOM(NMAX),MATRIX(NMAX2,NMAX2),
     /          DYN(NMAX),DAMP(NMAX)

      PSI=2.817E4*(PHI**5)-9469.7658*(PHI**4)+1107.3662*(PHI**3)
     /      -76.1191*(PHI**2)+2.7551*PHI+0.5337

      TSLOPE=2*(PSI/PHI**2)*PHI

      PSLOPE=1.4085e5*(PHI**4)-37879.06*(PHI**3)
     /         +3322.099*(PHI**2)-152.2382*PHI+2.7551

      DO 1 I=1,N
            DAMP(I)=-DYN(I)*(PHI/AREA(I)**2)
     /                  *SPEED*PI*D2*B2
1     CONTINUE

      DAMP(NP)=DAMP(NP)+(PSLOPE*SPEED/(2*PI*D2*B2))
      DAMP(NT)=DAMP(NT)-(TSLOPE*SPEED/(2*PI*D2*B2))

      RETURN
      END
*************************************************************************
****                    REDUCTION TO HESSENBERG FORM
****                           QR algorithm
*************************************************************************
      SUBROUTINE ELMHES(A,N,NP)
      DIMENSION A(NP,NP)
      IF (N.GT.2) THEN
            DO 17 M=2,N-1
                  X=0
                  I=M
                  DO 11 J=M,N
                        IF (ABS(A(J,M-1)).GT.ABS(X)) THEN
                              X=A(J,M-1)
                              I=J
                        ENDIF
11                CONTINUE
                  IF (I.NE.M) THEN
                        DO 12 J=M-1,N
                              Y=A(I,J)
                              A(I,J)=A(M,J)
```

```
                              A(M,J)=Y
12                        CONTINUE
                          DO 13 J=1,N
                              Y=A(J,I)
                              A(J,I)=A(J,M)
                              A(J,M)=Y
13                        CONTINUE
                    ENDIF
                    IF (X.NE.0) THEN
                          DO 16 I=M+1,N
                             Y=A(I,M-1)
                             IF (Y.NE.0) THEN
                                Y=Y/X
                                A(I,M-1)=Y
                                DO 14 J=M,N
                                   A(I,J)=A(I,J)-Y*A(M,J)
14                                 CONTINUE
                                DO 15 J=1,N
                                   A(J,M)=A(J,M)+Y*A(J,I)
15                                 CONTINUE
                             ENDIF
16                        CONTINUE
                    ENDIF
17            CONTINUE
      ENDIF
      RETURN
      END
*****************************************************************************
****        Eigenvalue extraction from the upper hessenebrg matrix
****                              QR algorithm
*****************************************************************************
      SUBROUTINE HQR(A,N,NP,WR,WI)
      DIMENSION A(NP,NP),WR(NP),WI(NP)
      ANORM=ABS(A(1,1))
      DO 12 I=2,N
            DO 11 J=I-1,N
                  ANORM=ANORM+ABS(A(I,J))
11          CONTINUE
12    CONTINUE
      NN=N
      T=0
1     IF (NN.GE.1) THEN
            ITS=0
2           DO 13 L=NN,2,-1
                  S=ABS(A(L-1,L-1))+ABS(A(L,L))
                  IF (S.EQ.0.) S=ANORM
                  IF (ABS(A(L,L-1))+S.EQ.S) GO TO 3
13          CONTINUE
            L=1
3           X=A(NN,NN)
            IF (L.EQ.NN) THEN
                  WR(NN)=X+T
                  WI(NN)=0
                  NN=NN-1
            ELSE
                  Y=A(NN-1,NN-1)
                  W=A(NN,NN-1)*A(NN-1,NN)
                  IF (L.EQ.NN-1) THEN
```

```
                        P=0.5*(Y-X)
                        Q=P**2+W
                        Z=SQRT(ABS(Q))
                        X=X+T
                        IF (Q.GE.0.) THEN
                              Z=P+SIGN(Z,P)
                              WR(NN)=X+Z
                              WR(NN-1)=WR(NN)
                              IF (Z.NE.0.) WR(NN)=X-W/Z
                              WI(NN)=0
                              WI(NN-1)=0
                        ELSE
                              WR(NN)=X+P
                              WR(NN-1)=WR(NN)
                              WI(NN)=Z
                              WI(NN-1)=-Z
                        ENDIF
                        NN=NN-2
                  ELSE
                        IF(ITS.EQ.30)PAUSE 'Too many its.'
                        IF(ITS.EQ.10.OR.ITS.EQ.20)THEN
                           T=T+X
                           DO 14 I=1,NN
                              A(I,I)=A(I,I)-X
14                         CONTINUE
                           S=ABS(A(NN,NN-1))+ABS(A(NN-1,NN-2))
                           X=0.75*S
                           Y=X
                           W=-0.4375*S**2
                        ENDIF
                        ITS=ITS+1
                        DO 15 M=NN-2,L,-1
                           Z=A(M,M)
                           R=X-Z
                           S=Y-Z
                           P=(R*S-W)/A(M+1,M)+A(M,M+1)
                           Q=A(M+1,M+1)-Z-R-S
                           R=A(M+2,M+1)
                           S=ABS(P)+ABS(Q)+ABS(R)
                           P=P/S
                           Q=Q/S
                           R=R/S
                           IF(M.EQ.L)GO TO 4
                           U=ABS(A(M,M-1))*(ABS(Q)+ABS(R))
                           V=ABS(P)*(ABS(A(M-1,M-1))+ABS(Z)
     /                               +ABS(A(M+1,M+1)))
                           IF (U+V.EQ.V)GO TO 4
15                      CONTINUE
4                       DO 16 I=M+2,NN
                           A(I,I-2)=0
                           IF (I.NE.M+2) A(I,I-3)=0
16                      CONTINUE
                        DO 19 K=M,NN-1
                           IF(K.NE.M)THEN
                              P=A(K,K-1)
                              Q=A(K+1,K-1)
                              R=0
                              IF(K.NE.NN-1)R=A(K+2,K-1)
```

```
                                X=ABS(P)+ABS(Q)+ABS(R)
                                IF(X.NE.0.)THEN
                                   P=P/X
                                   Q=Q/X
                                   R=R/X
                                ENDIF
                             ENDIF
                             S=SIGN(SQRT(P**2+Q**2+R**2),P)
                             IF(S.NE.0)THEN
                                IF(K.EQ.M)THEN
                                   IF(L.NE.M)A(K,K-1)=
     /                                    -A(K,K-1)
                                ELSE
                                   A(K,K-1)=-S*X
                                ENDIF
                                P=P+S
                                X=P/S
                                Y=Q/S
                                Z=R/S
                                Q=Q/P
                                R=R/P
                                DO 17 J=K,NN
                                   P=A(K,J)+Q*A(K+1,J)
                                   IF(K.NE.NN-1)THEN
                                      P=P+R*A(K+2,J)
                                      A(K+2,J)=A(K+2,J)-P*Z
                                   ENDIF
                                   A(K+1,J)=A(K+1,J)-P*Y
                                   A(K,J)=A(K,J)-P*X
17                              CONTINUE
                                DO 18 I=L,MIN(NN,K+3)
                                   P=X*A(I,K)+Y*A(I,K+1)
                                   IF(K.NE.NN-1)THEN
                                      P=P+Z*A(I,K+2)
                                      A(I,K+2)=A(I,K+2)-P*R
                                   ENDIF
                                   A(I,K+1)=A(I,K+1)-P*Q
                                   A(I,K)=A(I,K)-P
18                              CONTINUE
                             ENDIF
19                        CONTINUE
                          GO TO 2
                       ENDIF
                    ENDIF
                 GO TO 1
                 ENDIF
                 RETURN
                 END
```

The number of sections you chose:
2

Plenum Volume	Plenum Pressure
0.750	0.60E+05

N	Length	Ref. Area	Loss	Compl.Vol.	Compl.Pr.
1	1140E+01	5.601E-02	4.000	0.4	1.500E+05
2	1.80E+00	3.240E-02	0.000		

Speed	Pump Section	Throttle Section
13.5	1	2

Φ	Ψ	$\Im(\lambda)$	$\Re(\lambda)$	ω_{osc} (Hz)	B	ξ
.010	.475	0.000E-01	6.917E+00	0.000E-01	0.000E-01	0.000E-01
.012	.485	0.000E-01	6.271E+00	0.000E-01	0.000E-01	0.000E-01
.014	.495	0.000E-01	5.634E+00	0.000E-01	0.000E-01	0.000E-01
.016	.504	0.000E-01	4.999E+00	0.000E-01	0.000E-01	0.000E-01
.018	.512	0.000E-01	4.359E+00	0.000E-01	0.000E-01	0.000E-01
.020	.519	0.000E-01	3.693E+00	0.000E-01	0.000E-01	0.000E-01
.022	.526	0.000E-01	2.943E+00	0.000E-01	0.000E-01	0.000E-01
.024	.532	-4.897E-01	1.862E+00	7.794E-02	1.209E-00	1.823E+02
.028	.542	-1.317E+00	1.415E+00	2.097E-01	4.495E-01	1.698E+01
.030	.546	-1.519E+00	1.205E+00	2.417E-01	3.899E-01	1.035E+01
.032	.549	-1.665E+00	1.003E+00	2.651E-01	3.555E-01	6.861E+00
.034	.552	-1.774E+00	8.101E-01	2.824E-01	3.337E-01	4.716E+00
.036	.555	-1.855E+00	6.246E-01	2.952E-01	3.192E-01	3.260E+00
.038	.556	-1.913E+00	4.469E-01	3.045E-01	3.095E-01	2.201E+00
.040	.558	-1.953E+00	2.765E-01	3.108E-01	3.032E-01	1.389E+00
.042	***.559***	***-1.977E+00***	***1.133E-01***	***3.147E-01***	***2.995E-01***	***7.376E-01***
.044	.559	-1.988E+00	-4.306E-02	3.165E-01	2.978E-01	1.953E-01
.046	.559	-1.988E+00	-1.930E-01	3.165E-01	2.978E-01	-2.720E-01
.048	.559	-1.978E+00	-3.369E-01	3.149E-01	2.993E-01	-6.880E-01
.050	.558	-1.960E+00	-4.749E-01	3.119E-01	3.021E-01	-1.070E+00
.052	.556	-1.933E+00	-6.075E-01	3.077E-01	3.063E-01	-1.431E+00
.054	.555	-1.899E+00	-7.350E-01	3.023E-01	3.117E-01	-1.782E+00
.056	.553	-1.859E+00	-8.578E-01	2.959E-01	3.185E-01	-2.134E+00
.058	.551	-1.812E+00	-9.763E-01	2.884E-01	3.268E-01	-2.496E+00
.060	.548	-1.759E+00	-1.091E+00	2.799E-01	3.367E-01	-2.882E+00
.062	.545	-1.699E+00	-1.202E+00	2.704E-01	3.485E-01	-3.304E+00
.064	.542	-1.633E+00	-1.310E+00	2.599E-01	3.626E-01	-3.781E+00
.066	.538	-1.559E+00	-1.416E+00	2.482E-01	3.797E-01	-4.339E+00
.068	.534	-1.478E+00	-1.519E+00	2.352E-01	4.007E-01	-5.019E+00
.070	.530	-1.387E+00	-1.621E+00	2.207E-01	4.270E-01	-5.884E+00
.072	.526	-1.284E+00	-1.721E+00	2.043E-01	4.613E-01	-7.051E+00
.074	.521	-1.166E+00	-1.821E+00	1.855E-01	5.079E-01	-8.744E+00
.076	.516	-1.027E+00	-1.921E+00	1.634E-01	5.766E-01	-1.149E+01
.078	.511	-8.565E-01	-2.020E+00	1.363E-01	6.913E-01	-1.679E+01
.080	.506	-6.275E-01	-2.121E+00	9.988E-02	9.435E-01	-3.172E+01
.082	.500	-1.823E-01	-2.223E+00	2.901E-02	3.249E+00	-3.807E+02
.084	.494	0.000E-01	-2.920E+00	0.000E-01	0.000E-01	0.000E-01
.086	.487	0.000E-01	-3.307E+00	0.000E-01	0.000E-01	0.000E-01
.088	.481	0.000E-01	-3.640E+00	0.000E-01	0.000E-01	0.000E-01
.090	.474	0.000E-01	-3.952E+00	0.000E-01	0.000E-01	0.000E-01
.092	.466	0.000E-01	-4.254E+00	0.000E-01	0.000E-01	0.000E-01

APPENDIX E

Volute/impeller interaction code

and

Convergence history diagrams

```
*************************************************************************
*      Impeller volute interaction in the presence of leakage flows
*                           Version 5.0
*                   Include volute wall friction
*                         VAX/VMS 4.7 Version
*************************************************************************
*      Define variables of interest
*************************************************************************

       REAL*8 PHIT,PSIT,DELC,DELCM2,CTR,LOSSF,F,W,D2,B2,BETAB,BLB2
       REAL*8 LP,PI,DT,SIGMA,D1,U,ALPHA,REL,PDELCM2,SGCM2,PHIDES,BETA
       REAL*8 PHILT,PDELC,SGC,LAMBDA,DL,LOSSFV,PSIS,COT,ONE,CP,EFF
       INTEGER COUNT,N,TEST,LEAKF,LEAKCO,Z,INDEX
       PARAMETER (D2=0.6096,B2=0.0127,BETAB=0.5759586532)
       PARAMETER (BLB2=2,D1=0.2032,PHIDES=0.134)
       PARAMETER (U=13.5,N=100,LP=0.372872,PI=3.141592654)
       PARAMETER (LOSSF=0.5,DT=0.0014186,Z=8,LEAKCO=17000)
       PARAMETER (F=0.004123658,W=0.0635)
       PARAMETER (DL=0.0191511)
       REAL*8 A(0:101),AREF(0:101),DH(0:101),C(0:101),CM2(0:100)
       REAL*8 CU(0:100),VR(0:100),CLM(0:100),CLU(0:100),PHIV(0:101)
       REAL*8 PSIM(0:100),PSIV(0:101),DCM2(0:100),DELPSIV(0:100)
       REAL*8 C2(0:100),FLOW(1:15),VELD(0:100,15),PRESD(0:100,15)
       REAL*8 CD(0:100,15),CL(0:100,1:15)

       OPEN (UNIT=9,FILE='SYS$OUTPUT',STATUS='OLD')
       OPEN (UNIT=9,FILE='SYS$INPUT',STATUS='OLD')

*************************************************************************
*      Initialize variables
*************************************************************************

100    DELCM2=2
       PDELCM2=0.1
       PDELC=0.1
       SGCM2=1
       SGC=1

*************************************************************************
*      Enter user defined paramaters
*************************************************************************

       WRITE (9,*)'Enter tongue pressure coefficient.'
       READ (9,*) PSIV(0)
       WRITE (9,*)'Enter volute tongue loss factor.'
       READ (9,*) LOSSFV
       WRITE (9,*)'Enter impeller slip factor.'
       READ (9,*) SIGMA
       WRITE (9,*)'Enter shroud leakage factor
     / (0:No leakage/1:Full leakage).'
       READ (9,*) LEAKF
       WRITE (9,*)'Enter first guess at C(0).'
       READ (9,*) C(0)
       WRITE (9,*)'Enter first guess at Cm2(0).'
       READ (9,*) CM2(0)
       WRITE (9,*)'Enter relaxation coefficient.'
       READ (9,*) REL
```

```
*************************************************************************
*      Initialize more variables
*************************************************************************

       A(0)=0.00168
       AREF(0)=A(0)/(PI*D2*B2)
       DH(0)=4*W*A(0)/(2*(A(0)+W**2))
       COUNT=0
       ONE=1.
       BETA=BETAB

*************************************************************************
*      March through the volute (Theta from 0 to 360)
*************************************************************************

500    PHIV(0)=C(0)*AREF(0)/U
       CLM(0)=LEAKF*(U*DSQRT(PSIV(0)/LEAKCO))
       CLU(0)=CU(0)

       DO 1000 I=0,N

            A(I+1)=A(I)+(F/N)
            AREF(I+1)=A(I+1)/(PI*D2*B2)
            DH(I+1)=4*W*A(I+1)/(2*(A(I+1)+W**2))
            C2(I)=DSQRT(CM2(I)**2+
     /      (SIGMA*U-(CM2(I)/DTAN(BETA)))**2)
            CU(I)=SIGMA*U-(CM2(I)/DTAN(BETA))
            VR(I)=CM2(I)/DSIN(BETA)
            PSIM(I)=(2*CU(I)/U)-((C2(I)/U)**2)-(LOSSF*(VR(I)/U)**2)
            CLM(I)=DSIGN(ONE,PSIV(I))*LEAKF*
     /      (U*DSQRT(DABS(PSIV(I))/LEAKCO))
            CLU(I)=CU(I)
            PHIV(I+1)=PHIV(I)+(CM2(I)/(N*U))-(CLM(I)*BLB2/(N*U))
            C(I+1)=U*(PHIV(I+1)/AREF(I+1))
            DELPSIV(I)=PHIV(I)*C(I)/U
            DELPSIV(I)=DELPSIV(I)-(PHIV(I+1)*C(I+1)/U)
            DELPSIV(I)=DELPSIV(I)+(CM2(I)*CU(I)/(N*U**2))
            DELPSIV(I)=DELPSIV(I)-(BLB2*CLM(I)*CLU(I)/(N*U**2))
            DELPSIV(I)=DELPSIV(I)*(4/(AREF(I)+AREF(I+1)))
            DELPSIV(I)=DELPSIV(I)-((LAMBDA(C(I),DH(I))*DL/DH(I))
     /      *((C(I)/U)**2))
            PSIV(I+1)=PSIV(I)+DELPSIV(I)
            ALPHA=(DT*DSIN(BETA)*U**2)/(2*LP)
            DCM2(I)=ALPHA*(PSIM(I)-PSIV(I+1))
            CM2(I+1)=CM2(I)+DCM2(I)


1000   CONTINUE

*************************************************************************
*      Calculate error and control variables
*************************************************************************

       COT=C(0)
       CTR=DSQRT((C(100)/U)**2+DSIGN(ONE,COT)*(PSIV(100)-PSIV(0))*
     /      (1-LOSSFV))
       CTR=CTR*U*DSIGN(ONE,COT)
```

```
      DELC=CTR-C(0)
      DELCM2=CM2(100)-CM2(0)

*************************************************************************
*     Convergence criterion and iteration setup
*************************************************************************

      IF (DABS(DELC).LT.1E-5 .AND. DABS(DELCM2).LT.1E-5) THEN
            GOTO 2000
      ELSE
           C(0)=C(0)+
     /     5*REL*(DSIGN(ONE,(ABS(PDELC)-ABS(DELC)))*
     /     SGC*DABS(DELC))
           CM2(0)=CM2(0)+
     /     REL*(DSIGN(ONE,(ABS(PDELCM2)-ABS(DELCM2)))*
     /     SGCM2*DABS(DELCM2))
           SGCM2=DSIGN(ONE,(ABS(PDELCM2)-ABS(DELCM2)))*SGCM2
           SGC=DSIGN(ONE,(ABS(PDELC)-ABS(DELC)))*SGC
           PDELCM2=DELCM2
           PDELC=DELC
           IF ((DELC.GT.10).OR.(DELCM2.GT.10)) THEN
                 GOTO 3000
           ELSE
                 COUNT=COUNT+1
                       IF (MOD(COUNT,500).EQ.0) THEN
                       WRITE (9,*) 'New relaxation coefficient:'
                       READ (9,*) REL
                 ENDIF
                 IF (COUNT.GT.9999) THEN
                       GOTO 5000
                 ELSE
                             WRITE (9,4040) COUNT,DELC,DELCM2,
     /                                       C(0),CM2(0)

                       GOTO 500
                 ENDIF
           ENDIF
      ENDIF

*************************************************************************
*     Calculate relevant operating parameters
*************************************************************************

2000  PHIT=PHIV(100)-PHIV(0)
      PSIT=PSIV(100)+(C(100)/U)**2
      PSIS=PSIV(100)+CP(PHIT)*(PSIT-PSIV(100))
      PHILT=CLM(0)
      EFF=0
      DO 2005 I=1,100
           EFF=EFF+(CM2(I)*CU(I))
2005  CONTINUE
      EFF=(N*PHIT*PSIS*(U**2))/(2*EFF)
      EFF=EFF*100
      DO 2010 I=1,100
                 PHILT=PHILT+CLM(I)
2010  CONTINUE
      PHILT=PHILT*(BLB2/(N*U)
```

```
*************************************************************************
*      Screen display of results
*************************************************************************

       WRITE (9,4000) PSIV(0),LOSSFV,SIGMA,C(0),CM2(0),PHIT,
     / PSIT,PSIS,EFF,PHILT
       WRITE (9,*) ' Selected local volute pressure coefficients:'
       WRITE (9,*) '   90<      180<    270<     360<'
       WRITE (9,4050) PSIV(25),PSIV(50),PSIV(75),PSIV(100)
       WRITE (9,4015) CP(PHIT)
       WRITE (9,4060) (180/PI)*DASIN(CM2(100)/C2(100))
       WRITE (9,4005)COUNT
       WRITE (9,*) ' Enter index of data series (0 if reject).'
       READ (9,4030) INDEX
       IF ((INDEX.GT.0).AND.(INDEX.LT.16)) THEN
                FLOW(INDEX)=(PHIT/PHIDES)*N
            DO 2100 I=0,100
                VELD(I,INDEX)=20*CM2(I)
                PRESD(I,INDEX)=50*PSIV(I)
                CL(I,INDEX)=20*CLM(I)
2100        CONTINUE
       ENDIF
       WRITE (9,*) 'Another point (Y:0/N:1) ?'
       READ (9,*) TEST
       IF (TEST.EQ.1) THEN
                GOTO 5000
       ELSE
                GOTO 100
       ENDIF

3000   WRITE (9,*)' Divergence!!!'

*************************************************************************
*      Define formats
*************************************************************************

4000   FORMAT('  Tongue pressure coefficient:',F8.5,/,
     / '  Tongue loss factor:',F8.5,/,
     / '  Impeller slip factor:',F8.5,/,
     / '  C(0):',F8.5,' m/s',/,
     / '  Cm2(0):',F8.5,' m/s',/,
     / '  Overall flow coefficient:',F6.3,/,
     / '  Volute exit total pressure coefficient:',F6.3,/,
     / '  Overall static pressure coefficient:',F6.3,/,
     / '  Overall efficiency:',F6.3,' %',/,
     / '  Leakage flow coefficient',F6.3)
4005   FORMAT ('  Iteration count:',I5)
4010   FORMAT (6F12.8)
4015   FORMAT ('  Diffuser pressure recovery factor:',F6.3)
4020   FORMAT (4F12.8)
4030   FORMAT (I2)
4040   FORMAT ('  ',I4,2X,E11.5,2X,E11.5,2X,F9.5,2X,F9.5)
4050   FORMAT (4F9.5)
4060   FORMAT ('  Flow angle of attack on the volute tongue
     / (degrees):',F6.3)

5000   WRITE (9,*) ' Do you want to generate 3-D files (Y:0/N:1)?'
```

```
      READ (9,*)TEST

*************************************************************************
*     Write file subrotine should be calld at this point
*     IF (TEST.EQ.0) THEN CALL WRITEFILE
*************************************************************************

      PAUSE
      END

*************************************************************************
*     Definition function of Cp(Flow)
*************************************************************************

      FUNCTION CP(PHIT)
      REAL*8 CP,PHIT

      IF (PHIT.LE.0.06) THEN
           CP=0.75
      ELSE
           CP=0.75-6.4*(PHIT-0.06)
      ENDIF
      IF (CP.LE.0) THEN
           CP=0
      ENDIF

      RETURN
      END

*************************************************************************
*     Definition function of Lambda(Re)
*************************************************************************

      FUNCTION LAMBDA(C,DH)
      REAL*8 LAMBDA,C,DH

      LAMBDA=0.02-0.005*(DLOG10((C*DH)/1E-6)-5)

      RETURN
      END
```

Convergence history diagrams